JPL D–26280

Earth Observing System (EOS)

Microwave Limb Sounder (MLS)

EOS MLS
Instrument Calibration Report
Post-Launch Updates – Volume 4

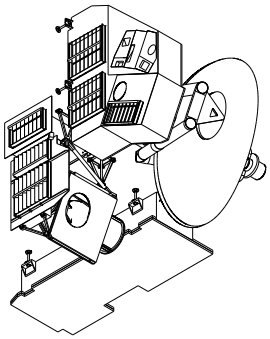

Robert F. Jarnot, Richard E. Cofield, Herbert M. Pickett, Paul C. Stek

February 11, 2025

Jet Propulsion Laboratory
California Institute of Technology
Pasadena, CA 91109-8099

The research was carried out at the Jet Propulsion Laboratory, California Institute of Technology, under a contract with the National Aeronautics and Space Administration (80NM0018D004).

Release Record

Version	Date	Comments
draft	12 Feb 2003	Start of working/draft version
	30 Mar 2004	Initial release for review
	7 Nov 2014	Add Oct 2014 Spectral Baseline Data
	2 Nov 2018	Add Oct 2018 Spectral Baseline Data
Public	11 Feb 2025	URS wording added to cover

Routine updates to Spectral Baseline measurement data are not included in the table above. These updates take place one or two times a year.

Contents

Chapter 1

Introduction

This volume of the EOS MLS Calibration Report addresses changes and updates to the results presented in the first three volumes.

- ❏ Some performance characteristics are influenced by the instrument environment (especially temperature, temperature stability, and air *vs* vacuum operation). In particular:
- ❏ Noise characteristics are typically improved in orbit (compared to ground-based performance) because of the relatively benign thermal environment experienced by the signal chain electronics, and the lack of convection-induced artifacts in filter spectrometer post-detector electronics:
  - ⇨ The total-power measurement mode of MLS is particularly impacted by instabilities due to the relatively long time between reference measurements (24.7 s nominally), and to its sensitivity to $\frac{1}{f}$ noise.
- ❏ The long data sets obtained in orbit provide high visibility into unusual behavior in any measurement channel, especially when higher level data products are being scrutinized.
  - ⇨ This allows ready identification of channels which display unwanted systematic behavior rather than just (possibly elevated) random noise.
  - ⇨ Some channels flagged as 'display excess noise' from pre-launch tests are thus now flagged as 'bad.'
- ❏ R4 relative sideband response changed after definitive pre-launch calibrations had been performed, but the calibration data files were not updated to reflect this situation until after launch (an oversight).
- ❏ The most important changes and updates arise in the FOV arena:
  - ⇨ Moon scans provide validation of pre-launch calibrations of FOV relative pointing between the radiometers. With the incorporation of data from multiple in-orbit moon scans, the precision and accuracy of these data are improved.
  - ⇨ It is anticipated that scans of the moon with the spacecraft executing a modest yaw maneuver will provide significant improvements in knowledge of *absolute* FOV pointing. At the time of writing such measurements have not been performed, but

discussions with the spacecraft operations team are underway to determine their feasibility.

- ⇨ One area of FOV calibration in which UARS MLS experience indicated that in-flight data would be necessary for model refinement was that of the estimation of the radiance offsets between Space and Limb Port views to cold space.
- ⇨ Another important UARS lesson, related to the previous bullet, was that the *spectrally-varying* component of the difference between cold space observed via the two ports would be both significant in magnitude and not well predicted from pre-launch data. Level 1 software was designed with this in mind, the plan being to incorporate appropriate forms of spectral and non-spectral baseline correction after evaluation of in-flight data.

These topics are the main subjects of this volume of the EOS MLS Calibration Report.

Non-inclusive (and non-ordered) list of topics:

(1) Bad channels

(2) Sensitivity

(3) 1/f characteristics + spectrally-averaged noise

(4) R4 Tsys

(5) R4 rsr

(6) FOV details + antenna offsets

(7) Spectral Baseline (AC and DC), including updates

(8) Linearity range verified over wider range by use of both GHz targets

(9) Gain compression

(10) Switching Mirror port scans

(11) Moon tracking data

(12) THz-related updates

Chapter 2

Radiometric Performance and Calibration

In the first volume of this report we indicated that several filter channels displayed slightly elevated noise compared to expectations because of internally-generated interference. All of the channels flagged from ground test data remained 'noisy' in orbit, but careful evaluation of the Level 2 residual data indicated that the increased noise was also accompanied by systematic offsets. These offsets tend to be poorly behaved in the time-series sense, and significantly larger than radiometric noise for the ensemble of radiances used in a retrieval. The channels which are currently marked as 'bad' at Level 1 (flagged with negative radiance precisions) are:

- Bands 3, 4 and 5, channel 22 (internally generated interference, observed before launch, but impact not decided)
- Bands 15 and 18, channel 21 (interference from a S/C transmitter, anticipated prior to launch)
- Band 27, channels 9 and 10 (internally generated interference)
- Band 32, channels 2 and 4 (instrumental problem, probably an unwanted oscillation or instability, not identified before launch)

In most cases the source of the systematic variations is interference from local oscillators within the instrument, or from the X-band transmitter on the spacecraft. These sources of interference were anticipated. The nature of the observed behavior of the data from the Wide Filters in the R1A 118 GHz radiometer implies that it is more likely that the source is either an oscillation, or near-oscillation, in the front-end receiver amplifier chain. Pre-launch expectations were that all of the channels currently flagged as 'bad' would merely exhibit elevated levels of noise, not ill-behaved systematics. This should be considered a lesson learned for future instrumentation of this type.

2.1 Sensitivity

The observed in-orbit T_{sys}, and corresponding noise on individual data integrations, are in general very similar to values observed during ground testing, and documented in Volume 1

of this report.

The pre-launch change out of the R4 1st. LO whisker-contacted tripler for a more reliable planar one resulted in a significant improvement, ∼20%, in T_{sys} for all channels of this radiometer. A representative set of in-orbit T_{sys} plots for all GHz bands is shown in Figures 2.1 and 2.2. An additional significant characteristic of this radiometer, not readily apparent in pre-launch test data, is that time-series noise for all channels *decreases* as input signal (radiance) *increases*. This is clearly evident in the in-orbit space view χ^2 data for this radiometer, which are substantially higher than pre-launch expectations, and shown in Figures 2.3 and 2.4. The T_{sys} and χ^2 data presented here should be compared to the pre-launch data presented in Volume 1. The unusual dependence of χ^2 on scene radiance becomes readily apparent when computing χ^2 for the internal target reference data. This was overlooked in the pre-launch instrument characterizations because sensitivity was invariably inferred from long-duration data sets taken with a stable ambient scene provided by a view to one of the two internal GHz calibration targets. Under such conditions the reference χ^2 are reasonably close to expectations. This measurement mode was chosen because it allowed long data sets to be taken without the need for maintaining LN_2-cooled targets.

Comparison of pre- and post-launch performance data for R4 indicate the likely presence of either an oscillation or gain peak (resonance) in the IF system at around 15 GHz. This is not unprecendented, since IF processors using similar amplifiers on other instruments at JPL have exhibited related oscillation-related problems that required rework by the vendor (Miteq). A low-level oscillation or high-Q gain peak that is affected by total signal power could readily explain the characteristics observed here. It is important to note that the elevated χ^2 only have impact upon the spectrally-averaged noise. Since the most challenging measurements in R4 (ClO and BrO) rely upon spectral contrast, Level 2 software was modified to estimate and remove a MIF-dependent spectrally-flat baseline for all R4 bands. The combined effect of MIF-dependent spectrally-flat baseline removal and reduction in T_{sys} arising from the tripler change out is a slight *improvement* in precision for the challenging ClO and BrO measurements, but a degradation in the precision of R4 measurements which rely on absolute radiances, such as those related to clouds.

It is interesting to note that the noise characteristics of the R3 Wide Filters are sufficiently improved in the orbital environment that the requirement for spectrally-varying noise in a single data integration are met. This was not the case for pre-launch data reported in Volume 1 of this report, and means that *all* measurement channels (except for those flagged as 'bad') meet spectrally-varying noise requirements.

Post-launch noise performance for the THz bands is in line with pre-launch expectations, with some minor improvement because of the more stable thermal environment and lack of local water vapor in the orbital environment.

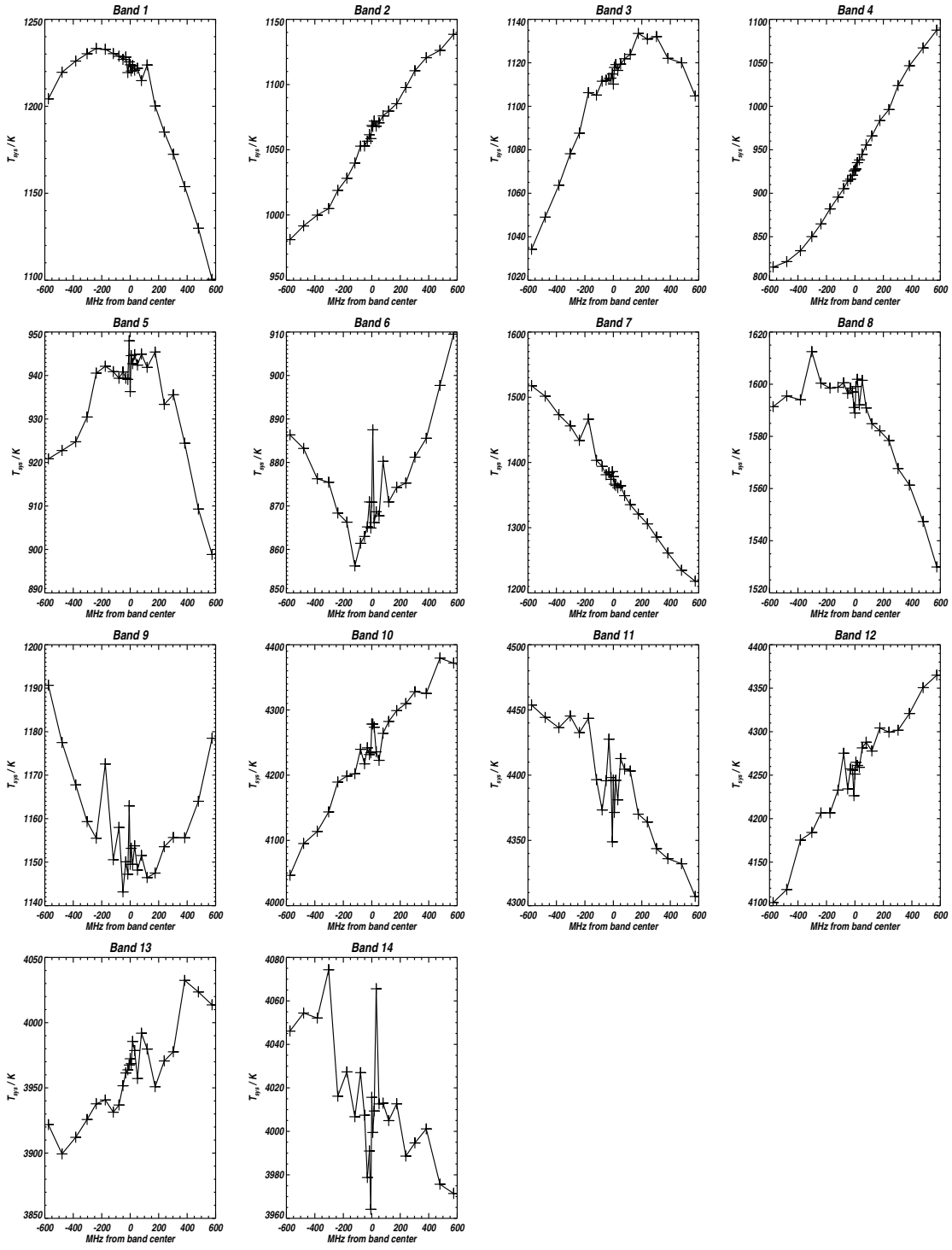

Figure 2.1: In-orbit T_{sys} for the GHz FB25 bands. These data are for a single MAF on 28 March 2005 (DOY087, MAF 10), and are representative of observed in-orbit performance since the start of routine instrument operation.

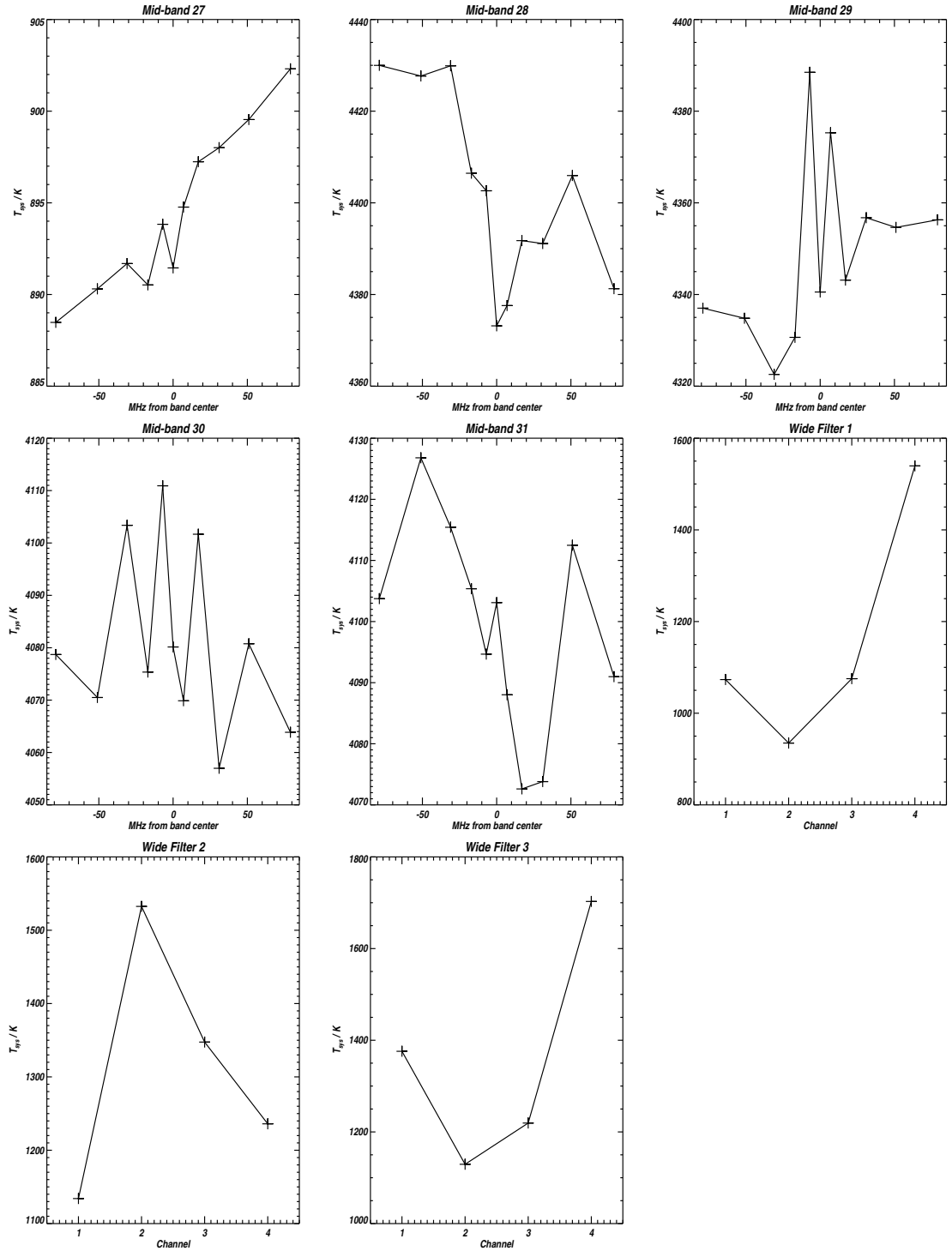

Figure 2.2: In-orbit T_{sys} for the GHz MB11 and Wide Filter bands. Wide Filters 1, 2 and 3 in this plot correspond to Bands 32, 34 and 33 respectively. These data are for a single MAF on 28 March 2005, and are representative of observed in-orbit performance since the start of routine instrument operation.

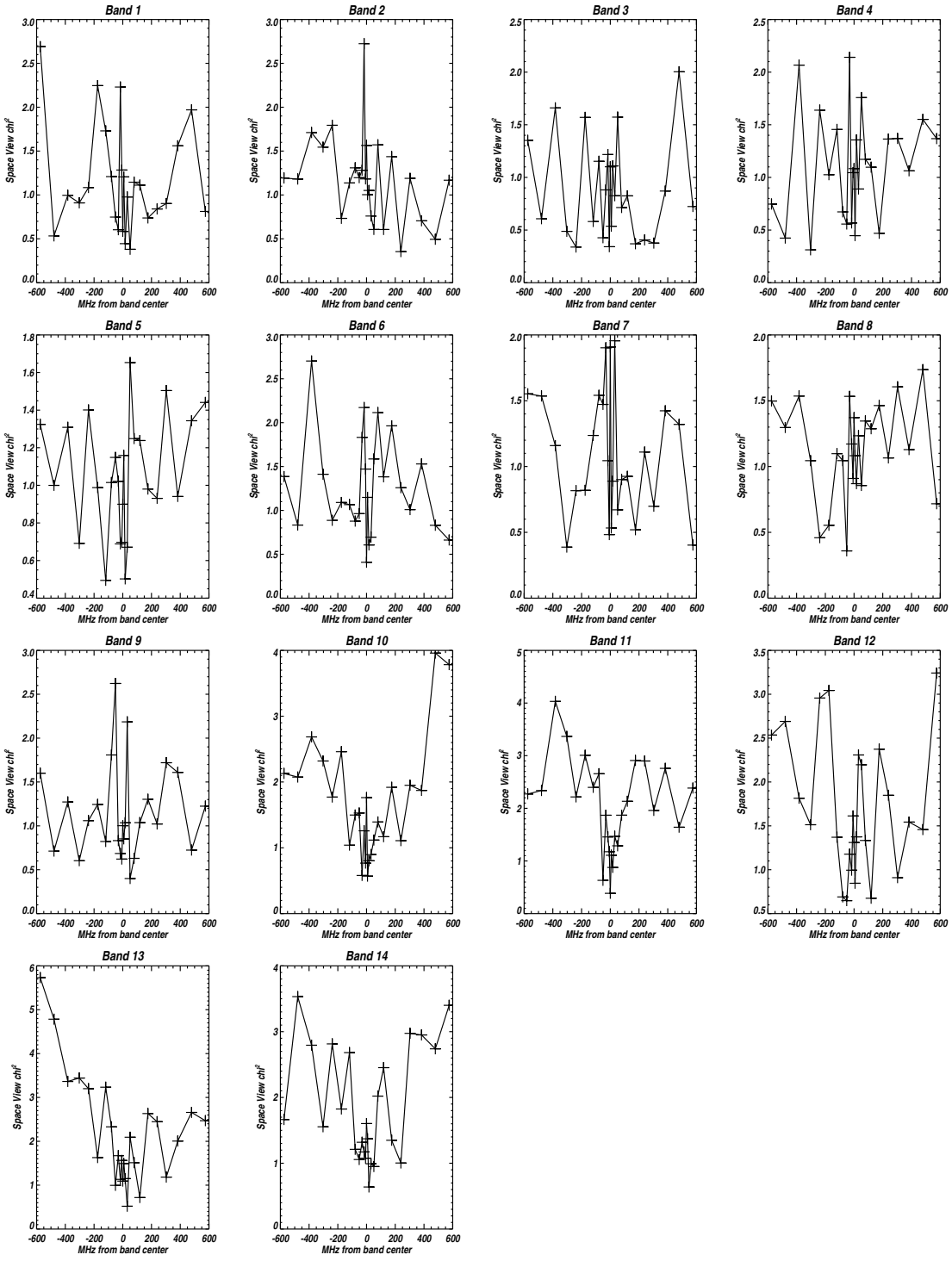

Figure 2.3: In-orbit Space View χ^2 for the GHz FB25 bands. These data are for a single MAF on 28 March 2005 (DOY087, MAF 10), and are representative of observed in-orbit performance since the start of routine instrument operation.

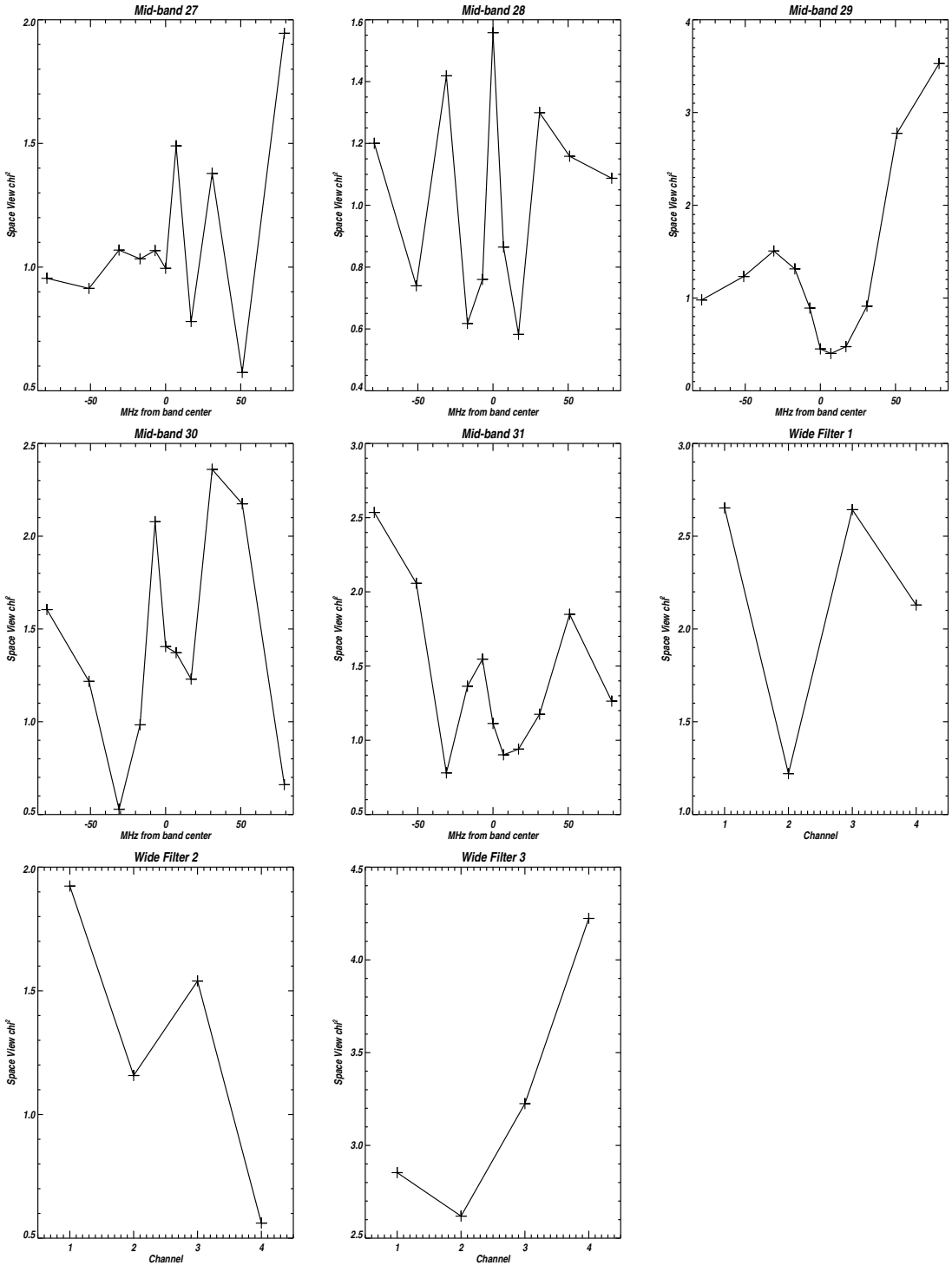

Figure 2.4: In-orbit Space View χ^2 for the GHz MB11 and Wide Filter bands. Wide Filters 1, 2 and 3 in this plot correspond to Bands 32, 34 and 33 respectively. These data are for a single MAF on 28 March 2005, and are representative of observed in-orbit performance since the start of routine instrument operation.

2.2 Noise Model

Pre-launch noise characterizations followed the model in the instrument Science Requirements document [1], namely determination of the spectrally-varying and spectrally-averaged noise components on individual calibrated limb data integrations. The noise, ΔT, on a single radiance measurement to a scene of brightness $\mathrm{T_{total}}$ is represented by the expression:

$$\Delta \mathrm{T} = \mathrm{T_{total}} \sqrt{\frac{1}{B\tau} + \left(\frac{\Delta G}{G}\right)^2} \tag{2.1}$$

where the $\frac{1}{B\tau}$ term represents the time-series (radiometer) noise on the, and term $\frac{\Delta G}{G}$ term represents the additional noise imparted by the measurement system in the form of gain variations. The radiometer noise components arise from the statistical nature of the observed photons in the measurement bandwidth covered by an individual channel, together with conversion loss in the front-end mixer. As a result, this source of noise is uncorrelated from channel to channel in a given radiometer. The gain variations on the other hand tend to be highly correlated between channels of a given radiometer, as one might expect.

Instrument performance requirements are stated in terms of radiometrically calibrated data. The radiometer noise contribution in Equation 2.1 is clearly in terms of uncalibrated data however, since no allowance is made for the precision of the radiometric reference measurements (cold space and internal target data). On the other hand, the gain variation component of Equation 2.1 contains implicit assumptions regarding both the calibration measurement timing and the Level 1 processing method used to convert raw limb data into calibrated radiances. A missing element in the simplified noise model of Equation 2.1 is that it does not cover measurement covariances at all. The total-power measurement scheme employed by EOS MLS introduces measurement-to-measurement covariances in a sequence of calibrated data points from a given channel due to the interpolation of a common set of reference data measurements. This topic is addressed quantitatively for EOS MLS in [4]. To summarize:

- ❏ Both the radiometer and gain variation noise components are 'smoothed' in time by the interpolation process, leading to correlated reference noise in sequences of measurements by a given channel.
- ❏ The gain variation component tends to be highly correlated between all channels of a given radiometer, imparting correlated reference noise between channels of a radiometer.
  - ⇨ In order to keep the noise on interpolated calibration measurements low, a 'calibration window' of several (6 – 10) MAFs is chosen, leading to the noise correlations having a 'length' exceeding 1 MAF.
- ❏ The net effect of these correlations is that the noise behavior of a measurement system of this kind ideally requires it to be expressed in the form of a variance-covariance matrix (or equivalent form) that captures all of the off-diagonal terms that are currently ignored in retrievals and sensitivity estimates.

The true noise behavior of calibrated radiance data is even more complex than just implied because the gain variation term inevitably exhibits $\frac{1}{f}$ noise. The main effect of this is increased covariances in the spectrally-averaged noise components. In order to illustrate the

importance of including gain variations in noise estimates, let us assume a spectrally-flat $\frac{\Delta G}{G}$ of 2×10^{-4}, or half of the amount allowed in the instrument performance requirements documentation. For a system temperature of 1,000 K, a typical value for many channels in this instrument, the noise on an individual, uncalibrated measurement is 0.2 K. This should be compared to noise requirements in [1], bearing in mind that correlated noise components do not integrate down in the same way as random (uncorrelated) ones. An additional issue is that the relatively long time between reference measurement groups (24.7 s nominally) means that post-detector $\frac{1}{f}$ noise must be considered. This source of low-frequency noise is *not* correlated between channels, and so particular care must be taken in the design of the post-detector electronics to keep its magnitude down to acceptable levels.

2.2.1 Noise Performance

The instrument requirements on noise specified in the Requirements document recognize the simplifications and assumptions of Equation 2.1 by specifying allowable ΔT with a suitable inflation factor to allow for the noise contibution from the reference measurements in the Level 1 radiometric calibration processing process/algorithms. The in-orbit noise characteristics and performance of the instrument are extremely close to those inferred from ground measurements with the exception of R4, discussed earlier. An analysis of the noise performance of EOS MLS GHz channels is given in [3], which includes information on the $\frac{1}{f}$ characteristics of the measurement system.

2.3 In-orbit IF Zeroes

IF zeroes[1] are only of peripheral concern because they have no impact on calibrated radiances, and minor impact upon estimated noise. Their long-term stability (drift) is of interest however because it provides an indication of the stability of the filter channel post-detector electronics, allowing us to determine spectrometer offset drift contributions to long-term drifts in channel outputs. Level 1 uses the 'most recent' values of IF zeroes when estimating noise. Until April of 2005, Level 1 used pre-launch values, at which point we stepped through all bands minimizing and restoring spectrometer input signal levels as a diagnostic to help understand further the source of decline of some raw signal levels. At this point Level 1 software automatically recognized and updated its record of these measurements, which are presented in Figures 2.5 to 2.6 below.

The zero levels of the filter channels are set by small offsets in the post-detector electronics together with a larger intentional offset generated by a resistive current path from the Spectrometer -5 V supply to each digitizer virtual ground input. The data are generally in keeping with expectations, with only a small number of channels having offsets that have changed by more than 100 counts since pre-launch testing. The offset changes in the Wide Filter channels are noticeably larger than those in the REMEC-built FB25 and MB11 spectrometers, which can be attributed to their somewhat more primitive manner of construction. Whereas the REMEC filterbanks comprised of collections of small surface-mount hybrid modules, the Wide Filters were built as large surface mount PCBs. A serious problem with the Wide Filters, detected and corrected prior to launch, was that some of the smaller resistors in the signal paths were subject to mechanical stress, evidenced by unstable signals

[1] IF zeroes are the channel DN with maximum attenuation of the spectrometer input signals.

and offset levels. Even though several of these resistors were changed for physically larger devices, we can probably attribute at least some of the observed offset changes to residual stress effects in the remaining components of these subassemblies.

2.3.1 IF Zero Interactions and Recovery Time

In addition to updating the IF Zero information used at Level 1, the data from the 5th and 6th of April 2005 measurements were used to look for signs of degradation in the filterbank voltage regulators. These regulators were added to the spectrometer shearplates to overcome the interactions between spectrometers arising from inadequate regulation in the primary spectrometer power supply, and interactions between the pair of spectrometers on a given shearplate arising from the drops in the common supply wiring from the central power distribution assembly. Prior to the addition of the local shearplate regulators, changing the signal level into a filterbank would impact the levels of the channel outputs of the spectrometer which shared the shearplate. In a similar manner, signal level changes in all spectrometers arising from routine limb scans would modulate the outputs of all other filterbanks. In both cases the interactions between filterbanks are such that they are not readily correctable by post-processing.

The performance of the regulators was verified before launch, but the declining signals observed in many bands after launch led to the speculation that the regulators (National Semiconductor LP2953) were 'failing' in some manner. Radiation testing of these parts indicated that not only were they quite susceptible to low-dose-rate radiation, but that two distinct degradation mechanisms had to be taken into account:

(1) The initial manifestation of radiation damage is a drift in the internal reference circuitry, seemingly always in the direction of decreased output voltage. This degradation is not accompanied by any other apparent loss of 'quality' in the output voltage.

(2) The final manifestation is a loss in output drive ability, resulting in a far more dramatic 'loss of regulation.'

The IF zero measurements were performed with timing that eased the task of looking for interactions between spectrometers such as would be caused by a 'softening' of the regulated outputs from the regulators. No such effect was observed in the data from these tests.

The data in Figure 2.8 show the raw count data from the 4 Wide Filters in R3 (Band 33) during the attenuation test. The upper panels show the data from the first two filter channels, the lower panels the data from the other two channels. The timing of this test was to set maximum attenuation for the first two filters, and to do the same for the second set with the subsequent command. Latencies in the command system show up as interactions in these data. Wide Filter 6 (B33W.C3) appears to have a plateau at about 12,000 counts, but this is merely a drop in signal level caused by the attenuation of Wide Filter 4 (B33W.C1). Similarly, Wide Filter 4 appears to overshoot when its gain is reset to nominal, but this is merely a manifestation of an interaction with the setting of Filter 6 which is reset to nominal shortly after Wide Filter 4. This behavior was expected from ground test data, and has no impact on data quality during nominal instrument operation.

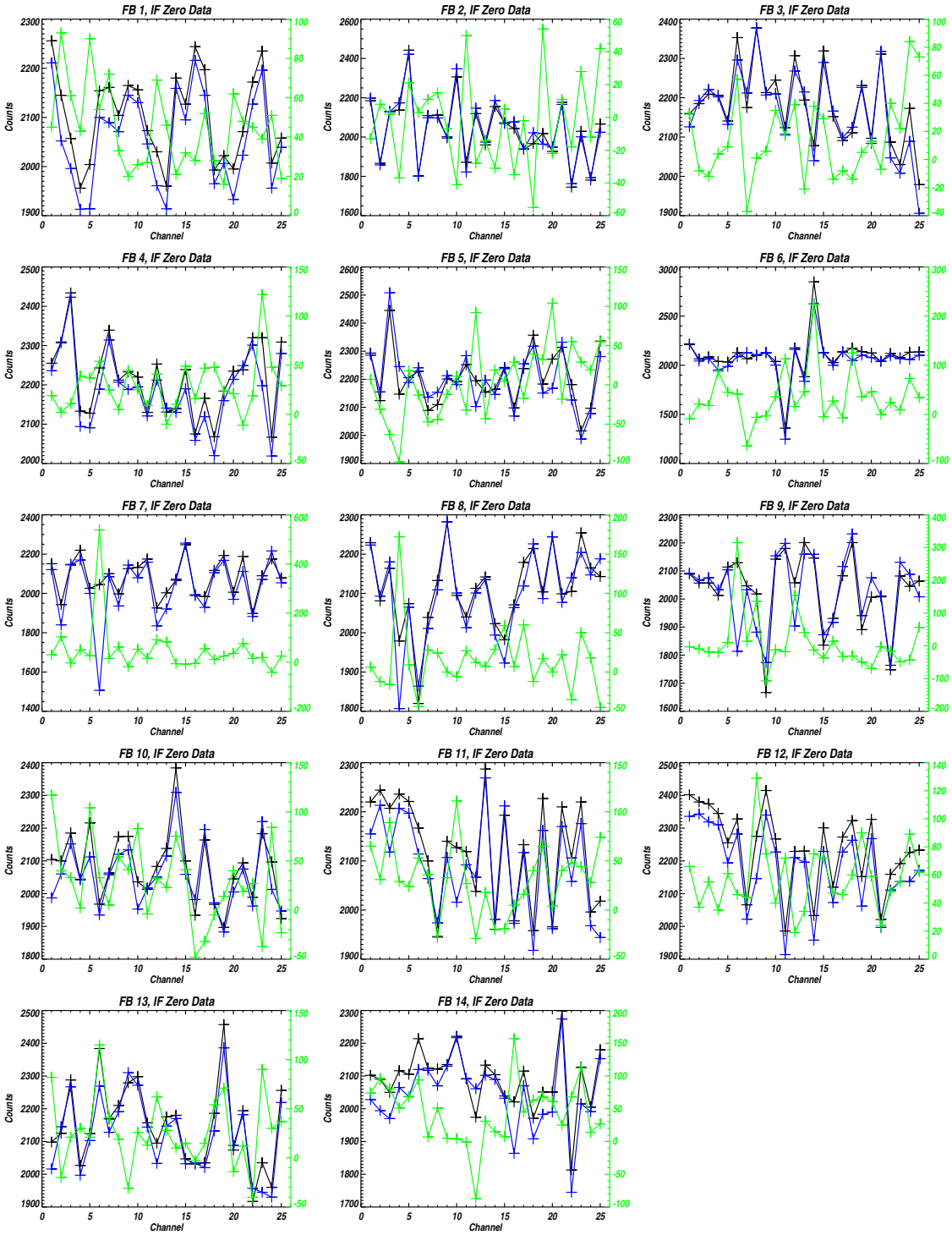

Figure 2.5: Pre- and post-launch (black and blue data) IF zero data for the GHz FB25 spectrometers. The post launch data were taken on 6 April 2005 (DOY096). The green plot is the difference between pre- and post-launch data.

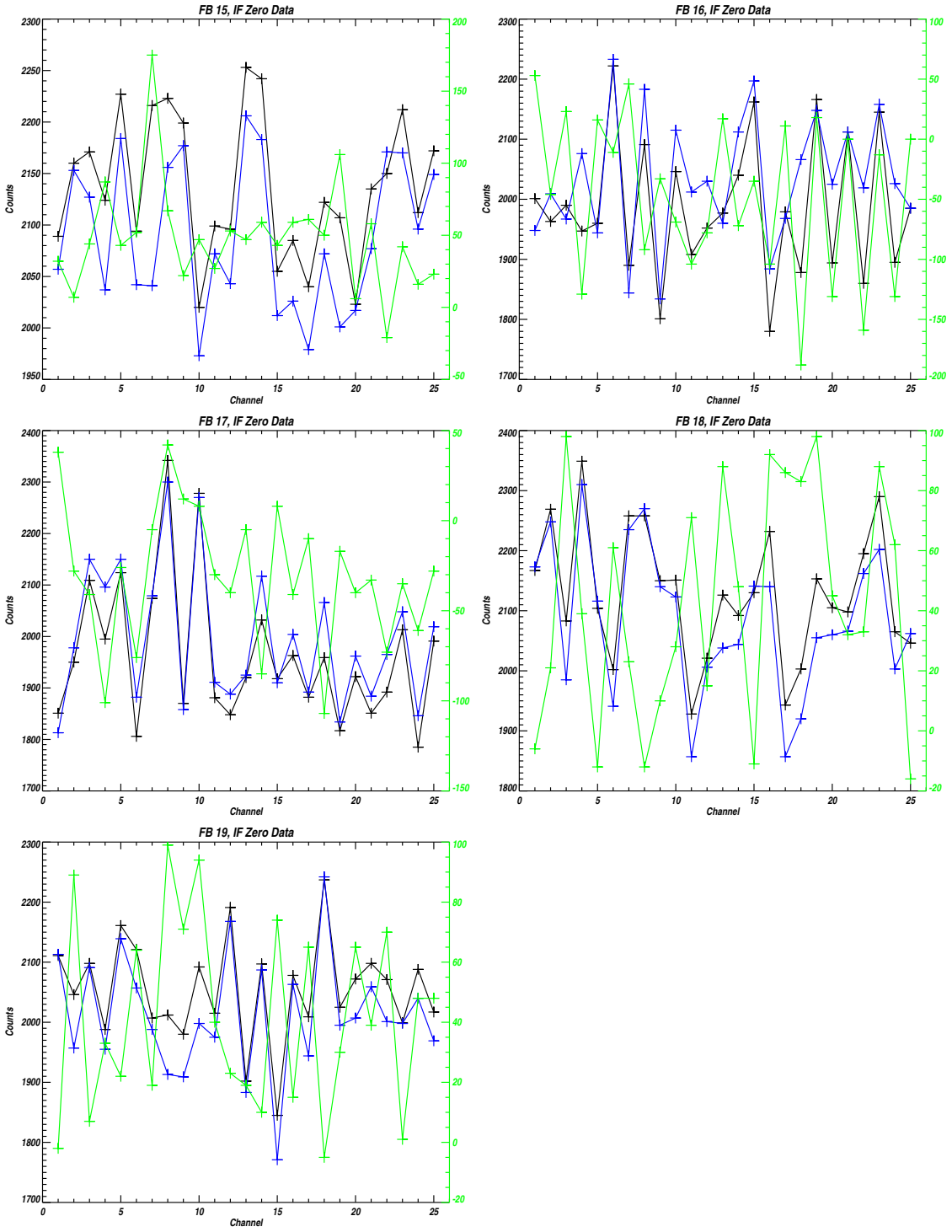

Figure 2.6: Pre- and post-launch (black and blue data) IF zero data for the THz FB25 spectrometers. The post launch data were taken on 6 April 2005 (DOY096). The green plot is the difference between pre- and post-launch data.

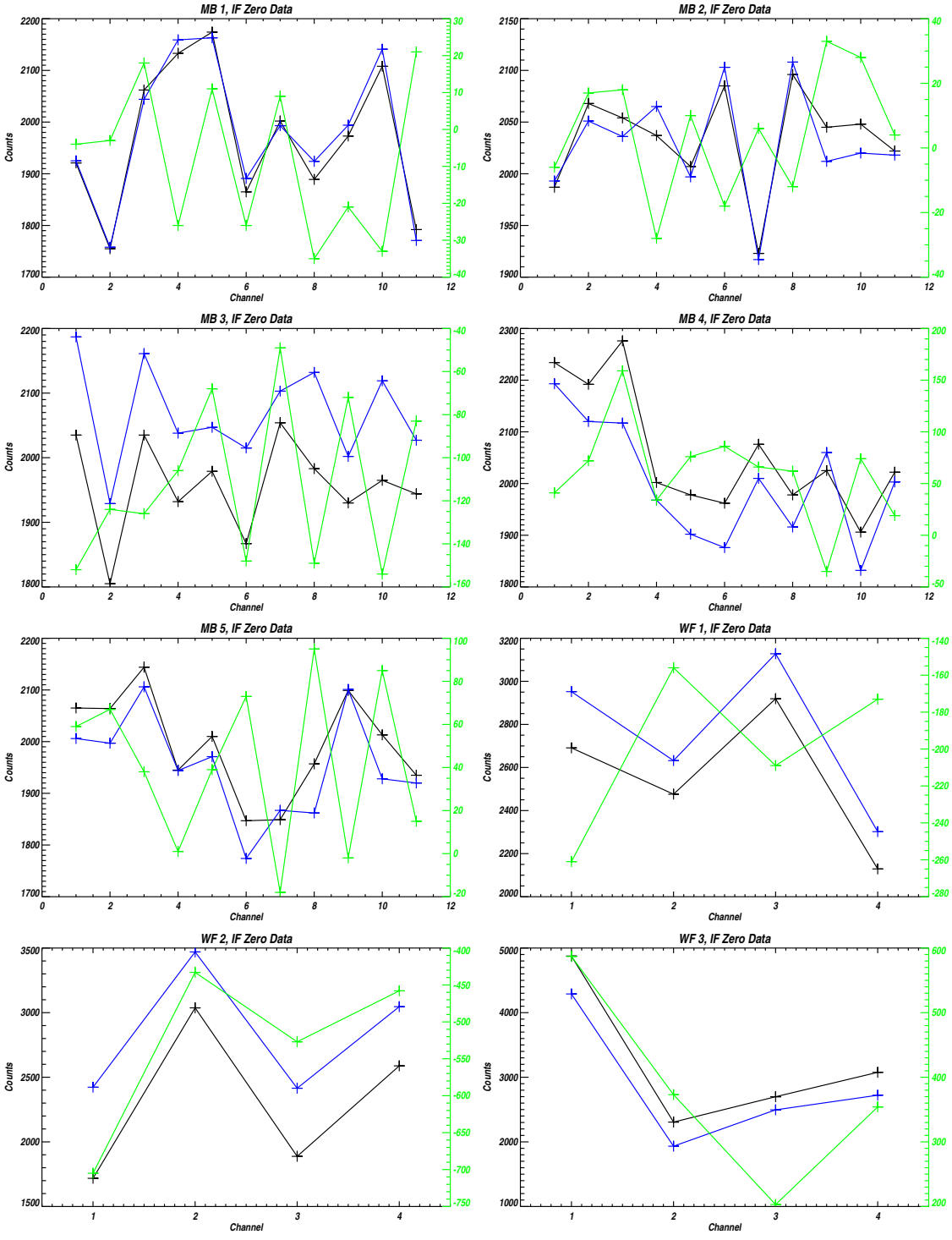

Figure 2.7: Pre- and post-launch (black and blue data) IF zero data for the GHz MB11 and Wide Filter spectrometers. MB 1 to MB 4 correspond to bands 27 to 31, and WF 1 to WF 3 correspond to bands 32, 34 and 33 respectively. The post launch data were taken on 6 April 2005 (DOY096). The green plot is the difference between pre- and post-launch data.

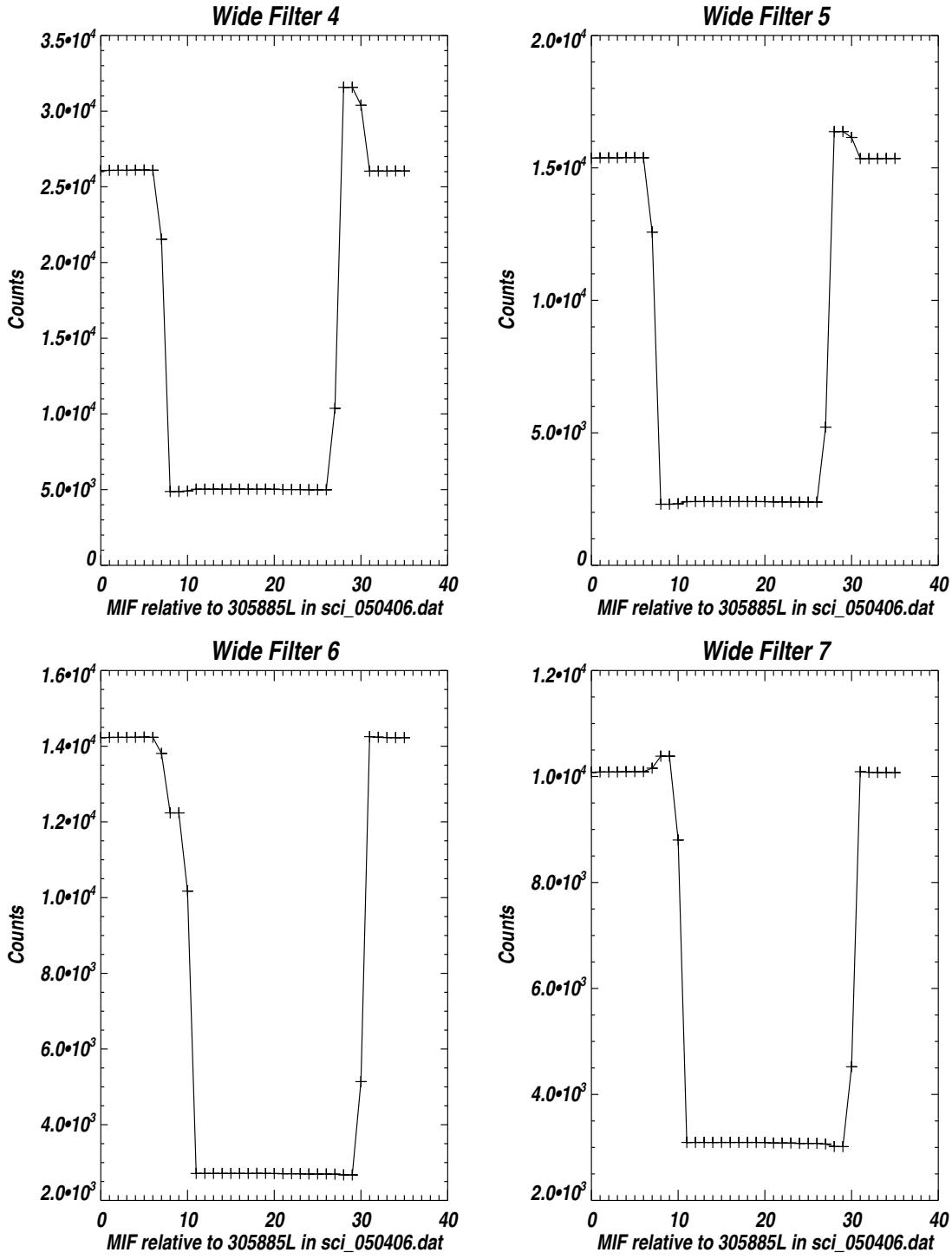

Figure 2.8: Data from the 6 April 2005 in-orbit test during which the IF attenuators for the Wide Filter in R3 were commanded for maximum attenuation, and then restored to their nominal settings. See text for a discussion of these data.

Note that when these channels were being manipulated for this test, the counts in all of the FB25 or R3 bands were affected, as expected, due to changes in the matches of the loads sampling the IF signal for this radiometer.

The corresponding data from the FB25 channels are also of interest, and the data for FB08 (R3, Band 8) for channels 1, 9, 17 and 25 are shown in Figure 2.9. This figure emphasizes the data as the channels settle to their maximum attenuation and nominal states. The panels are grouped in four groups of two, with the upper and lower panels of each group expanding the data in the vertical to emphasize settling effects. It can be seen that the channel outputs settle cleanly to their 'zero' values (lower panels of each pair), but have a noticeable settling of up to $\sim \frac{1}{2}$ s when the attenuators are reset to nominal. The average gain in Band 8 is $\sim$14 Counts K^{-1}. The recovery 'tails' in Figure 2.9 are of order 100 Counts, or 7 K, of sufficient magnitude to be a concern if similar behavior is present when switching between the Switching Mirror ports during routine operation. There are three potential reasons for the observed settling behavior:

- ❑ Filtering in the analog electronics of the digitally-controlled IF attenuators, as is potentially likely for reasons of noise immunity.
  - ⇨ This would not be an issue during routine instrument operation since we do not change the attenuator settings.
- ❑ The filter post-detector amplifiers are bandwidth-limited both by intent and by component performance, with a -3 dB response at $\sim$2 kHz.
  - ⇨ This time constant is far too short to explain the observations.
- ❑ The significant change in signal level brought about by the IF attenuator changes can be expected to change the temperature of the amplifiers in the affected portions of the signal paths to change the RF gain.
  - ⇨ This explanation is consistent with the observed clean settling to the IF zero level, and the slower settling when signal levels are restored.

We investigate this phenomenon more closely using data taken 5 April 2005 when the GHz switching mirror was moving with equal dwell time at each of the four ports. Figure 2.10 shows the count changes in channel 1 of Band 4 and channel 25 of Band 7 as the switching mirror view traverses from the Space port to the Controlled Target. This transition provides the largest signal change, and the chosen channels have good T_{sys} (800 K and 1,200 K dsb) and consequently high gains (19 and 18 Counts K^{-1}), easing the task of observing settling-related artifacts. The two data points in the transition between the low and high signal levels arise from the 3 MIFs that it takes for the Switching Mirror to traverse between the views. There is no evidence of any electronic settling time in these data, or in the data from any other channel. This leads us to conclude that the settling time issue discussed earlier is mostly likely an artifact of the IF attenuator electronics, and of no concern operationally.

2.4 Baseline

The significantly different optical paths to cold space via the switching mirror and GHz antenna result in spectral differences between the two data sets of order several $\frac{1}{10}$'s of a K.

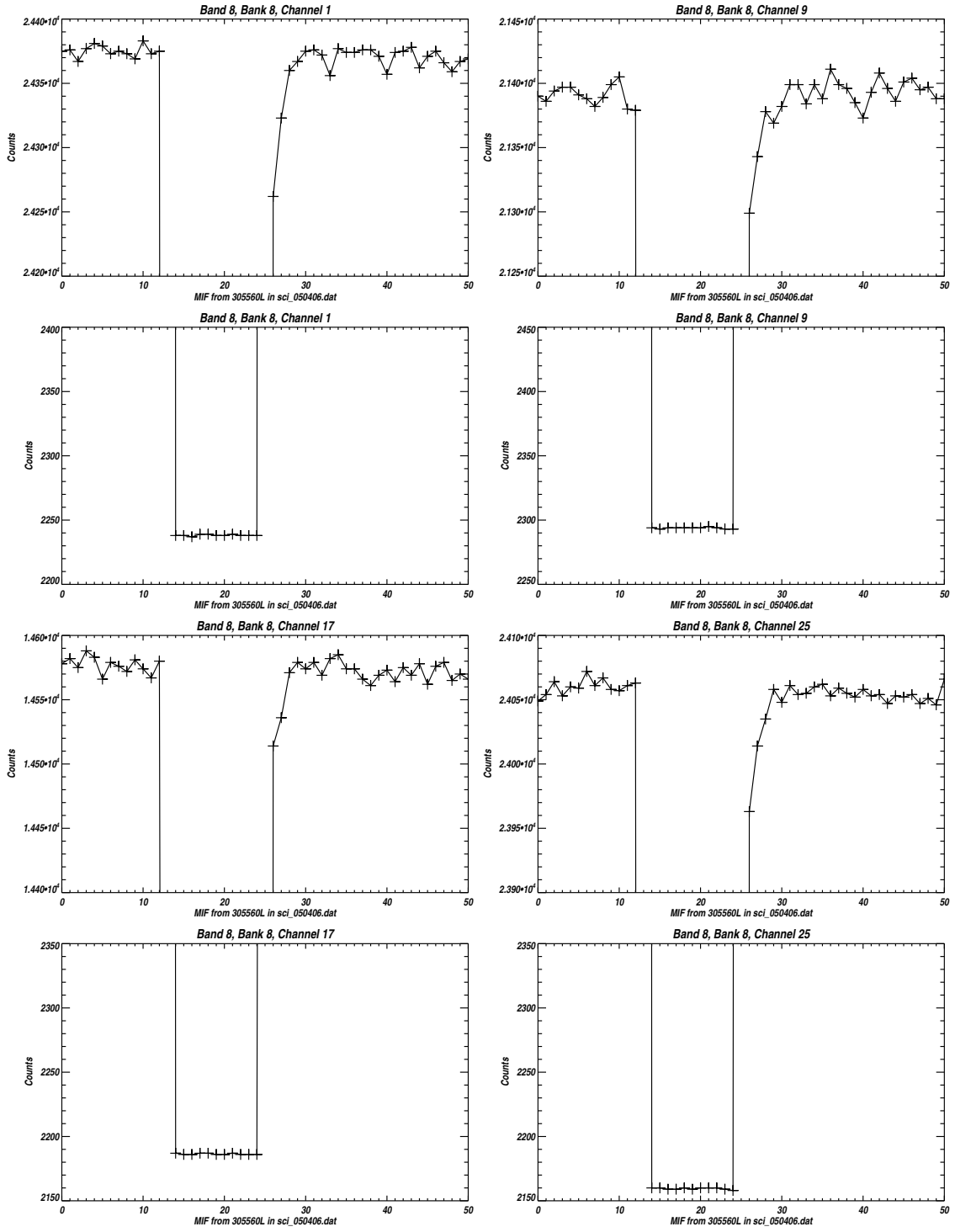

Figure 2.9: Data from the 6 April 2005 in-orbit test during which the IF attenuator for FB08 in R3 was commanded for maximum attenuation, and then restored to its nominal setting. See text for a discussion of these data.

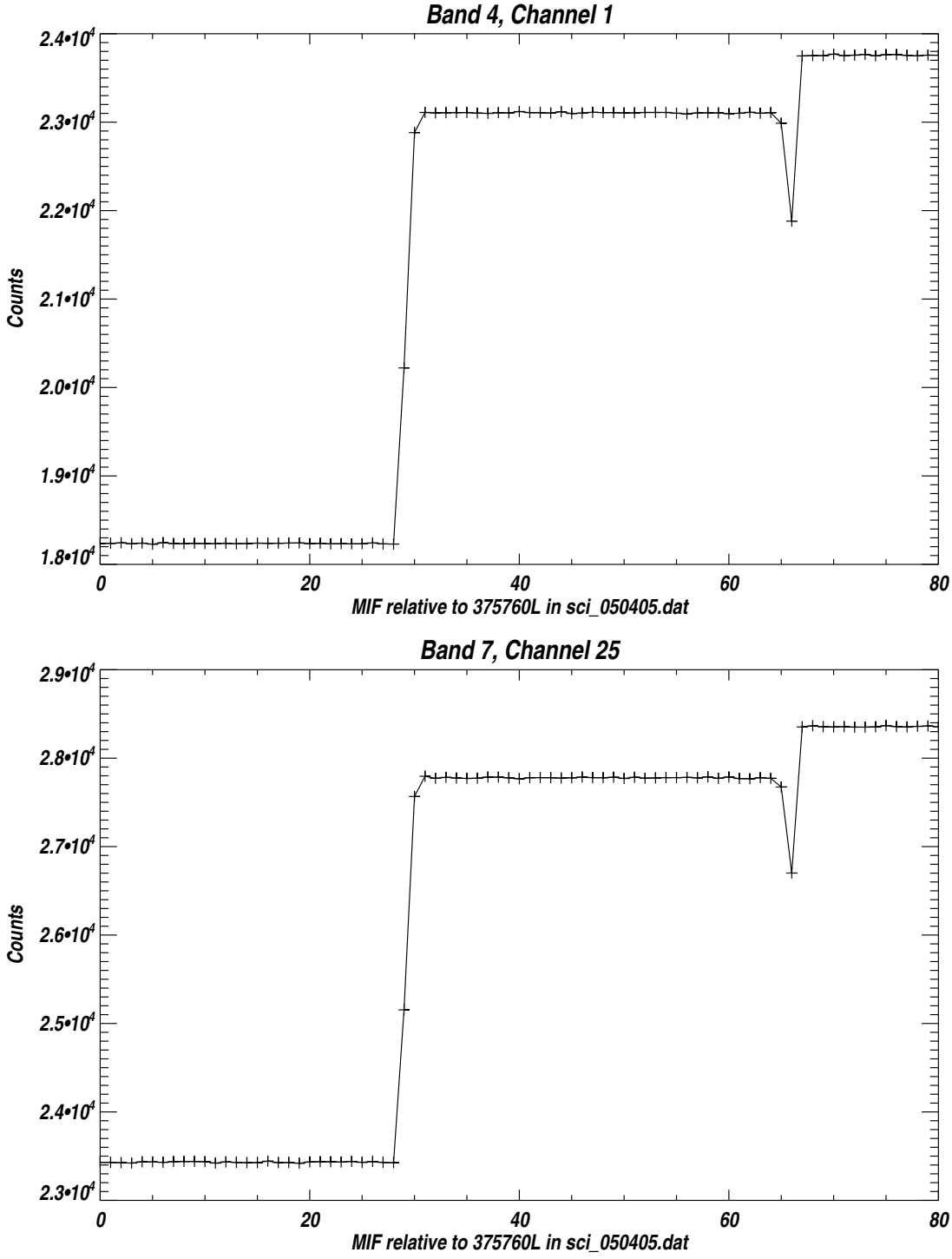

Figure 2.10: Data from the 5 April 2005 in-orbit test for channel 1 of Band 4 and channel 25 of Band 7, used to demonstrate the lack of any settling time constant in science data during routine operation. See text for a discussion of these data.

In addition to this spectral signature there is a significantly larger offset component between these two views to space, up to ∼10 K for R3 and R4, with orbital variation of about 2 K. Level 1 processing includes a simple model to 'take out' both the offset and its variation, but the differences between model and observed radiances are significant. Modeling of this offset is discussed further in the FOV chapter of this document. There are no corresponding baseline effects for the THz module because of its common switching/scanning mirror.

The calibrated limb port radiances in the Level 1 radiance file are not corrected for any of the baseline effects described above. For each MAF of radiance data we include separate estimates of the spectral and non-spectral baseline, together with an estimate of the uncertainty in the non-spectral component. Baseline-corrected limb radiances are easily determined by adding the two baseline corrections to each limb port radiance. The reason for generating uncorrected radiances together with the baseline corrections is to provide visibility into the quality of the calibrated limb port radiances to both users of Level 1 data, and to those providing higher levels of data processing. It also allows Level 2 processing to use its own 'experimental' forms of baseline correction without competition from Level 1 processing. We now discuss these two baseline components further.

2.4.1 Non-spectral Baseline

Baseline performance can be considered a radiometric or spectral topic since it has impacts in both areas. In this report we treat the AC component spectral baseline as a spectral performance issue (in the following chapter), and the offset component as a radiometric issue.

The non-spectral baseline component has substantial orbital variation, requiring it to be determined dynamically. The reported non-spectral baseline for each measurement band is the weighted mean of the limb-space port radiance difference for those limb views with sufficient tangent height. The weighting is by nominal channel bandwidth. To provide some additional allowance for the orbital variation of this offset, the reported value is the average of the computed baseline for the current and previous MAF. The uncertainty in this data is estimated as the rms of the variation of the observed offset in each channel in a 6 MAF window encompassing the targetted MAF. An example of the baseline offset between limb and space ports for several orbits is shown in Figure 2.11. These data are for a single channel from each of the GHz radiometers (except R1B), and were generated using the trapezoidal high-scan data of DOY210 (2004) taken during instrument activation. The vertical axes of all plots are the same to help with visual comparison of the differences in offsets between radiometers. This topic is discussed further in the FOV chapter of this volume.

The GHz antenna routinely scans to only ∼90 km tangent altitude, insufficient to provide limb views with insignificant atmospheric radiance contribution in all channels. Table 2.1 indicates which channels are *not* included in the non-spectral baseline determination. Only radiances above 80 km tangent height in each MAF are used.

2.5 Band 5 internal interference

Channel 22 of Band 5 is declared 'bad' at Level 1 due to low-level instability in its raw time series data. A behavior related to this problem is made clear from the data presented in Figure 2.12. This figure plots the raw count data from Channels 21 to 23 of Band 5 as the

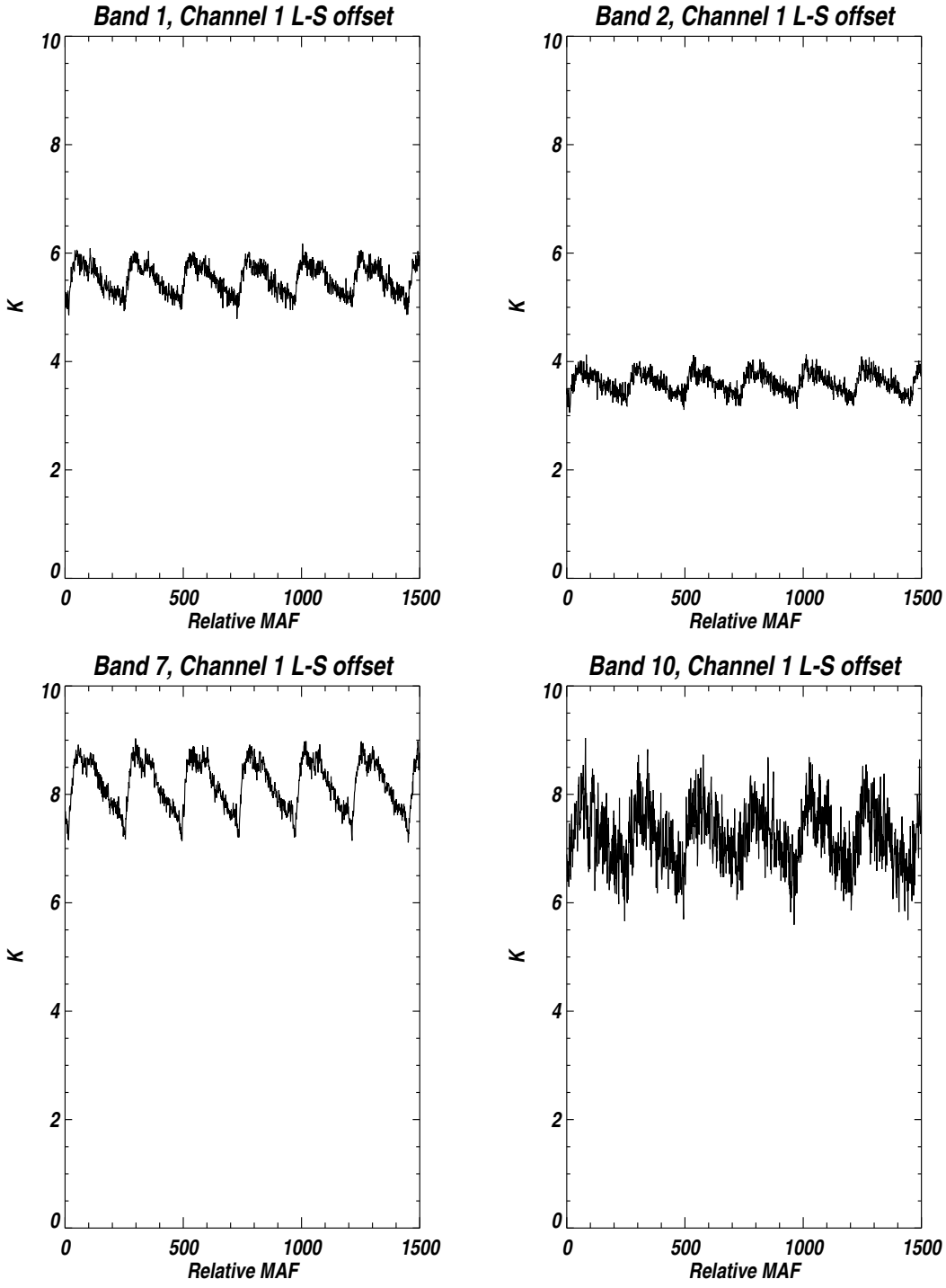

Figure 2.11: Limb - Space port differences for Channel 1 of Bands 1, 2, 7 and 10 for several orbits. The tangent heights of the limb views were sufficient to provide negligible atmospheric spectral contribution. These data were taken on DOY210 (2004), and processed with a modified version of Level 1 software which did not provide baseline corrections.

Table 2.1: Channels excluded from the baseline offset (non-spectral baseline) determination at Level 1. Note that excluded channels are included for the THz bands even though no baseline processing is currently performed for any of these bands.

Band	Channel(s)	Band	Channel(s)
1	8:18	18	11:17
2	12:14	19	11:17
3	2	20	12:14
4	none	21	8:18
5	none	22	25:84
6	none	23	36:69
7	13	24	33:74
8	12:14	25	32:71
9	13	26	25:84
10	none	27	none
11	none	28	6
12	none	29	none
13	11:15	30	6
14	13	31	none
15	11:17	32	none
16	11:17	33	none
17	12:14	34	none

Switching Mirror (GSM) slowly rotates. The signals from Channels 21 and 23 of Band 5 are seen to change as expected. Channel 22 exhibits noisy data for views to either side of the GSM space and limb ports with apparently elevated brightness temperatures, on the order of ∼600 K. This behavior suggests that views slightly to either side of the space and limb ports are subject to significant reflections, and that the R2 mixer is probably emitting a signal within the passband of the afflicted channel (sideband unknown). It is also noteworthy that Channel 22 of Bands 3 and 4 are also declared 'bad' because of instability, implying a possibly related cause.

2.6 Band 13

In the November 2005 timeframe a noticeable increase in the rate of decline of the raw counts in Band 13 was observed, and is shown in Figure 2.13 for channel 4 when viewing the controlled radiometric calibration target. The lower panel of this figure shows the relatively dramatic increase in daily average decline, from ∼20 counts per day which is the level observed in many other bands (and thought to be due to radiation effects in the low dropout regulators on each spectrometer shearplate) to ∼200 counts per day after a period of only $1\frac{1}{2}$ months. With this behavior it was clear that only a few weeks of usable life remained, and the Band was turned off. The surmised reason for the failure is that a transistor in the Band 13 signal path was suffering from 'wear out' due to a manufacturing defect[2], and this hypothesis was

[2]The possibility of such a failure was known before instrument launch, but too late to be able to take any corrective action.

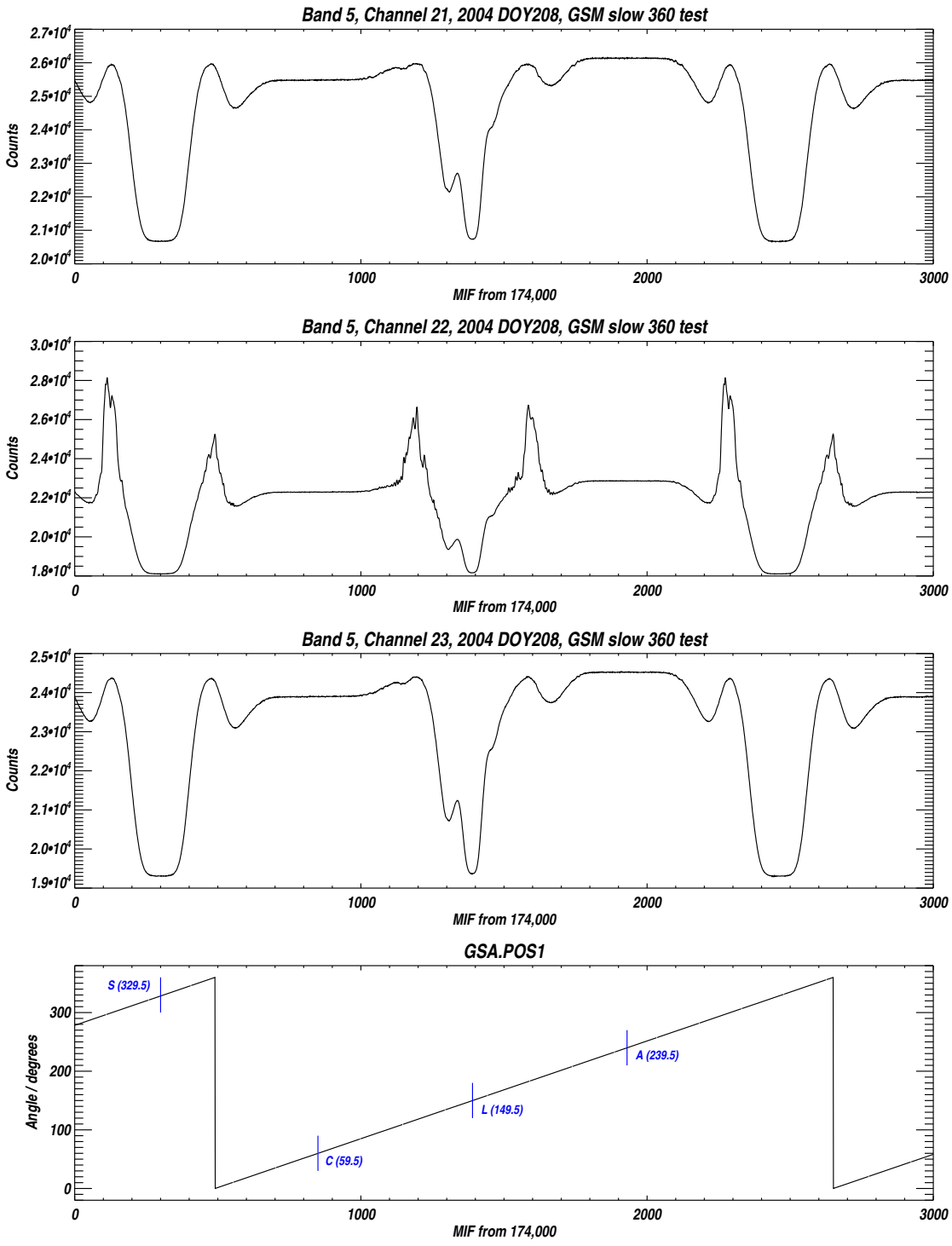

Figure 2.12: Raw counts from Channels 21, 22 and 23 of Band 5. The GHz Switching Mirror was rotating at $\sim 1^\circ\,\mathrm{s}^{-1}$, and the time period shown here encompasses just over one complete mirror rotation. The lower panel indicate mirror angle, and the 4 prime dwell locations used operationally are indicated by the blue lines.

tested by turning the Band off for a week, and then back on again for a day. From this data it was clear that the count decline was directly related to signal chain operating hours, not a radiation related issue.

2.7 Count Decline Monitoring

The general count decline in all filter spectrometer channels is monitored in near real time as data packets are received at JPL. Automated tools are in place which issue warnings (via e-mail and text messages) if suspicious behavior is detected. The long-term trend plots maintained by the Instrument Flight Operations team allow the count declines, and changes in many other useful raw and derived quatities, to be evaluated conveniently.

2.8 Gain Compression

Pre-launch linearity measurements (see Volume 1 of this report) appeared to indicate excellent linearity performance, in accordance with performance requirements. Additional thinking after launch revealed a major flaw in the pre-launch thinking however, arising from the fact that the pre-launch linearity measurements were performed viewing spectrally-flat scenes. Consider the following: instrument requirements were such that a gain compression of $\sim$0.5% was possible in some bands as the scene ranged from cold space to ambient target. A strong but narrow atmospheric spectral feature can thus appear to change in amplitude by up to $\sim$0.5% as the average scene seen in the rest of the IF for that receiver traverses from cold space to target radiance. In addition, the gain compression applies to the sum of scene and system temperature, so what initially may be thought of as $\sim$1 K error source can easily become a 5 K error. In addition, the nature of this problem is that is introduces spectral distortion.

A full description of this problem is given in [5], and some of the plots from that publication a reproduced below (one band from each GHz radiometer). The format of each plot is the same: the top panel shows an idealized set of radiances for the band, the center panel shows the corresponding radiances for an instrument with gain compression levels corresponding to what we expect is happening in EOS MLS, and the bottom panel shows the difference between idealised and measured spectra, clearly showing the significant spectral nature of the problem in addition to the offset component.

2.9 Band 6 Attenuator Margins

Bands 6 and 27 share a common attenuator. Band 6 counts decline in a manner similar to the other FB25 bands, but Band 27 counts have remained relatively stable. This leads to the question of how much we can increase the signal levels in Band 6 before the signal paths in Band 27 exhibit nonlinearity due to the VFCs beginning to saturate. On 12 February 2013 a stepped attenuator test was run during which the common attenuator was adjusted to provide several MAFs of data with 0.5 dB, 1 dB and 1.5 dB increases in signal levels. The signals during this test period are shown in Figures 2.18 and 2.19 below. The gain change in each spectrometer channel is not the same for a given pair of attenuator settings (due to mismatch and impedance changes), requiring a more subtle data analysis strategy.

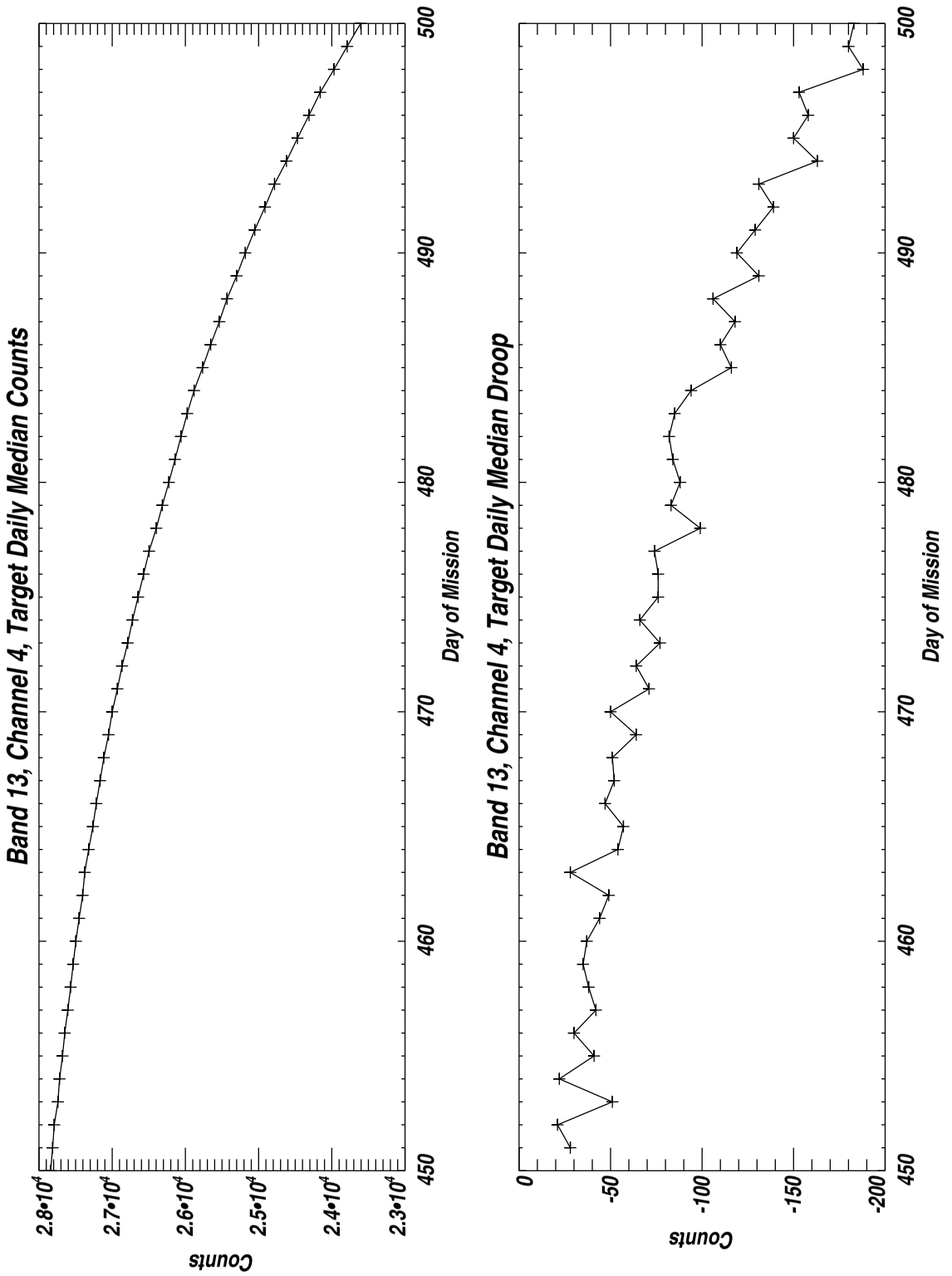

Figure 2.13: Daily mean target view raw counts (upper panel) from Channel 4 of Band 13. The lower panel shows the daily average count decline. Day of mission 450 corresponds to 8 October 2005.

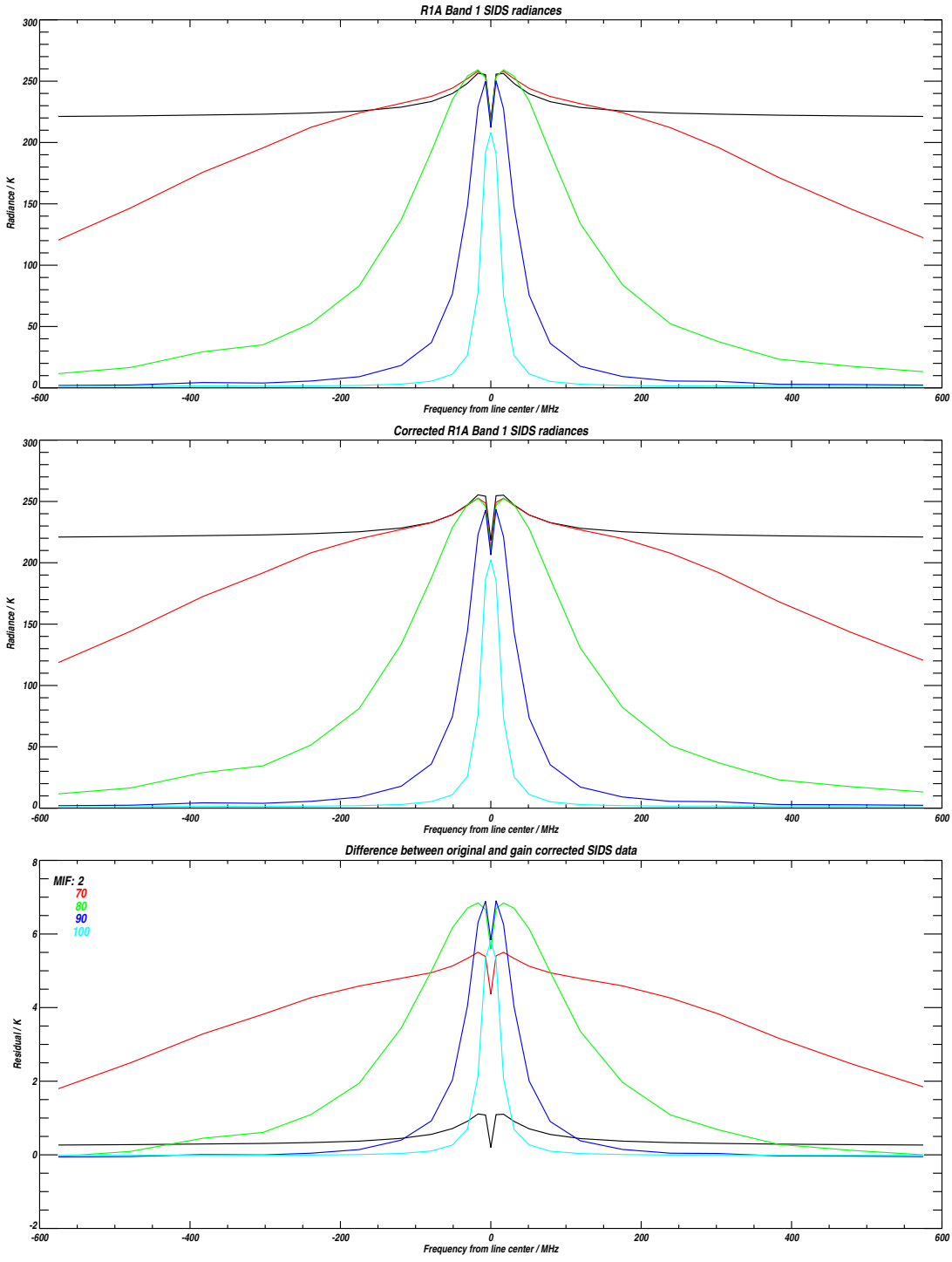

Figure 2.14: SIDS radiances for Band 1 (top panel). The same data, after correction for gain compression is shown in the middle panel, with the differences between the data (residuals) in the bottom panel. The same MIF's are plotted in each panel, and indicated in the bottom panel.

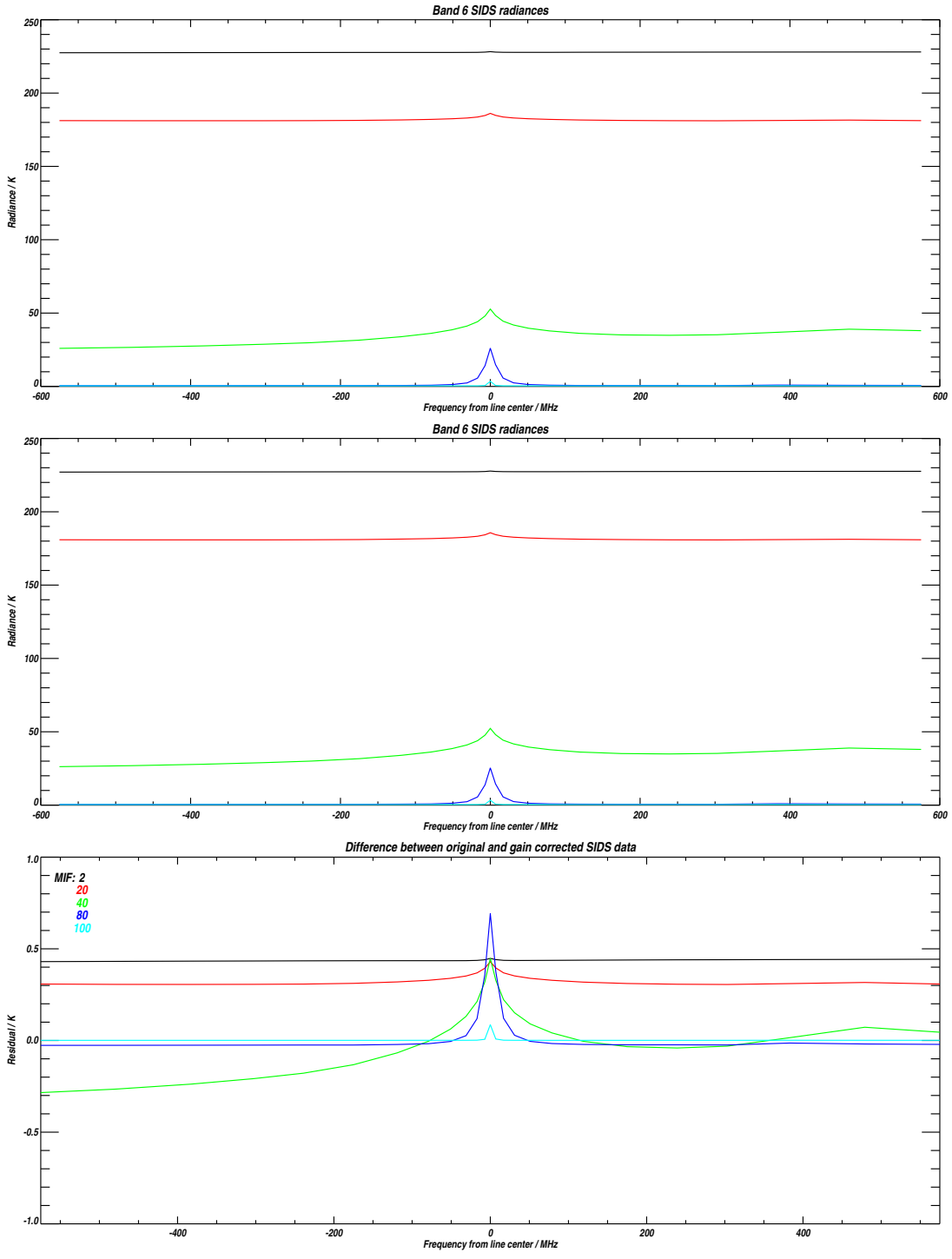

Figure 2.15: SIDS radiances for Band 6 (top panel). The same data, after correction for gain compression is shown in the middle panel, with the differences between the data (residuals) in the bottom panel. The same MIF's are plotted in each panel, and indicated in the bottom panel.

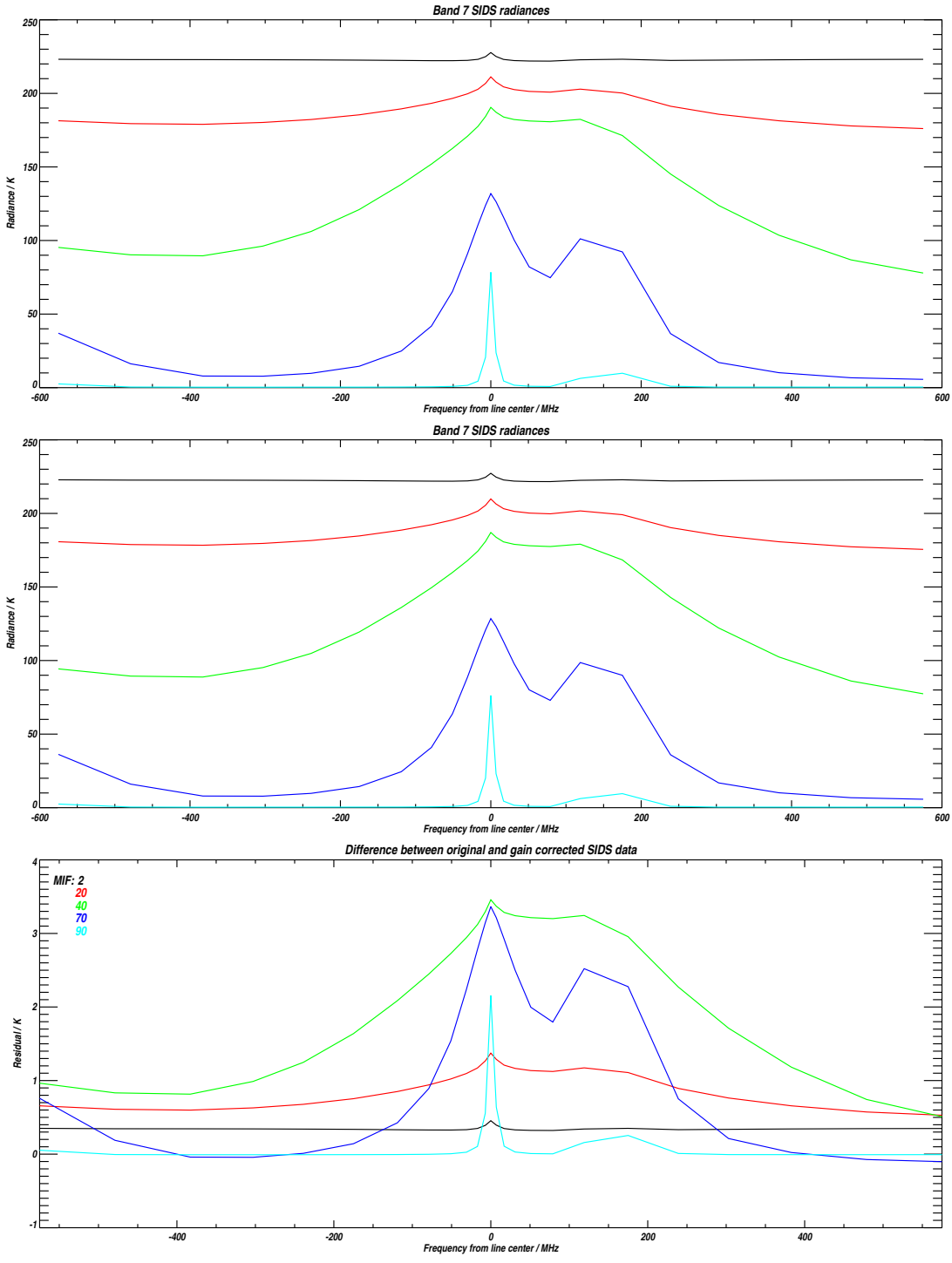

Figure 2.16: SIDS radiances for Band 7 (top panel). The same data, after correction for gain compression is shown in the middle panel, with the differences between the data (residuals) in the bottom panel. The same MIF's are plotted in each panel, and indicated in the bottom panel.

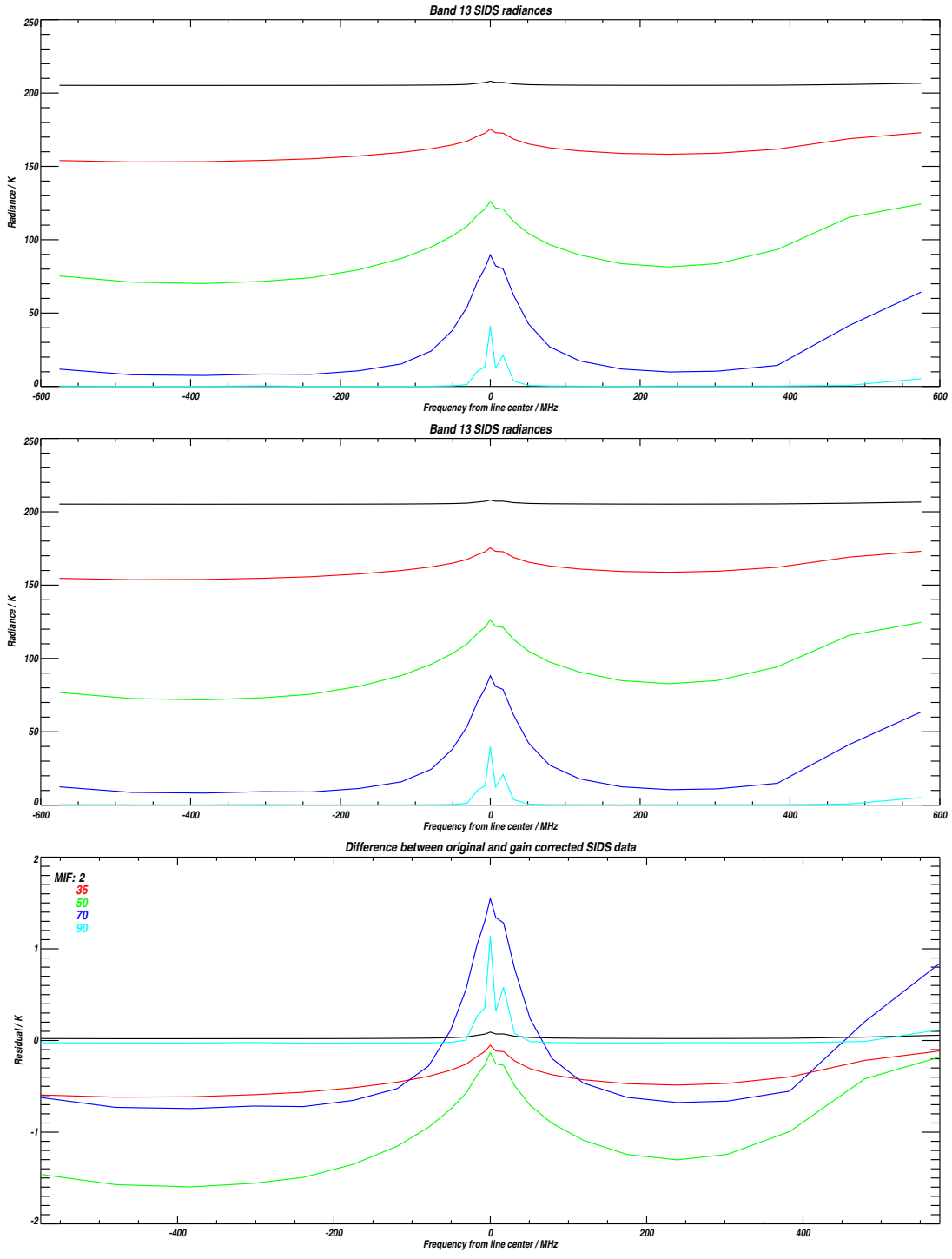

Figure 2.17: SIDS radiances for Band 13 (top panel). The same data, after correction for gain compression is shown in the middle panel, with the differences between the data (residuals) in the bottom panel. The same MIF's are plotted in each panel, and indicated in the bottom panel.

From the data at two different attenuator settings we can infer the system temperature of the receiver and the 'zero' counts of the spectrometer. In Figure 2.20 we show the inferred system temperature for the 3 non-standard attenuator settings, using the default setting as the other data set. The black and red curves are for 0.5 dB and 1 dB attenuation decreases, and show no adverse effects. The green curve (1.5 dB signal level increase) shows that channels 9 and 10 of Band 27 suffer from VFC nonlinearity however. The available margin of 1 dB in attenuator adjustment is sufficient for many more years of unimpaired B6/B27 operation at the current rates of signal level decline.

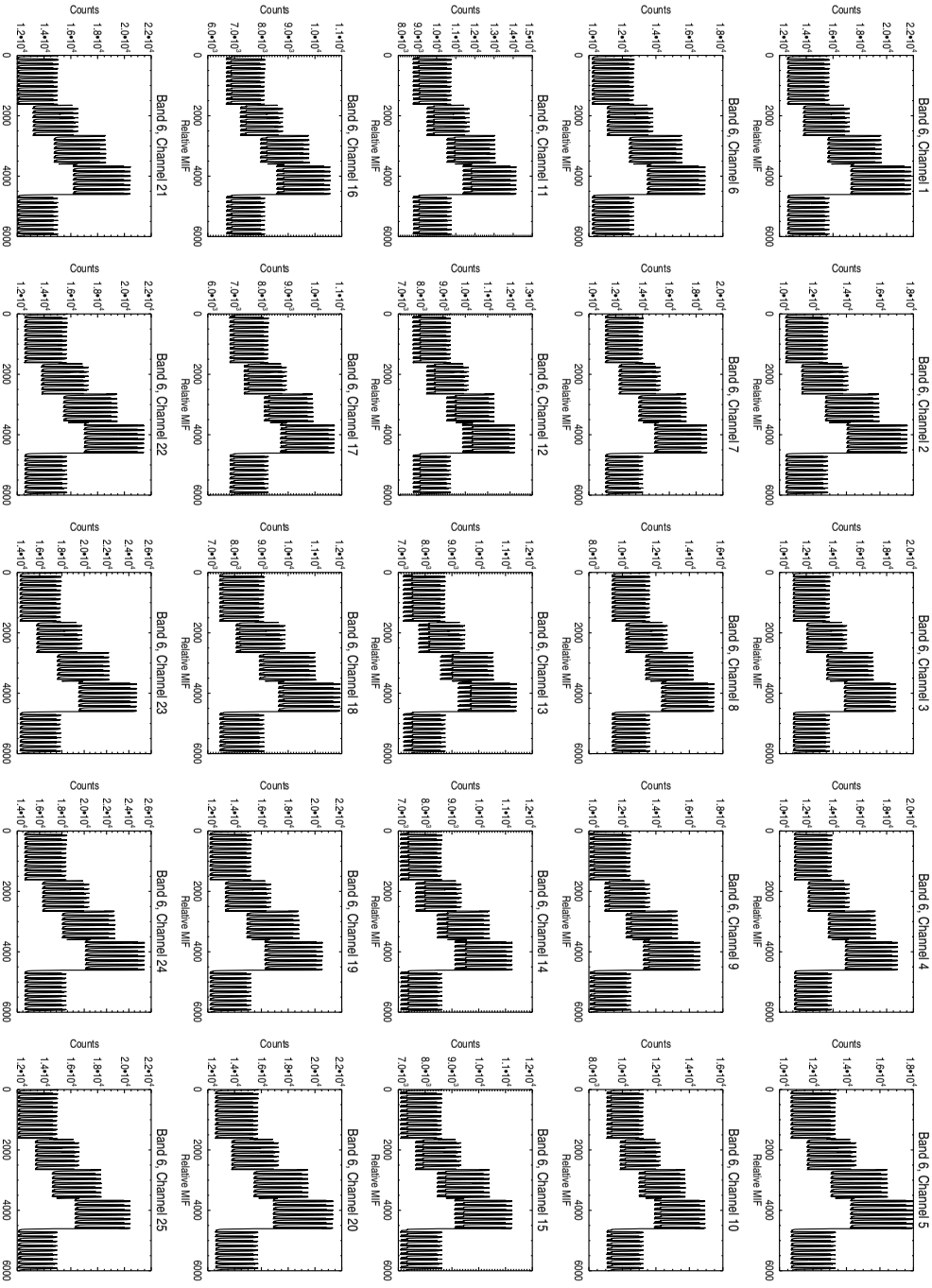

Figure 2.18: Raw counts for Band 6 channels during the 12 February 2013 attenuator step test.

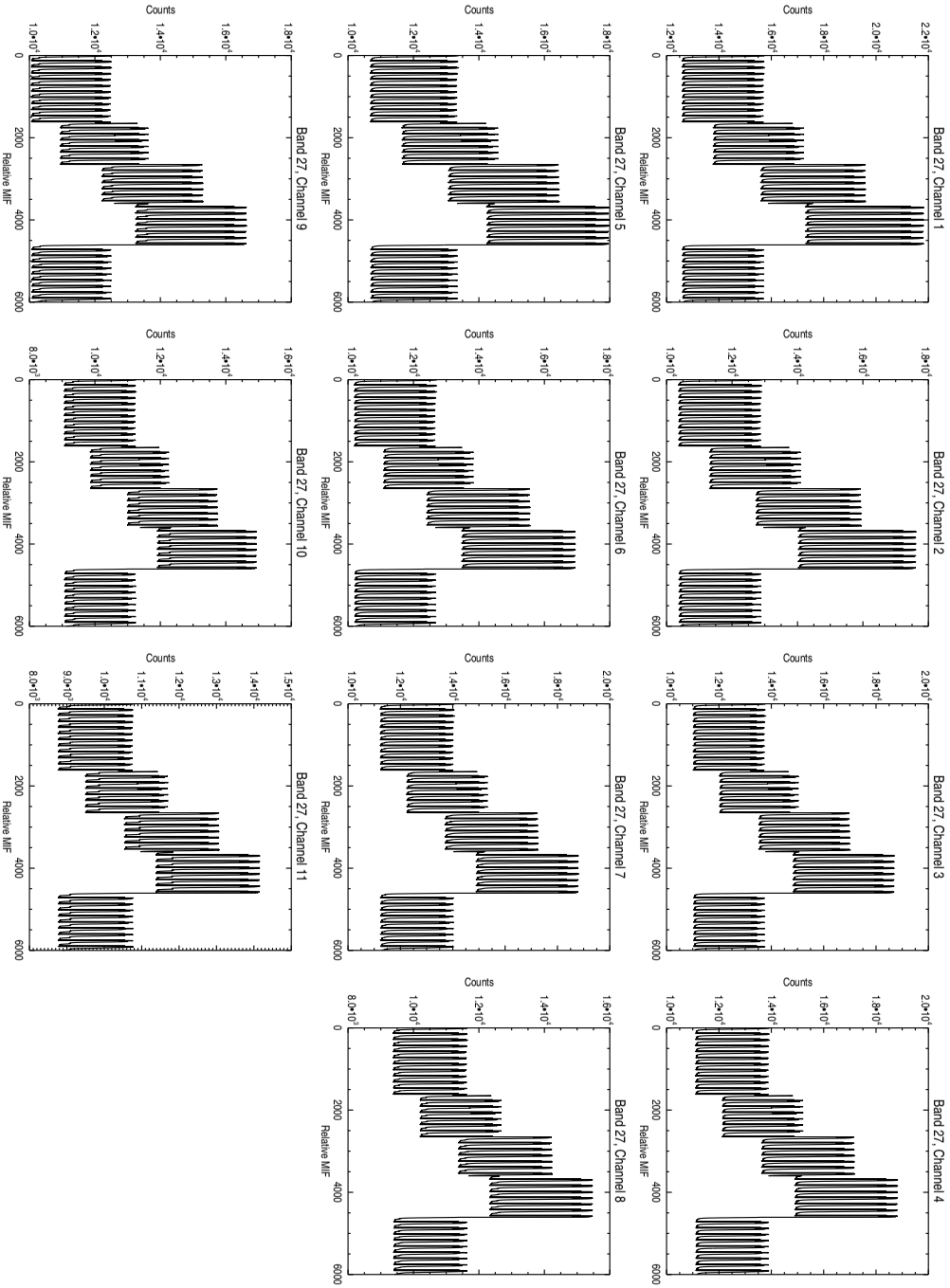

Figure 2.19: Raw counts for Band 27 channels during the 12 February 2013 attenuator step test.

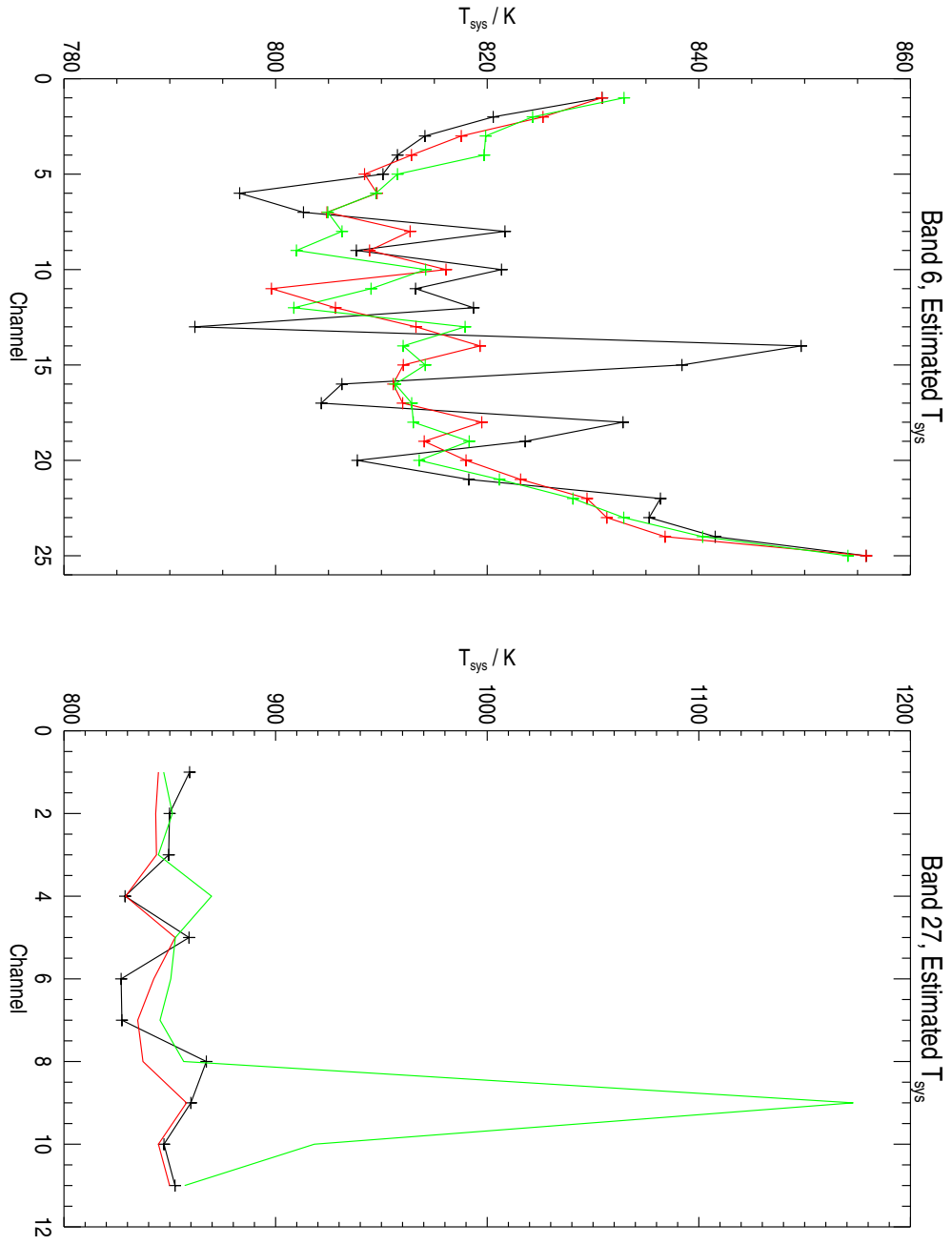

Figure 2.20: Inferred system temperature for Bands 6 and 27 channels during the 12 February 2013 attenuator step test.

Chapter 3

Spectral Performance and Calibration

Level 2 radiance residuals provide visibility into instances of channel position errors such as could arise from launch shifts or unexpected drifts. No such errors have been noted. The MLS instrument has a built-in sweeper (synthesizer) capable of performing a simultaneous sweep of all of the 11- and 25-channel filterbanks, and can in principle be used to measure drift in filter channel placement. The in-orbit demise of Band 13 led to the realization that operation of the sweeper would cause unwanted thermal cycling of some R4 IF signal chain components suspected of being partially responsible for the decline in raw counts observed throughout the mission in Bands 10 and 29. We have thus chosen, for the time being at least, not to consider using the sweeper in orbit.

Prior to instrument launch the R4 1st LO whisker-contacted tripler was replaced with a more reliable planar one. This operation was performed after instrument delivery, and eliminated any opportunity to perform relative sideband response measurements at the system level. The tripler changout was known to lead to small changes in receiver noise and relative sideband response, and so a limited set of sideband measurements were performed at the receiver subsystem level. These measurements consisted of taking measurements of relative sideband response at 3 points in the 1st IF using a planar Fabry-Pérot (FP) in a simple setup that merely swept the grid spacings while alternating between a direct view to an ambient target and a view to an LN_2 target through the FP.

By performing these measurements before and after the tripler changout, the intent was to apply the *changes* in observed sideband response to the sideband calibration data taken with the more elaborate setup described in Volume 1 of this report. The ratio of the relative sideband responses (upper/lower) reported in Volume 1 were then scaled on a band-by-band basis as follows:

- ❏ Bands 10 and 11: 1.0409
- ❏ Band 12: 1.0326
- ❏ Bands 13 and 14: 1.0493

These data indicate that the relative sideband responses in all R4 bands became more balanced (i.e., closer to 1:1) as a result of the tripler changeout.

These updated relative sideband responses are the ones used in Level 2 V1.5+ software. This document will be updated if future changes are make to any relative sideband information used in data processing, or if any in-orbit high-resolution sweeps of the filter spectrometers are performed.

3.1 GHz Spectral Baseline

Spectral Baseline refers to the difference between the routine reference view to cold space via the switching mirror and the "true" space view observed via the antenna. This is only of concern for the GHz measurements, as the THz module obtains its space reference view via its telescope primary. The GHz spectral baseline signatures are monitored annually by performing high elevation antenna scans (120 km tangent point and above) for several orbits. These data have remained remarkably stable for the duration of the mission to date, as shown in the plots below which overlay spectral baseline signatures for all GHz bands except for those in R4, and for the Wide Filter channels. The reason for omitting the R4 bands is that no clear evidence of a spectral baseline has ever been captured. It is unlikely that there is no spectral baseline signature, and we suspect that it changes too rapidly to be seen. The relatively high noise levels of the R4 bands contribute to the difficulty of capturing any such signature.

The spectral baseline plots typically average 4 complete orbits of data, and include an approximate indication of the rms noise in the edge and center channels. Other points of note include:

- ❏ The long-term variation of orbital average spectral baseline is typically on the order of 10 to 20 mK
- ❏ The brown spectral plot (with the star symbol) was taken during the period when we had switched over to the GME-B electronics, but the switching mirror had a small ($\sim 0.2^\circ$) pointing error. The data for the period when the switching mirror had the pointing error was processed using appropriate spectral baseline data.

3.1.1 Potential impact of orbit changes

Since Spring of 2023 the Aura spacecraft has no longer actively maintained its orbital altitude, and the orbital period has begun to slowly diminish. This has required the Flight Operations team (mainly Ryan Fuller) to monitor and update the MIF duration in order to maintain Orbit Sync, and operation that will have to be repeated every few months. The spectral baseline plots below have the 9 April 2024 data in bold, and there are hints that spectral baseline has begun to change in some bands. This can also be seen in the R4 spectral baseline data which are not included in this report since these data tend to be 'washed out' by rapid orbital changes.

3.1.2 Orbital Spectral Baseline Variations

The spectral baseline data have been analyzed to try to observe orbital variations. Since the signature is so stable, this becomes an exercise in which we balance sensitivity against temporal resolution. The only band for which we have been able to observe a consistent

orbital variation is Band 1, shown in Figure 3.12. The average spectral baseline signature for 6 orbits is shown, with the black and blue curves each representing half an orbit of data, with the same orbital phasing for each panel. This analysis has been repeated for Band 1 for all spectral baseline data sets, and each data set can be shown to produce pairs of curves in which one half of the orbit produces a baseline signature offset similarly from that for the other half of the orbit.

It is strongly suspected that the source of this variation is the broad space port view "seeing" the limb of the Earth at its edge. For a diffraction limited system, the edge of the beams are the regions with the strongest spectral variations. The level of orbital variation shown in the figure in not an accuracy concern for the Band 1 measurements. Attempts to reduce the window sizes significantly below half an orbit in order to obtain a clearer picture of the orbital behavior rapidly become swamped by increasing measurement noise.

When the spectral baseline data for all Bands are examined carefully, there are hints of long-term and/or orbital variations, but at such a low level as not to be a concern for this instrument.

3.1.3 Band 7 Spectral Baseline Anomaly on 18 October 2016

The spectral baseline data for Bands 7 through 9 for the data taken before the Moon was in the antenna FOV on 18 October 2016 are plotted in bold (red, dot-dash pattern, square markers). For Band 7 alone we observe that the spectral baseline signature for channel 24 (the second channel from the right) is offset by $\sim$40 mK. The same signature exists for the data taken after the Moon was in the FOV, and this shift in spectral baseline is confirmed by Level 2 analyses performed by Bill Read. This anomaly is still under investigation.

3.1.4 Spectral Baseline Data on 3 March 2018

The spectral baseline data taken on 3 March 2018 was afflicted with minor corruption (26 bad MAFs) due to a spacecraft FMU anomaly. The data analysis software was updated to use radiance precision data to remove the bad data from the analysis.

3.1.5 Spectral Baseline Data on 13/14 November 2019

The spectral baseline data planned to be taken on 13 November 2019 was afflicted by a minor operational anomaly which delayed the start of the activity, meaning that the data set spanned into the following day. The plots include only data taken on 14 November.

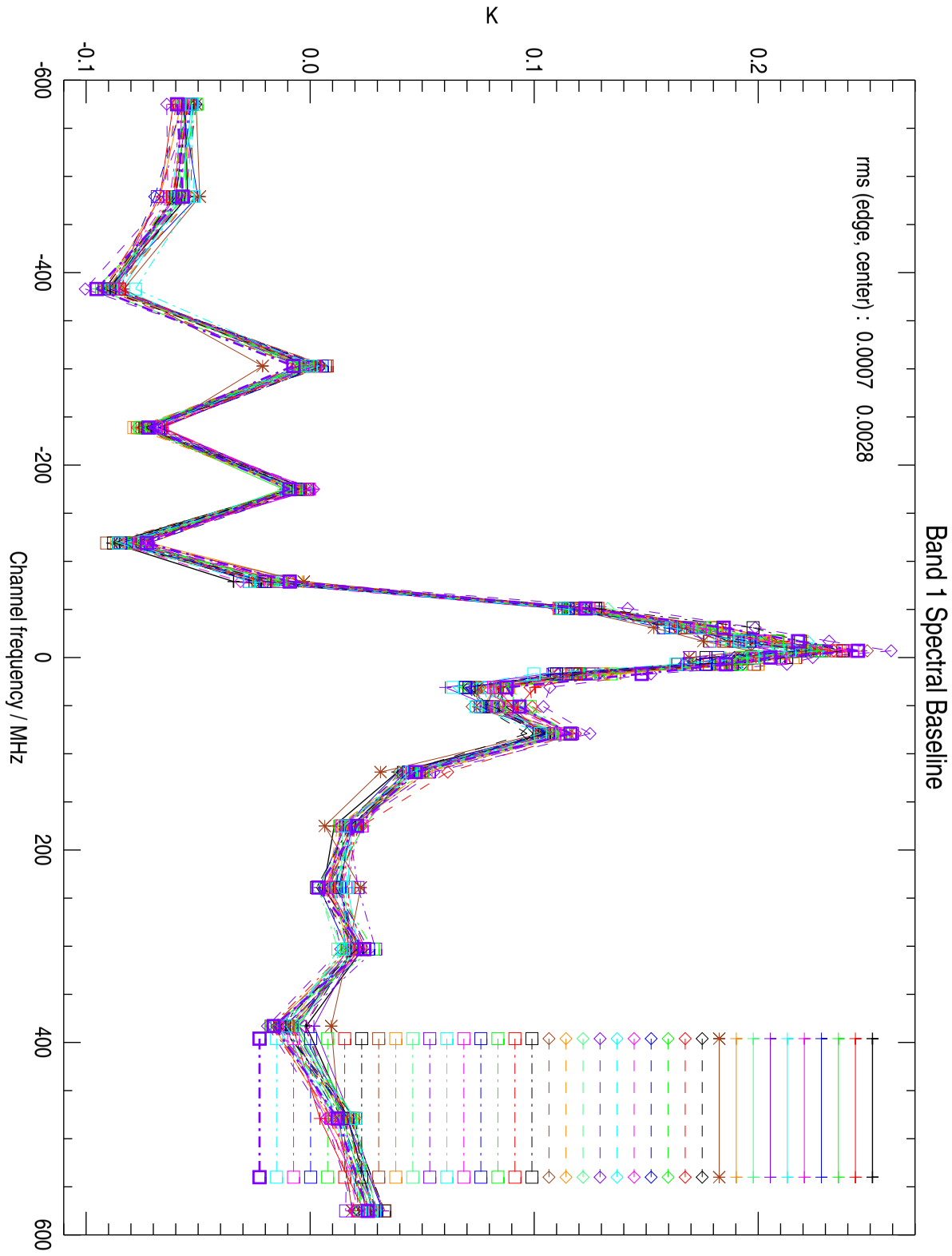

Figure 3.1: Spectral baseline data for Band 1 (R1A) taken between 2005 and 2024

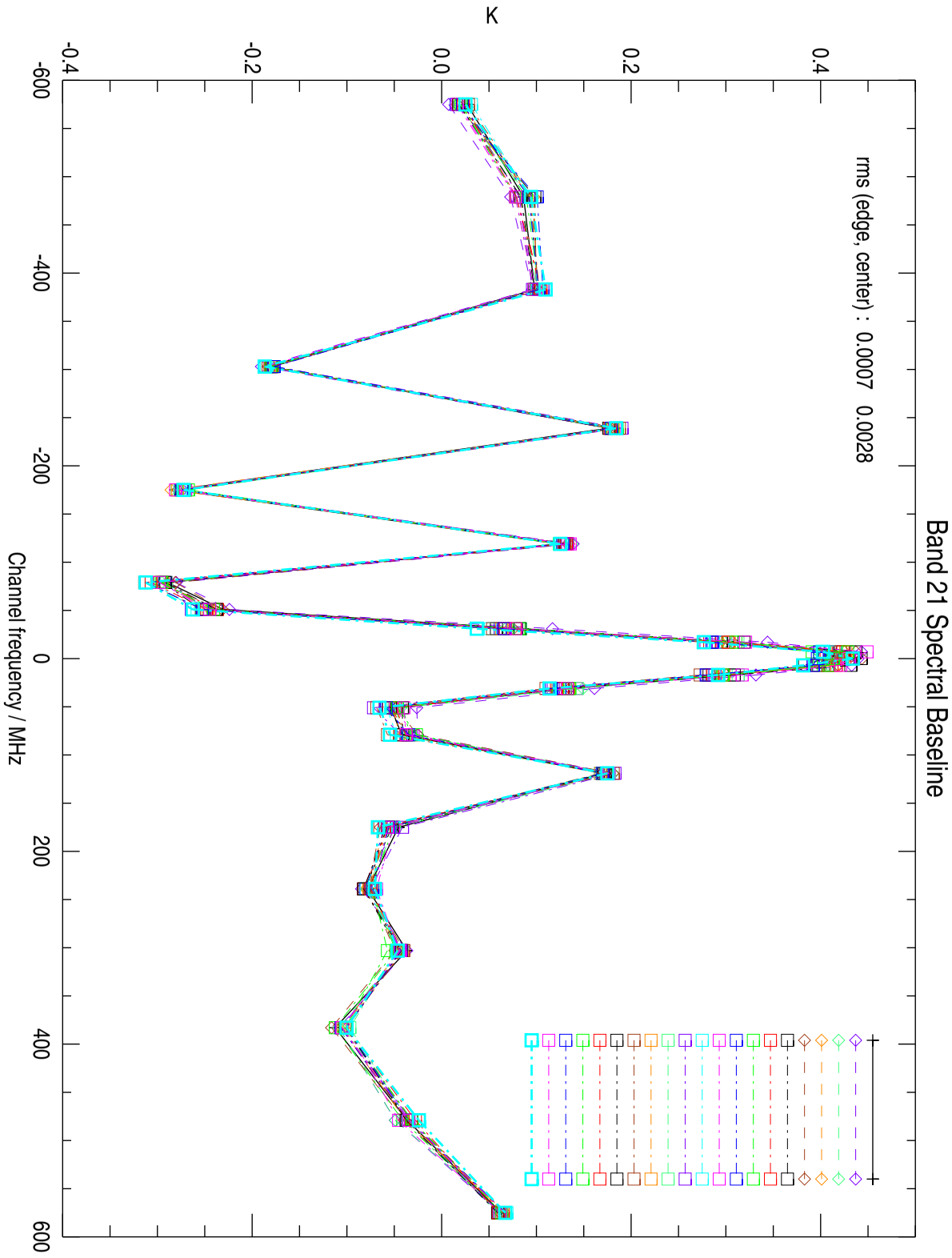

Figure 3.2: Spectral baseline data for Band 21 (R1B) taken from 7 October 2013 until 2024.

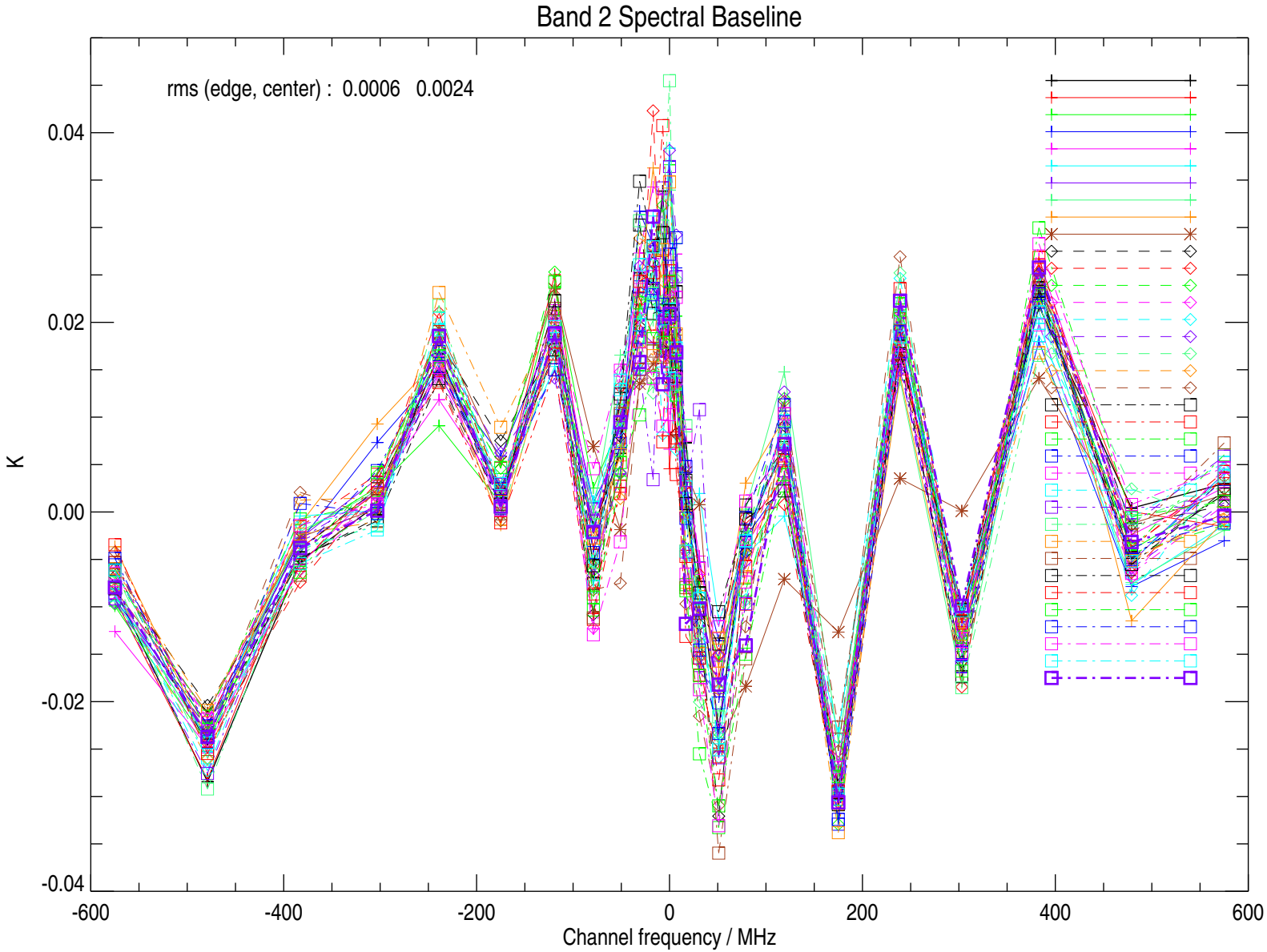

Figure 3.3: Spectral baseline data for Band 2 taken between 2005 and 2024.

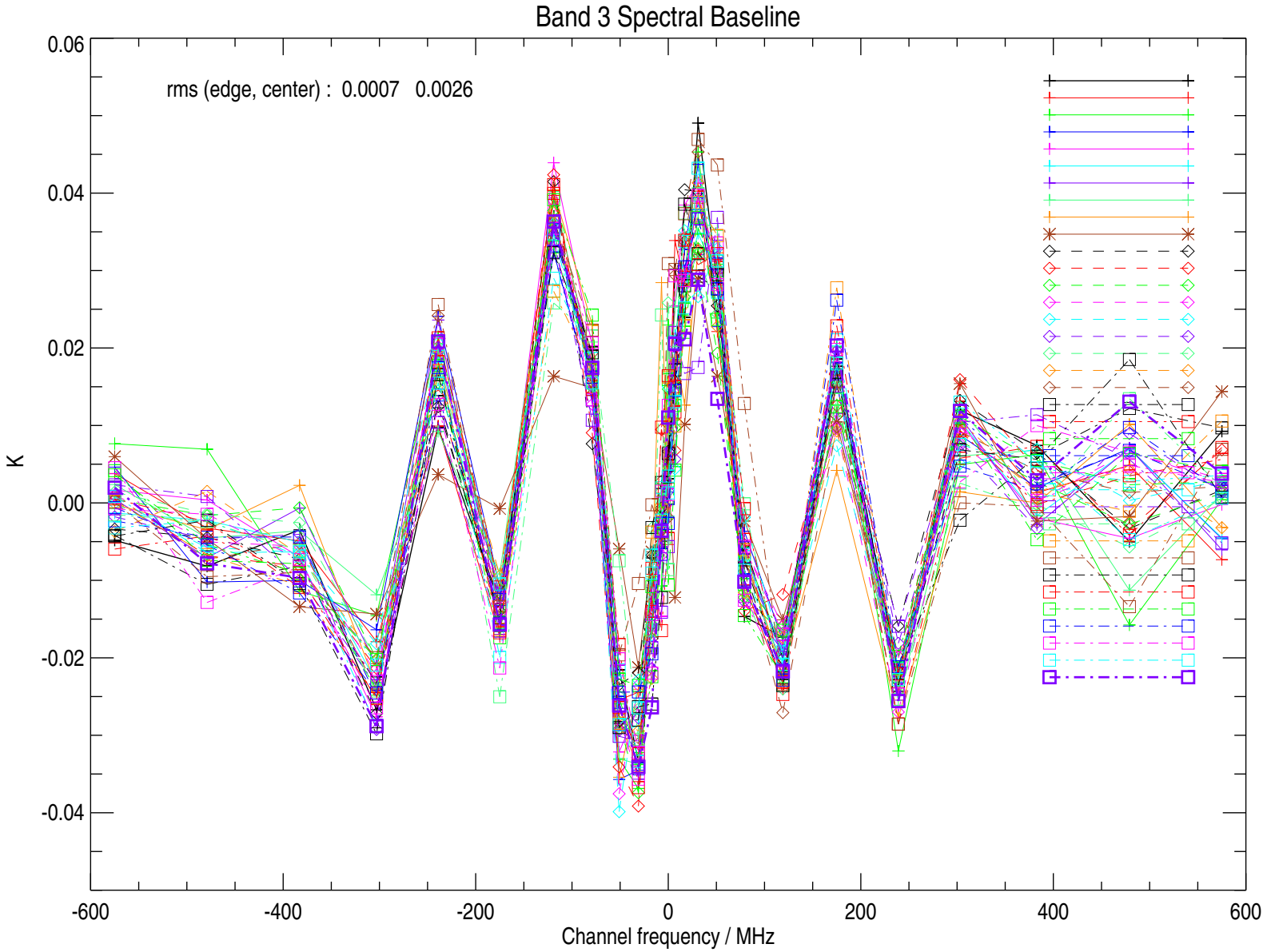

Figure 3.4: Spectral baseline data for Band 3 taken between 2005 and 2024.

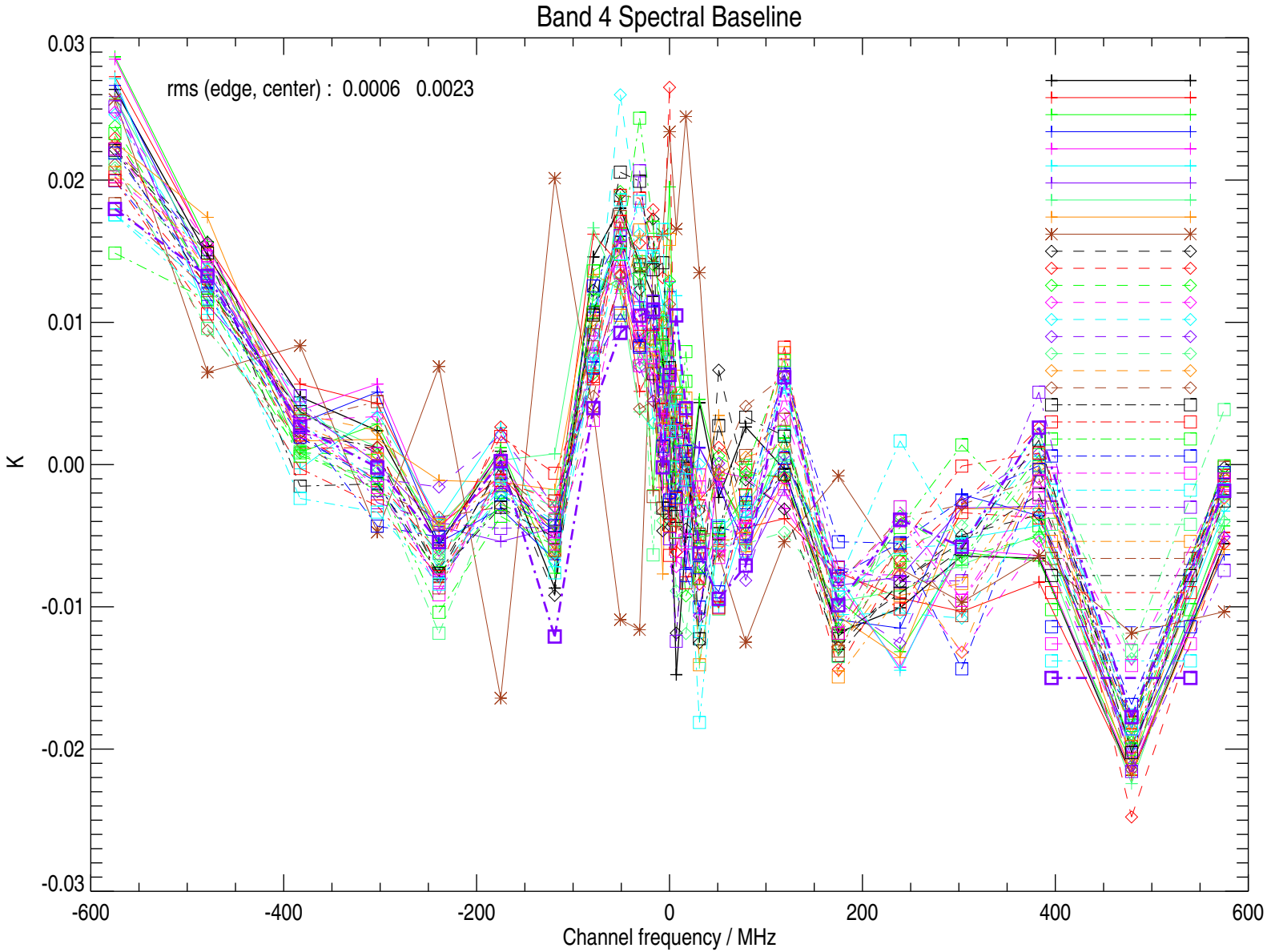

Figure 3.5: Spectral baseline data for Band 4 taken between 2005 and 2023.

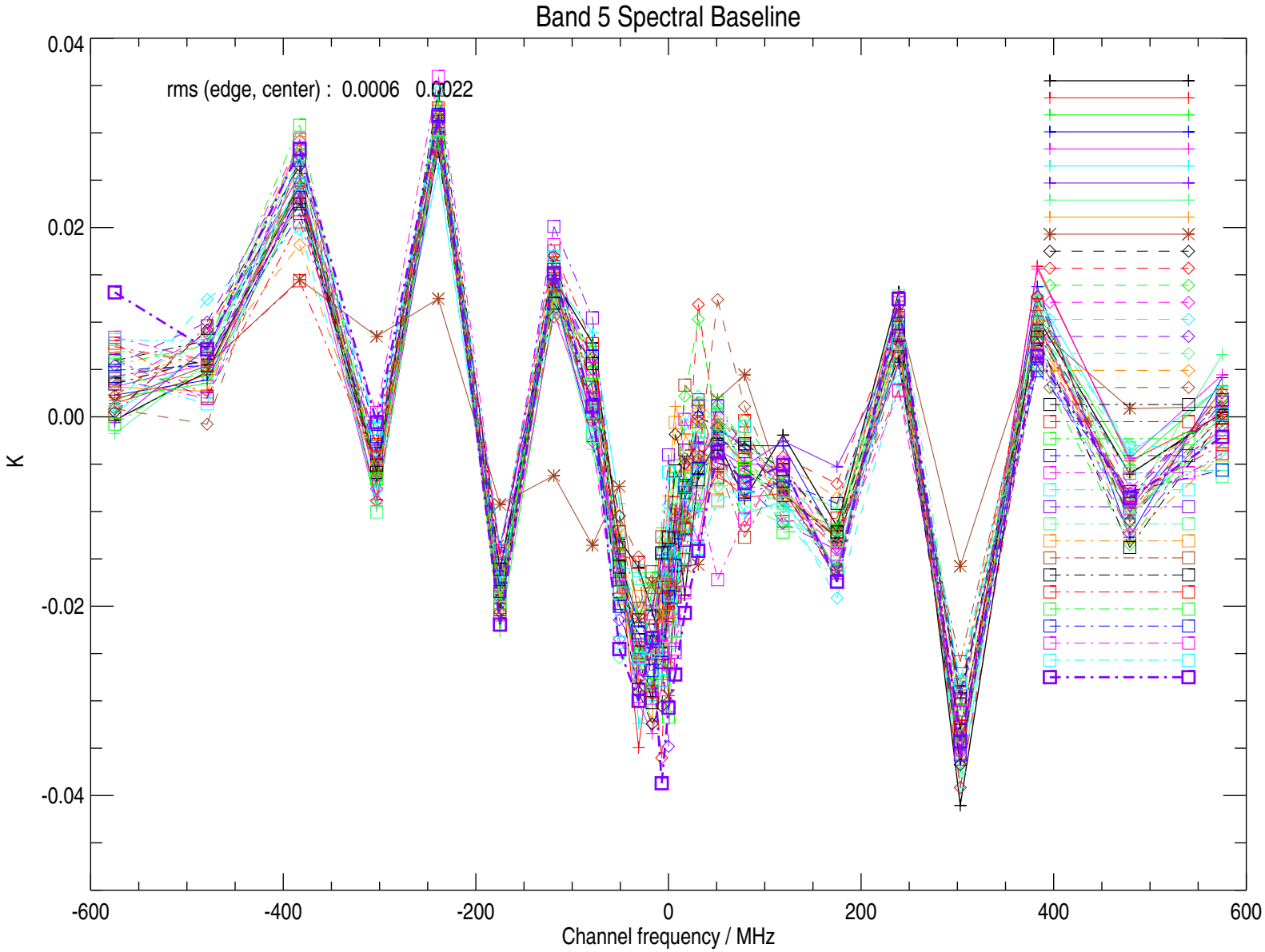

Figure 3.6: Spectral baseline data for Band 5 taken between 2005 and 2024.

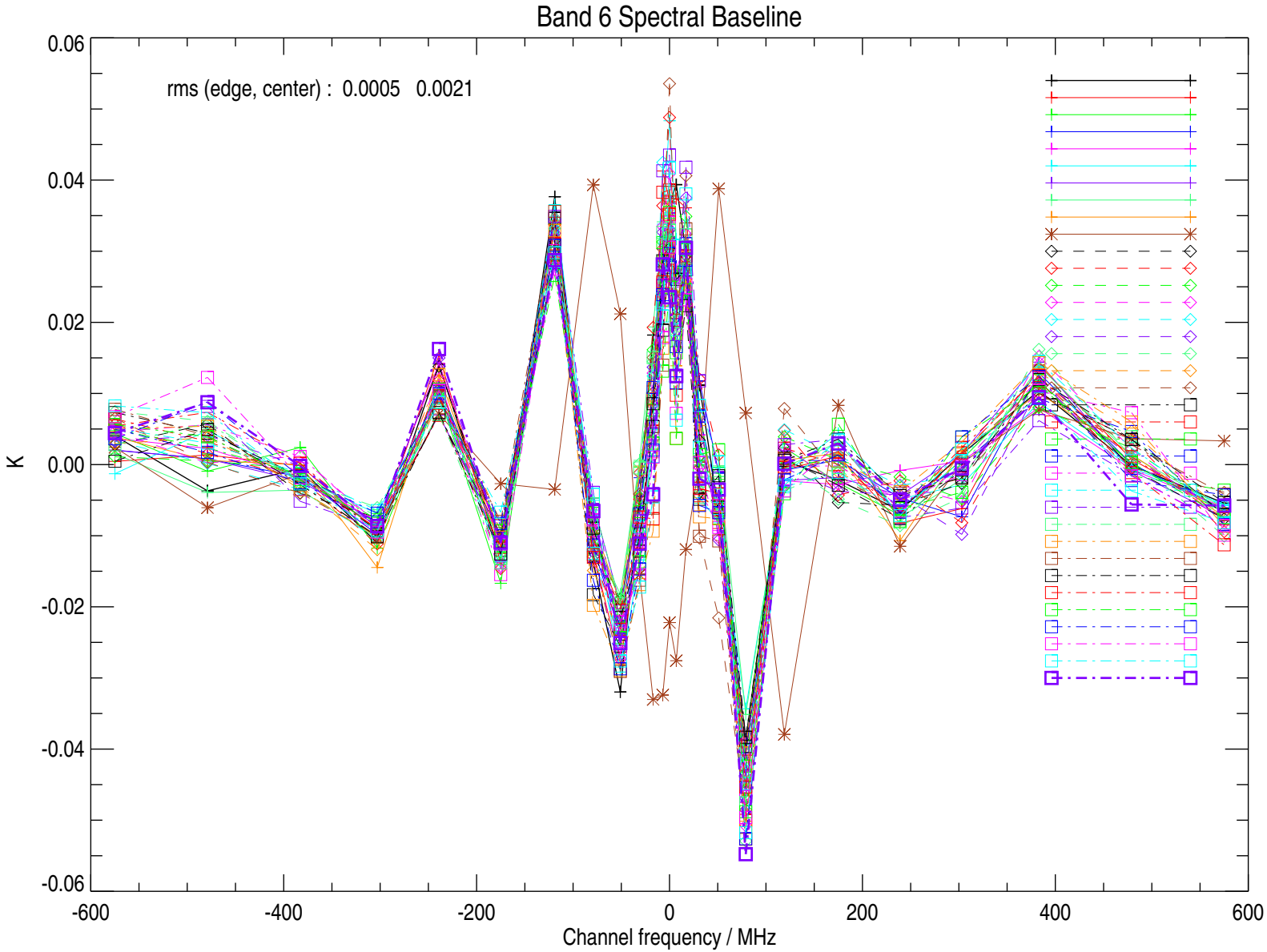

Figure 3.7: Spectral baseline data for Band 6 taken between 2005 and 2024.

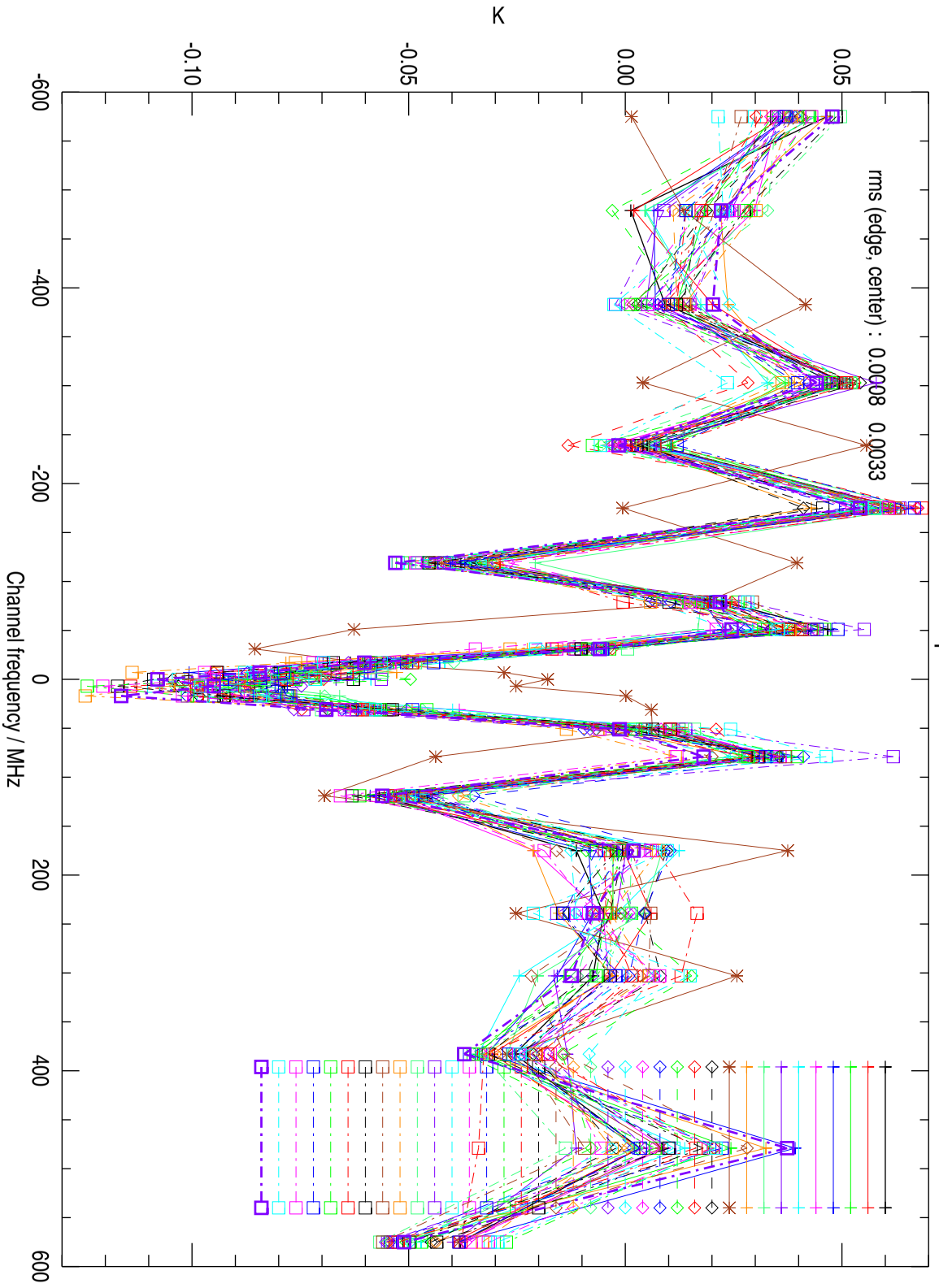

Figure 3.8: Spectral baseline data for Band 7 taken between 2005 and 2024.

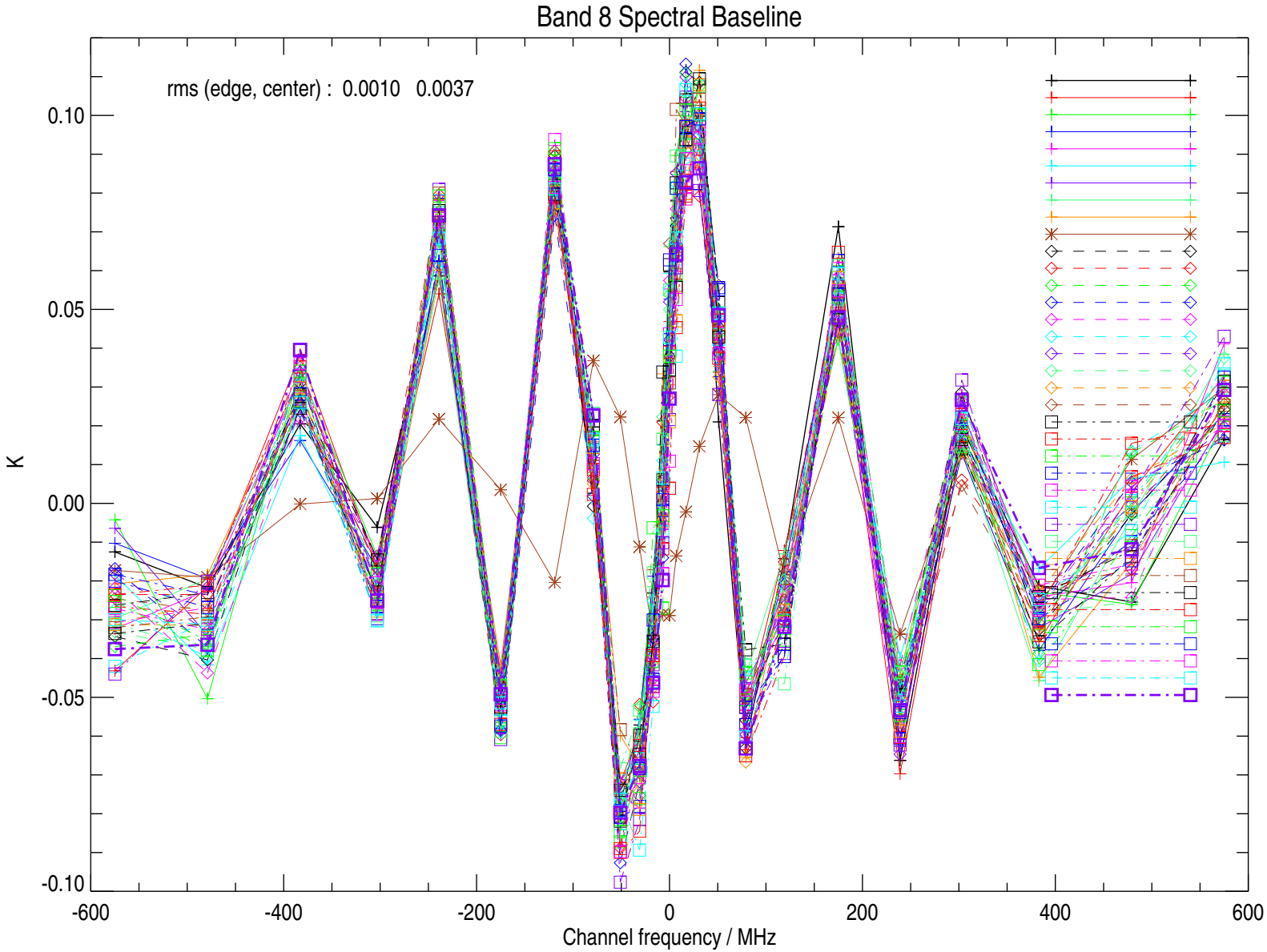

Figure 3.9: Spectral baseline data for Band 8 taken between 2005 and 2024.

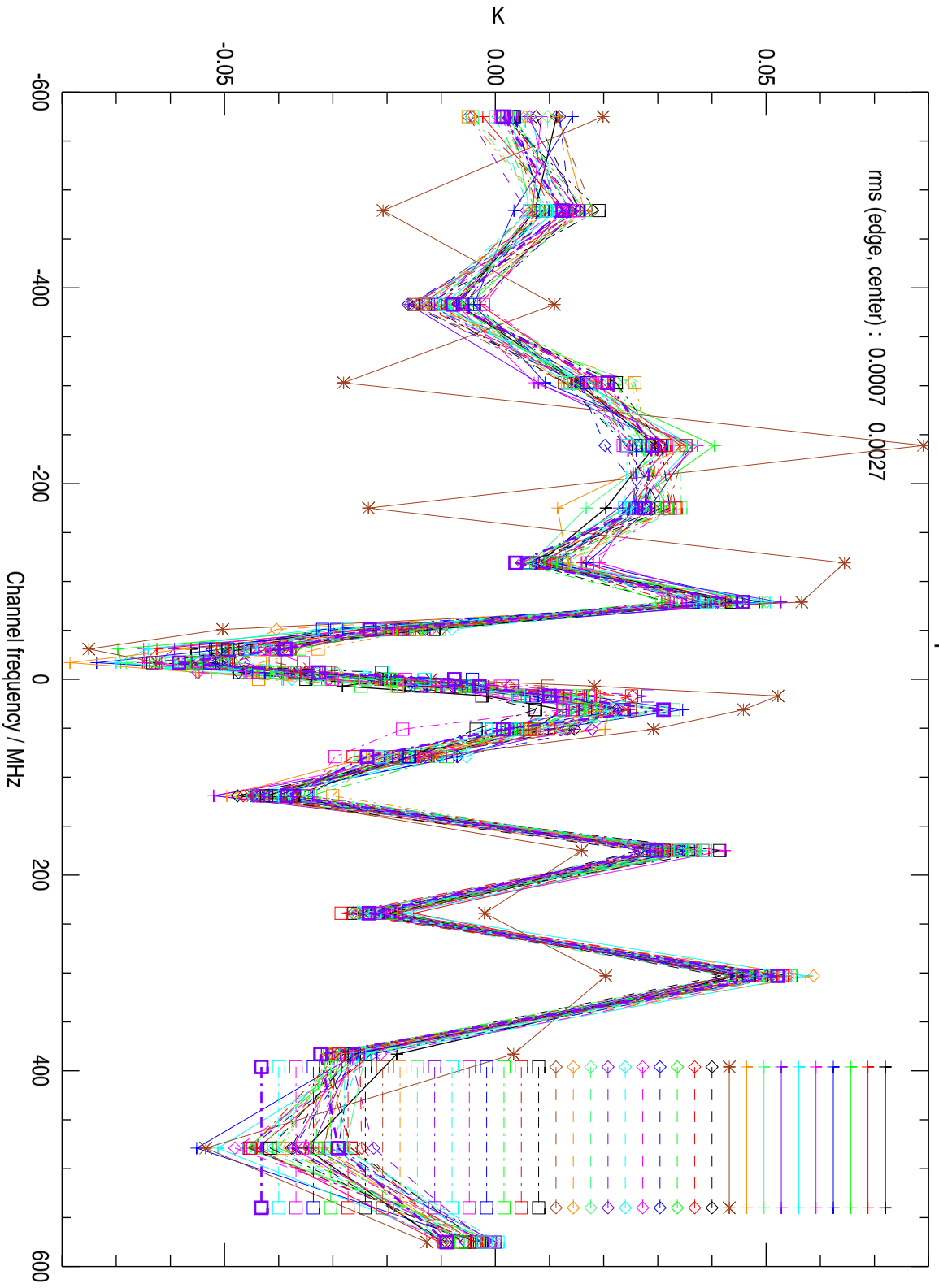

Figure 3.10: Spectral baseline data for Band 9 taken between 2005 and 2024.

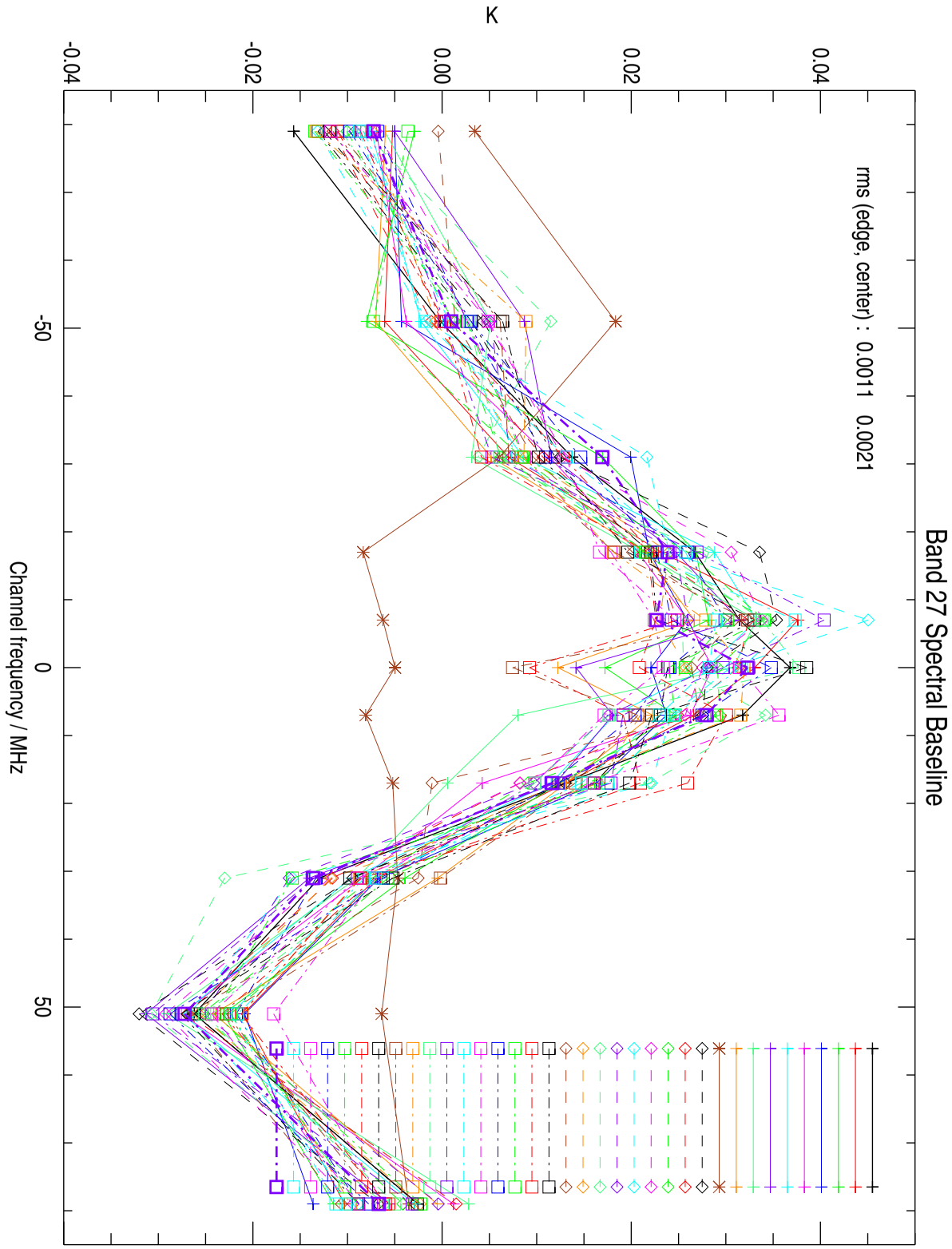

Figure 3.11: Spectral baseline data for Band 27 taken between 2005 and 2023.

Figure 3.12: Variation in Band 1 spectral baseline for six sequential orbits. See text for more information.

3.2 Switching Mirror Port Scans

Although the spectral baseline data just presented provides a certain level of confidence in the long-term stability of MLS measurements, it provides a far from complete picture of spectral artifacts present in the data. The first step taken to obtain a better picture of the situation was to scan the Switching Mirror slowly past its four prime positions with the antenna positioned well above the atmospheric limb. Data from two ports at very different radiative temperatures can then be used to radiometrically calibrate the data from the port under investigation, and all four ports can be calibrated this way.
There are two primary pieces of information to be gleaned from this data:

(1) We can see how well the FOV's are centered on the Switching Mirror ports, and

(2) we can look for evidence of standing waves.

Figures 3.13 to 3.15 show calibrated radiance at the three switching mirror ports used operationally by the GHz radiometers. At each port the mirror was slowly scanned past the nominal rest position (indicated by the black vertical line near the center of each panel). The antenna was positioned well above the atmospheric limb for these measurements. The band-average (weighted by channel noise bandwidth) radiance is plotted in each case. The color scheme used plots the bands indicated in the title of each panel in the order black, red, green, blue, cyan and magenta.

Several important things can be discerned in the data shown in these plots. For example, for none of the bands do we see minimum radiance when 'looking' directly at the space or limb ports. In all bands we see 'wiggles' in the band average radiances as the mirror is scanned, clear evidence of standing waves. When the same data are plotted channel by channel, the evidence for standing waves at the switching mirror rest positions is even clearer. Since the data being used to radiometrically calibrate the data from the port under investigation is subject to standing waves, it is not possible to determine the actual standing wave levels an any port. Another serious limitation arises from the double sideband nature of most MLS measurements – even if we were able to obtain a good measure of the spectral artifacts in each band, we have no way of partitioning the artifacts between sidebands.

3.3 Switching Mirror Port Scans – 25 May 2011

The switch over to GME B-side electronics (see Section 3.1) resulted in a suspected 0.2° Switching Mirror pointing error. Port scans similar to those just described (but including the ambient target port) were performed on 25 May 2011, and the data presented in Figures 3.16 to 3.19 appear to confirm this error. The data in these figures were obtained from a special run of Level 1 software which did not include antenna offsets.

3.4 Moon Tracking Data

The interesting results from the Switching Mirror port scan test led us to try a much more difficult, and potentially much more valuable, in-orbit characterization – tracking the Moon with the main antenna while is was well above the atmospheric limb. Full and new Moon tracking data are shown in Figures 3.20 and 3.21 respectively.

The full Moon data set was divided into four consecutive segments each of 64 MIFs duration. Filterbank 12 was connected to R1B, and Band 13 was turned off at the time of these measurements (DOY 76 of 2006). The consistency between the four groups of data taken in each band clearly show that the data represent real standing waves in the meausurement system, not noise. The radiance difference between the measurement groups that is strongly evident in the data for R1A (FB1) and R3 (Bands 7 to 9) arises from the slow drift of the Moon in the FOV over the course of the measurement. It is interesting to note that the observed standing wave levels are at the 1 K to 4 K level. The test in which a new Moon was tracked (DOY 208 of 2006, shown in Figure 3.21) resulted in observed radiance of about $\frac{1}{3}$ to $\frac{1}{2}$ of those obtained when viewing a full Moon. Filterbank 12 was connected to Band 12 for this measurement. These data show standing wave artifacts scaled down in magnitude according to the relative radiance of the two scenes, an indicator that they arise largely as a result of standing wave-induced ripples in the radiometric gain estimate. The differences in the standing wave patterns between the two data sets show that although these artifacts are substantial, unlike the spectral baseline observed when viewing cold space through the antenna, they do not have good long-term temporal stability. If this were not the case, large artifacts like those presented in the plots would be evident in Level 2 residuals. As with the port scan data, these results only give us a double sideband picture of what is taking place. IDL code was used for radiometric calibration, since Level 1 processing software 'throws away' limb data taken during MIF's which are nominally allocated to radiometric calibration views.

The full Moon tracking measurements were repeated in March 2008 (Figure 3.22), at which time Band 13 was turned off, and R1B data was not available since FB12 was connected to the THz radiometer system. As with the DOY 76 of 2006 data, these data were radiometrically calibrated using IDL code. The black, red, blue and green spectra are averages of contiguous 60 MIF duration Moon tracking data. These data are to be compared with the corresponding data shown in Figure 3.20. The measurements were repeated again in March 2009, shown in Figure 3.23. The four data chunks are 64 MIF's in duration for this data set, and although the standing wave magnitudes are similar to other full Moon track data, the details are different.

Full Moon tracking measurements were repeated again in March 2010 (Figure 3.24. As with the March 2008 data, Band 13 was off, and R1B data was not available. These data were calibrated using a modified version of Level 1 software, and omit the lunar data that were taken during the nominal radiometric calibration MIFs. The 201 MIF of clean views data were divided into 3 sets of 67 MIFs (black, red, green) to show the level of consistency during the tracking event.

For the full Moon tracking event of 21 March 2011 a different analysis approach was chosen. The Lunar brightness was first calibrated in each band, and fixed to the same value for all channels in a given band. Four groups of Space-Target view (two on either side of the Lunar view) where then used to determine Controlled Target radiance, plotted in Figure 3.25. This alternative analysis was chosen to see if similar patterns could be seen in the Target radiances, indicating persistent standing waves. The plotted data show no such patterns, and have precision consistent with the measurement time. We thus conclude that although the Lunar tracking data are very useful for FOV refinement, they provide no additional quantitative data on standing waves within MLS.

The full Moon tracking data shown in Figure 3.26 were calibrated using Level 1 software. For this tracking event the GME was accidently left in operation (GME-A was disabled,

but we were running on GME-B), and there were calibration events at the start and end of the lunar observation, as well as one in the middle. The time-series calibrated radiance data show a small discontinuity near the center of the tracking event, not yet explained, but probably an artifact introduced in the Level 1 processing. No other features of this data set are remarkable.

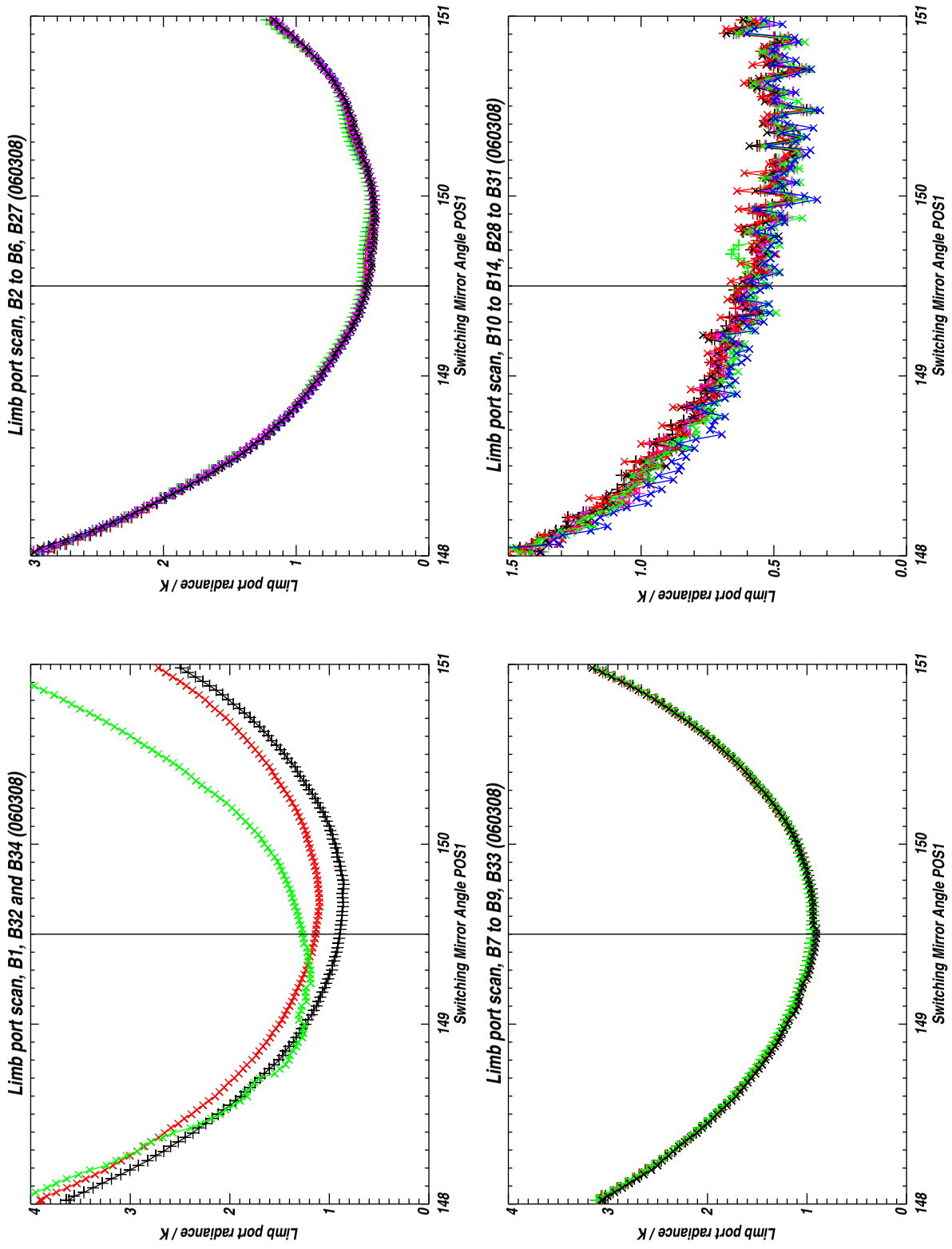

Figure 3.13: Observed radiances at the GHz limb port with the switching mirror slowly scanning past its prime rest position. See text for additional details.

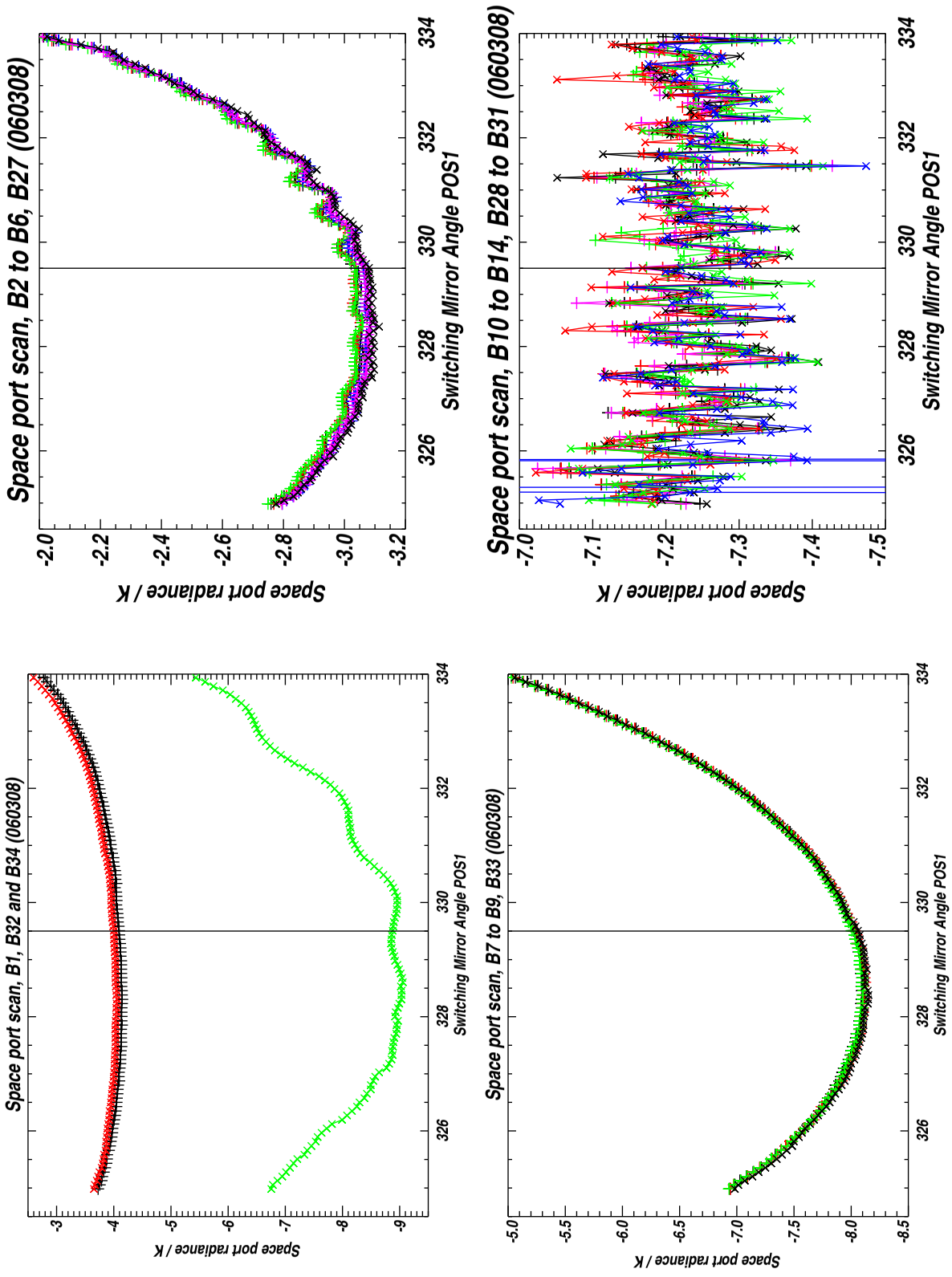

Figure 3.14: Observed radiances at the GHz space port with the switching mirror slowly scanning past its prime rest position. See text for additional details.

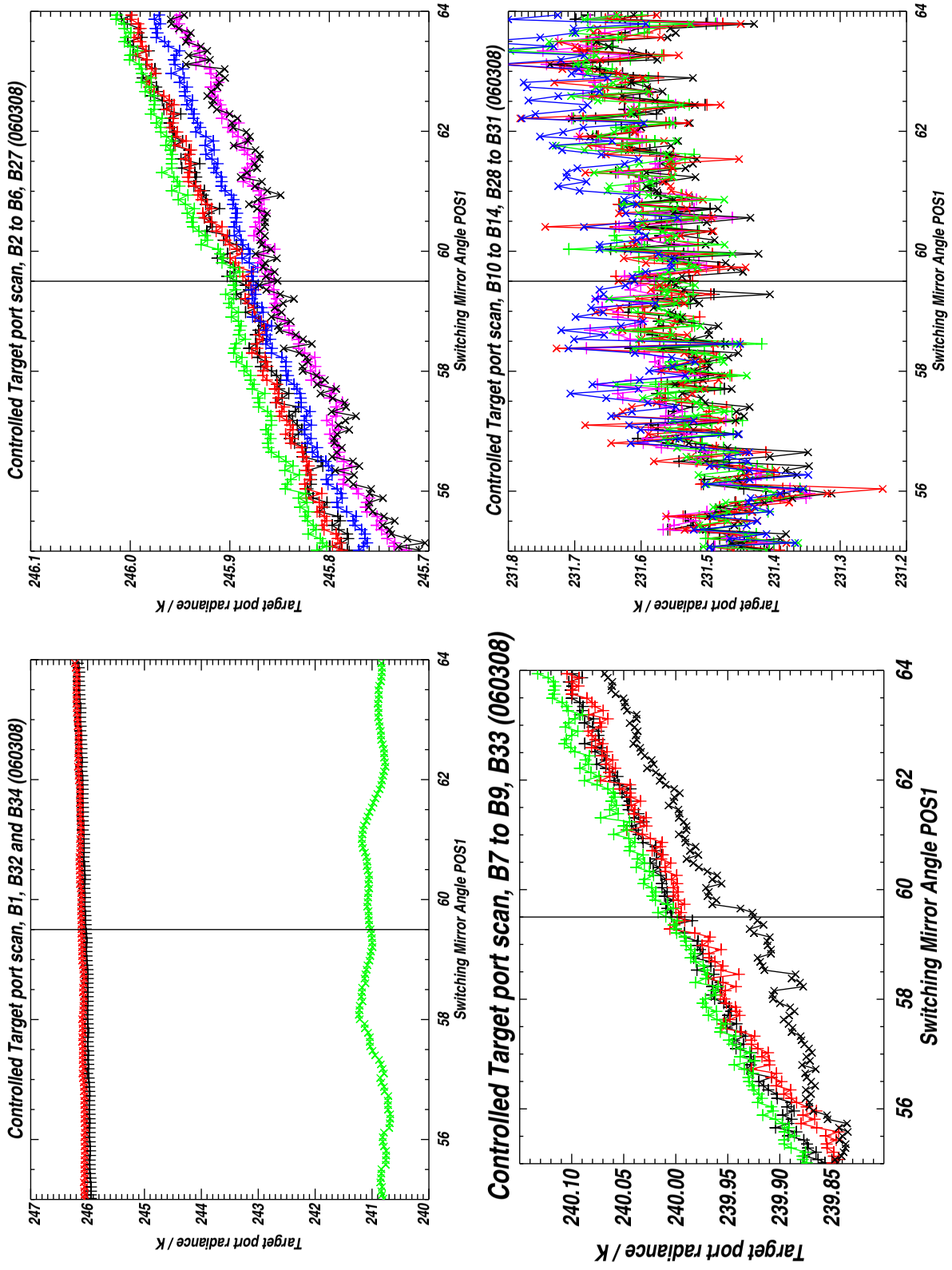

Figure 3.15: Observed radiances at the GHz controlled target port with the switching mirror slowly scanning past its prime rest position. See text for additional details.

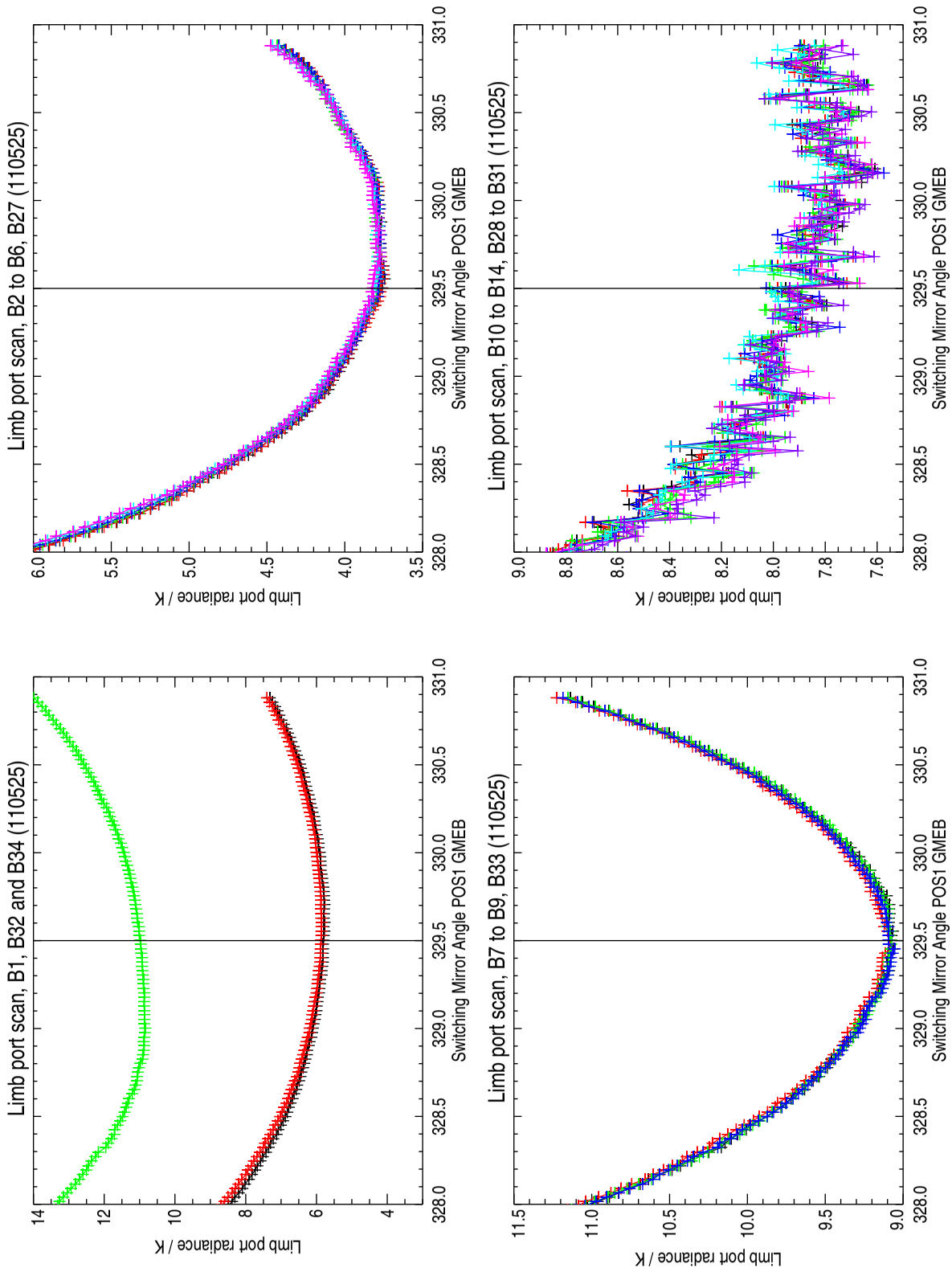

Figure 3.16: Observed radiances at the GHz limb port with the switching mirror slowly scanning past its prime rest position. See text for additional details.

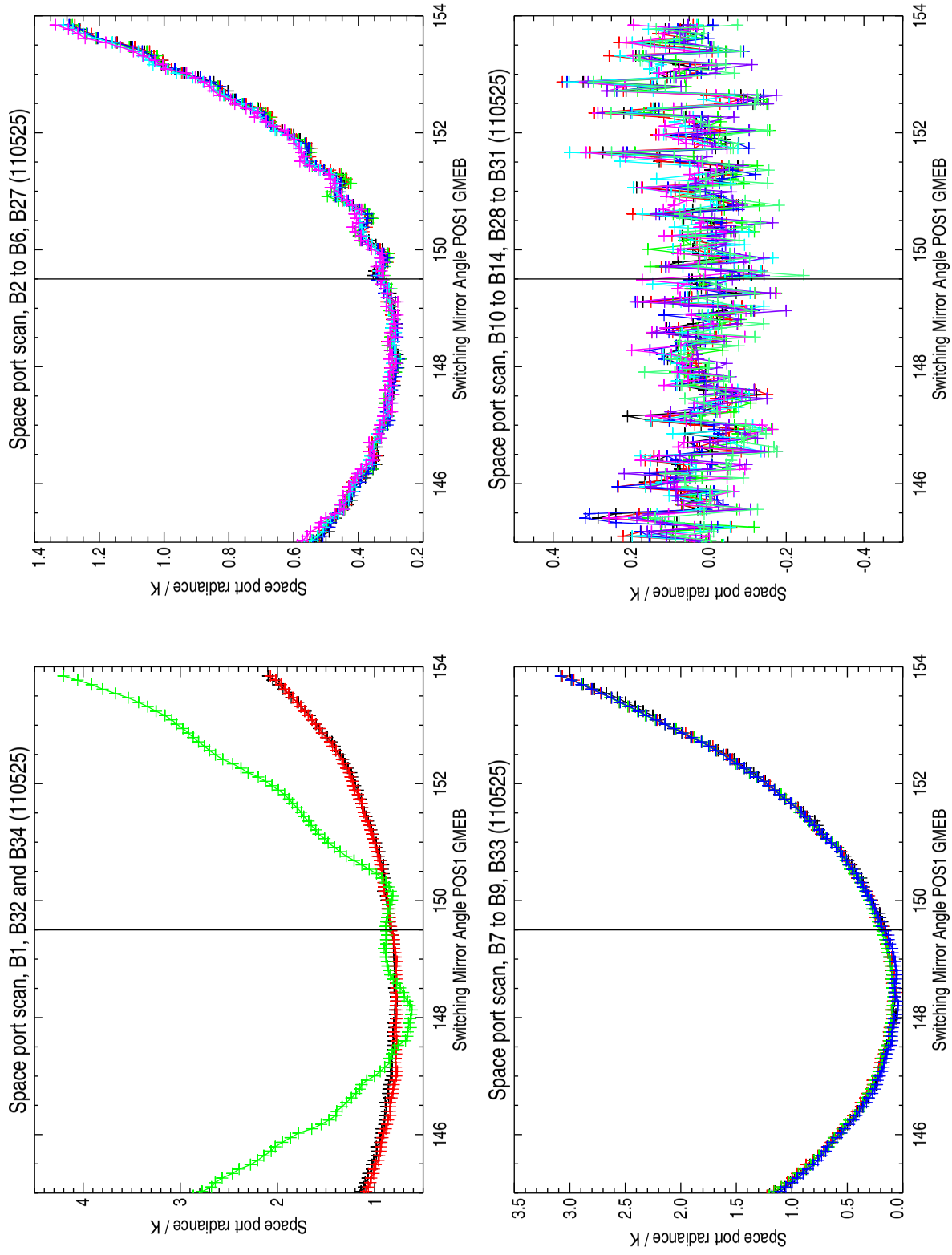

Figure 3.17: Observed radiances at the GHz space port with the switching mirror slowly scanning past its prime rest position. See text for additional details.

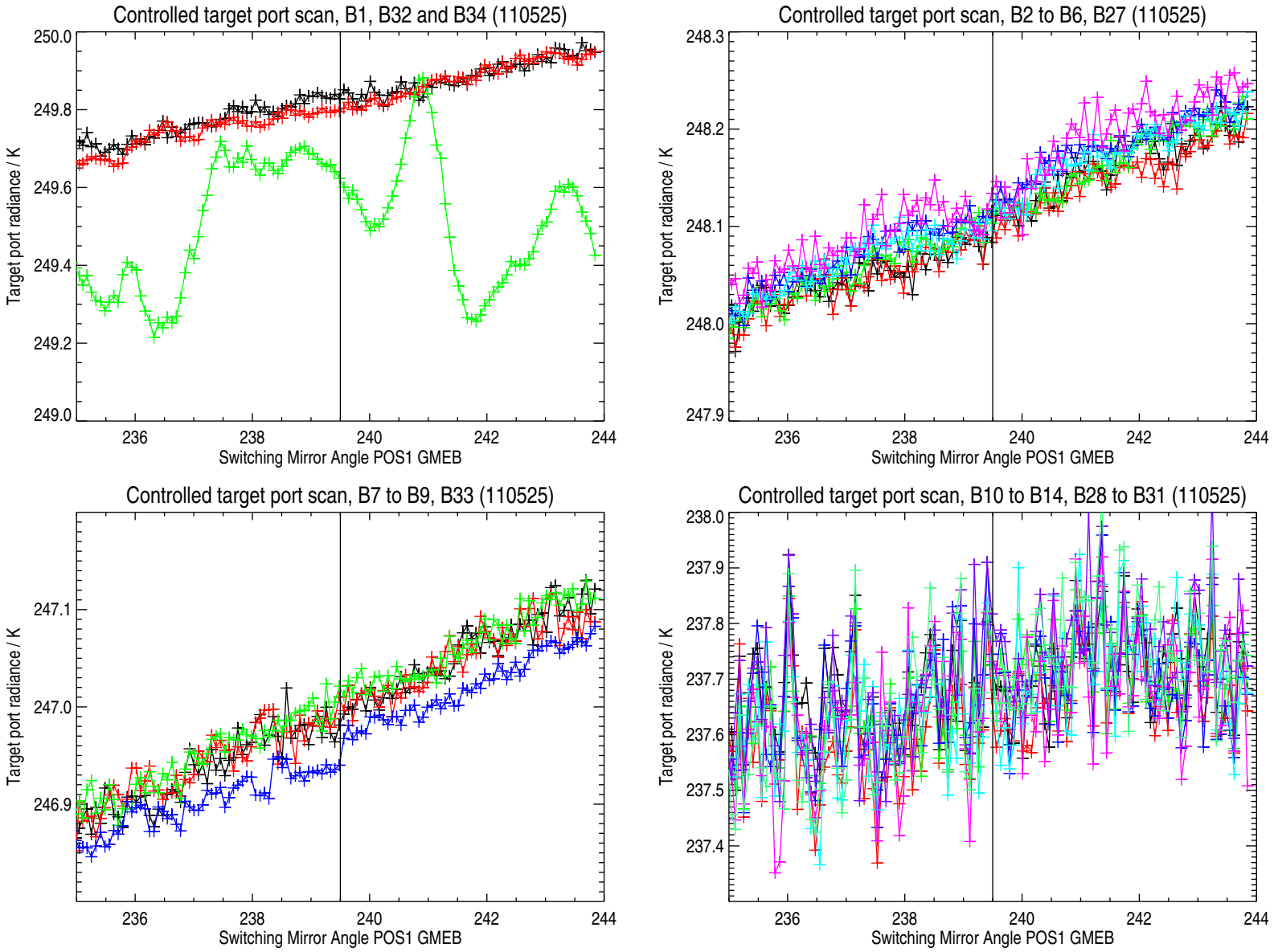

Figure 3.18: Observed radiances at the GHz controlled target port with the switching mirror slowly scanning past its prime rest position. See text for additional details.

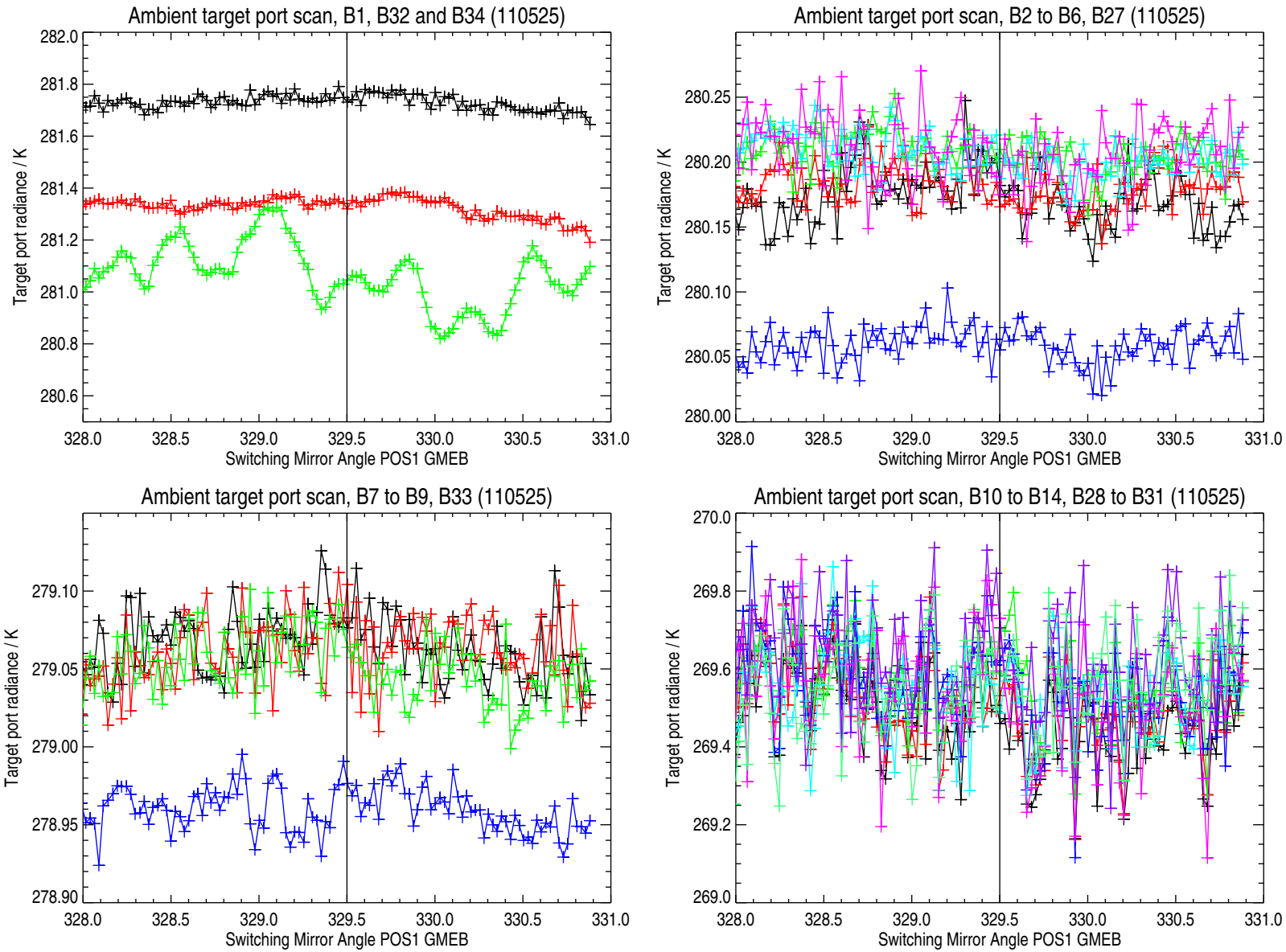

Figure 3.19: Observed radiances at the GHz ambient target port with the switching mirror slowly scanning past its prime rest position. See text for additional details.

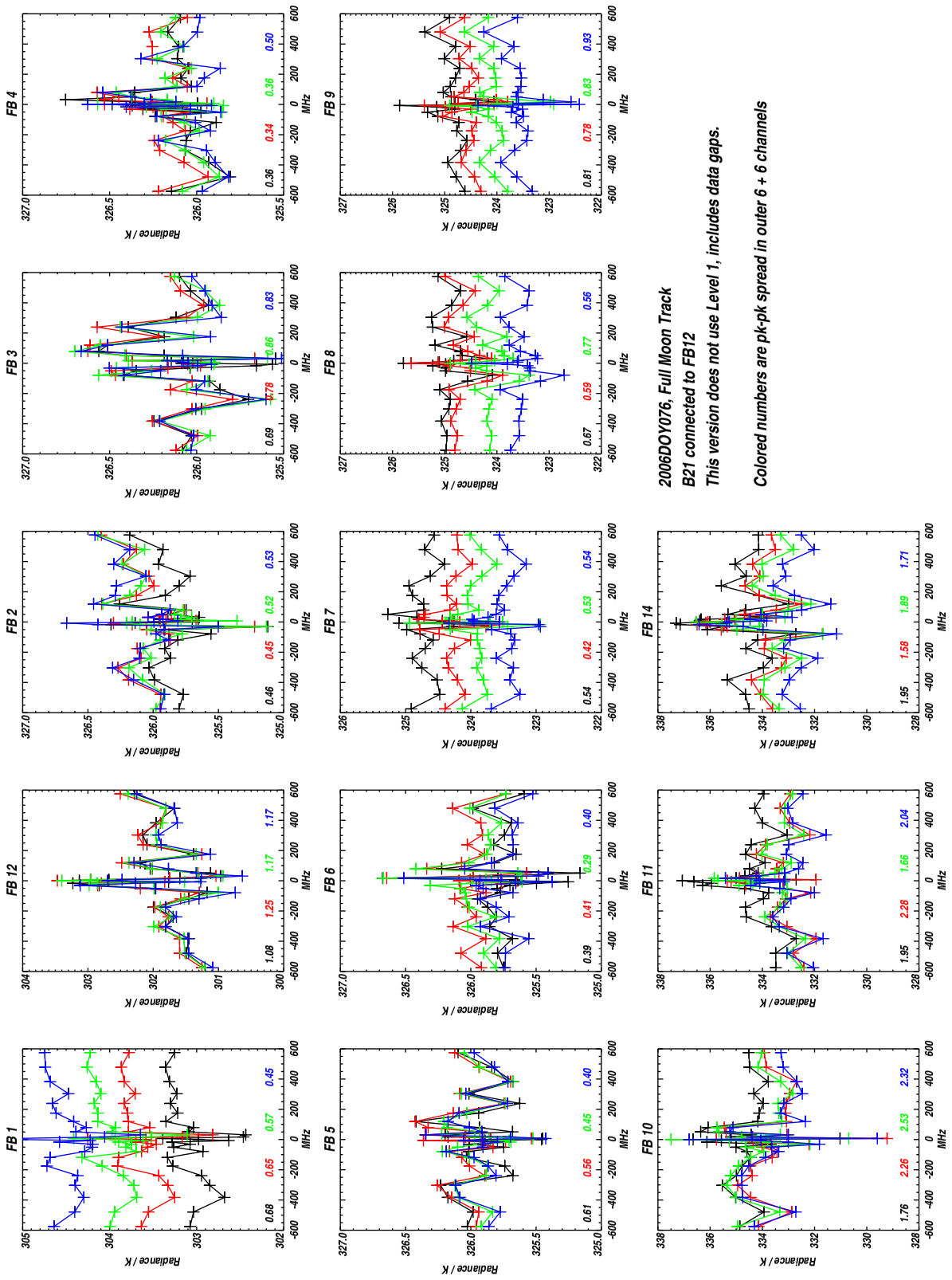

Figure 3.20: Limb radiances while tracking the full Moon. The time series data has been divided into four consecutive segments to give an indication of the noise level. See text for additional details.

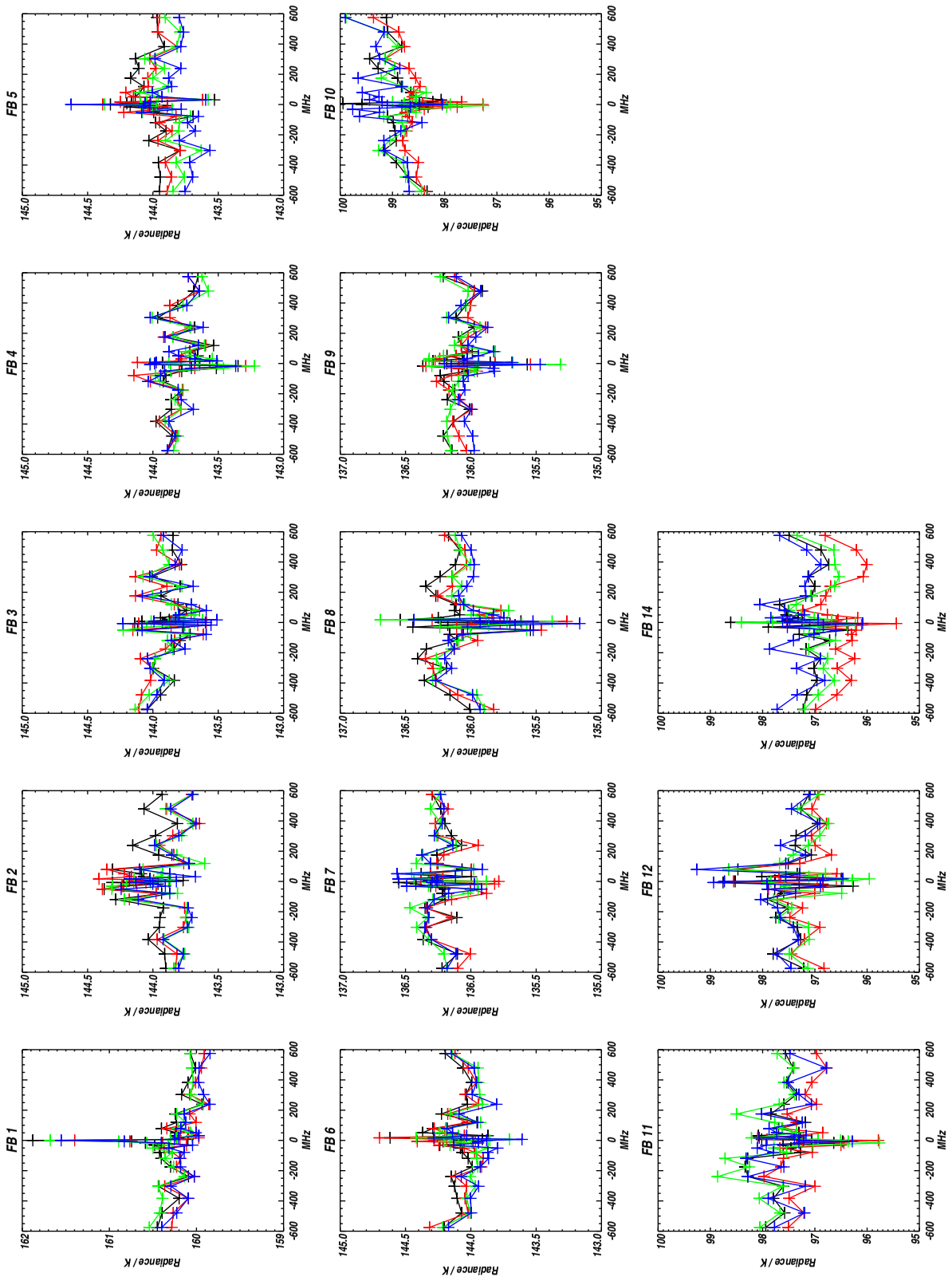

Figure 3.21: Limb radiances while tracking the new Moon. The time series data has been divided into four consecutive segments to give an indication of the noise level. See text for additional details.

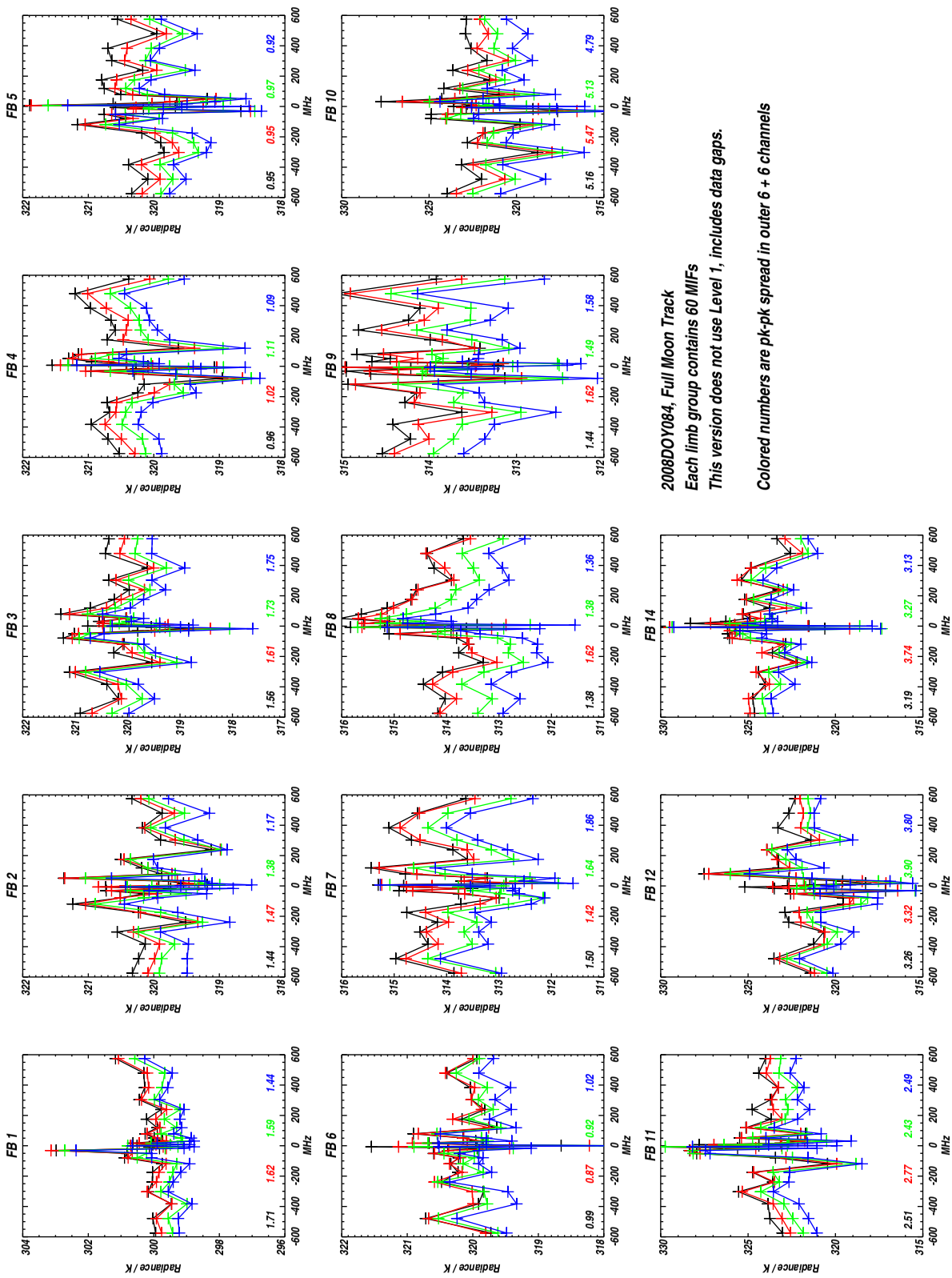

Figure 3.22: Limb radiances while tracking the full Moon on DOY084 of 2008. The time series data has been divided into four segments to give an indication of the noise levels and variations in radiometric calibration between consecutive major frames. See text for additional details.

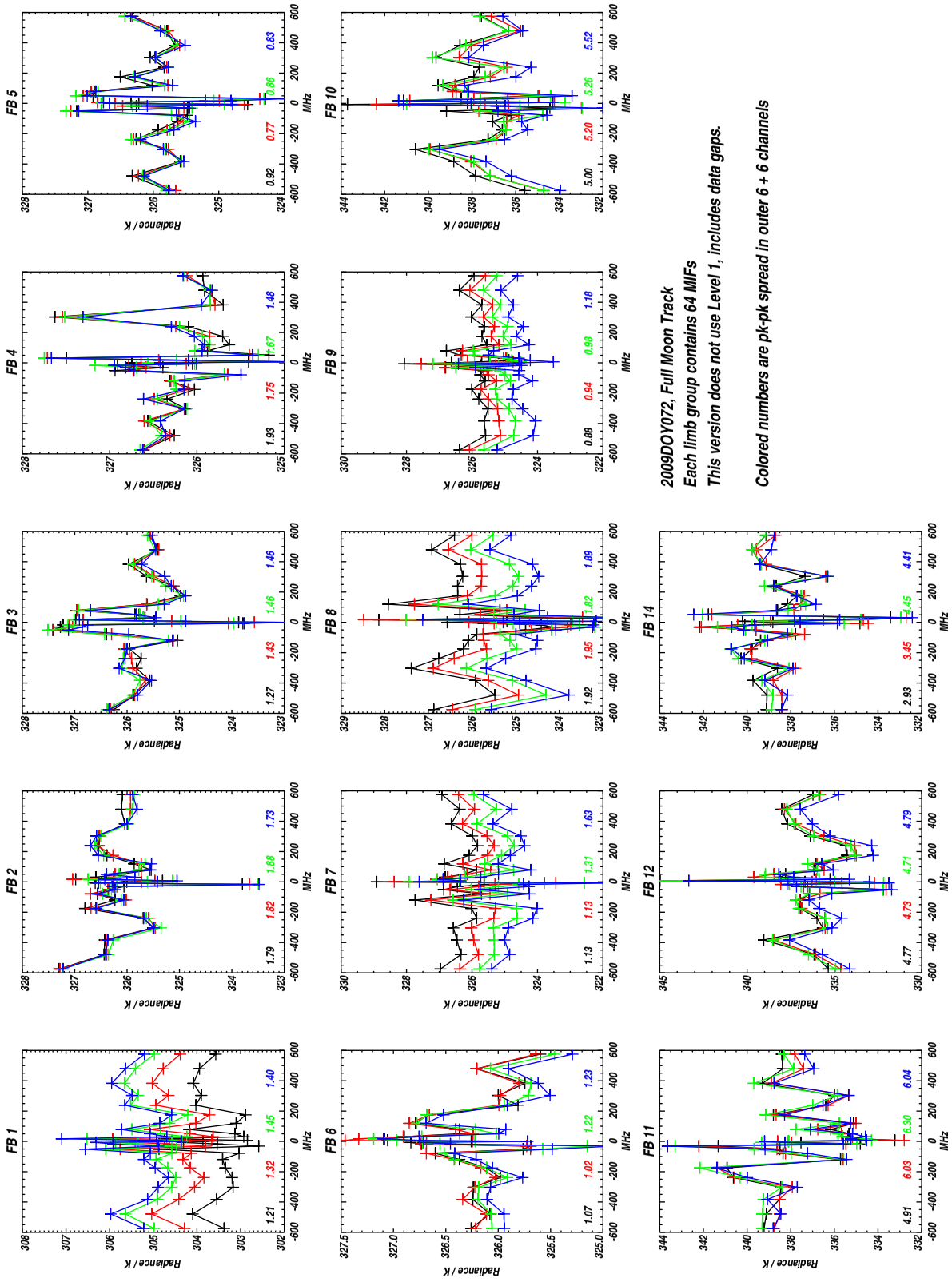

Figure 3.23: Limb radiances while tracking the full Moon on DOY072 of 2009. The time series data has been divided into four segments to give an indication of the noise levels and variations in radiometric calibration between consecutive major frames. See text for additional details.

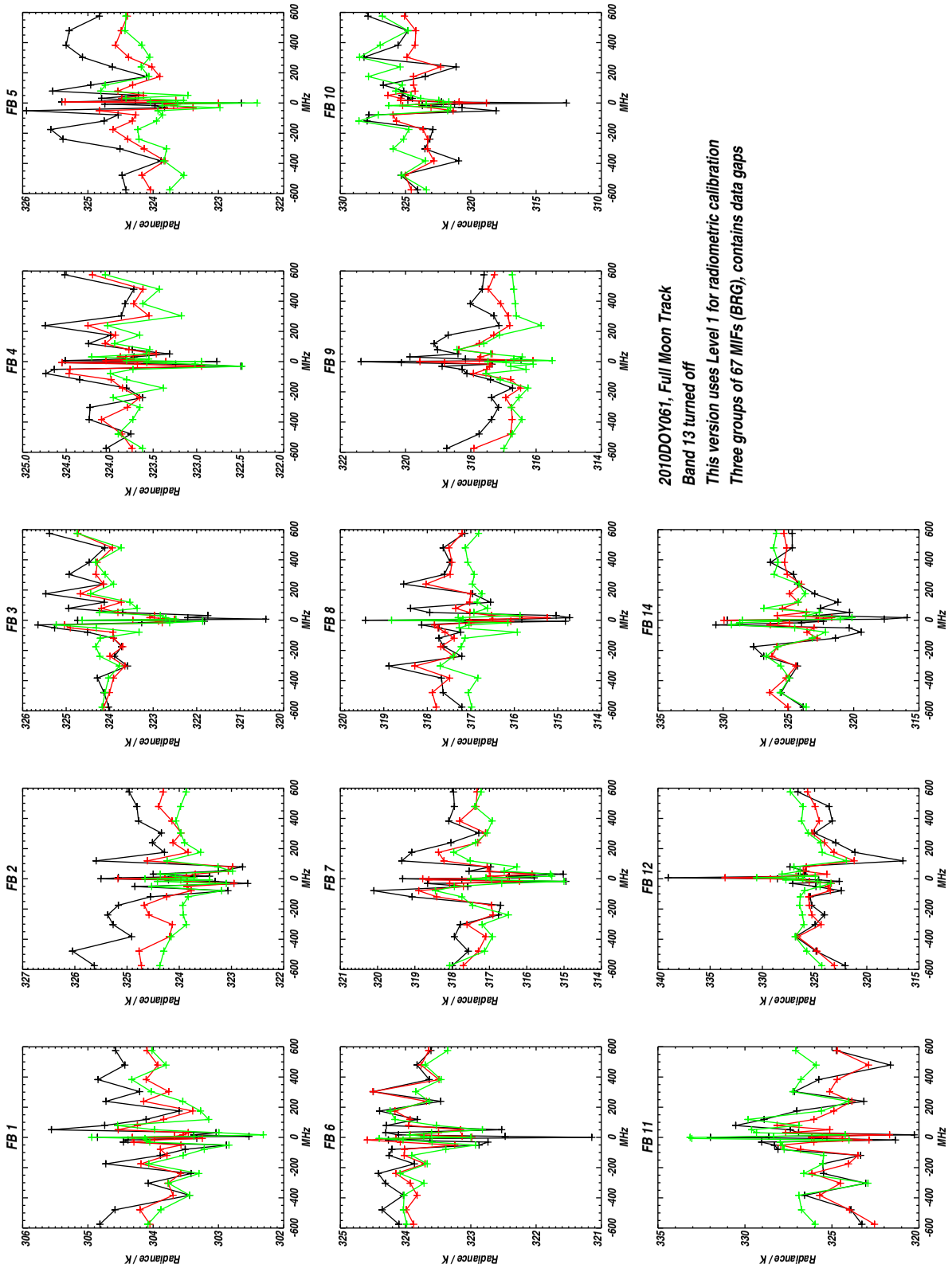

Figure 3.24: Limb radiances while tracking the full Moon on DOY061 of 2010. The time series data has been divided into three segments to give an indication of the noise levels and variations in radiometric calibration between consecutive major frames. These data were created using a modified version of Level 1 software, and hence omit the Moon tracking data taken during the nominal radiometric calibration period. See text for additional details.

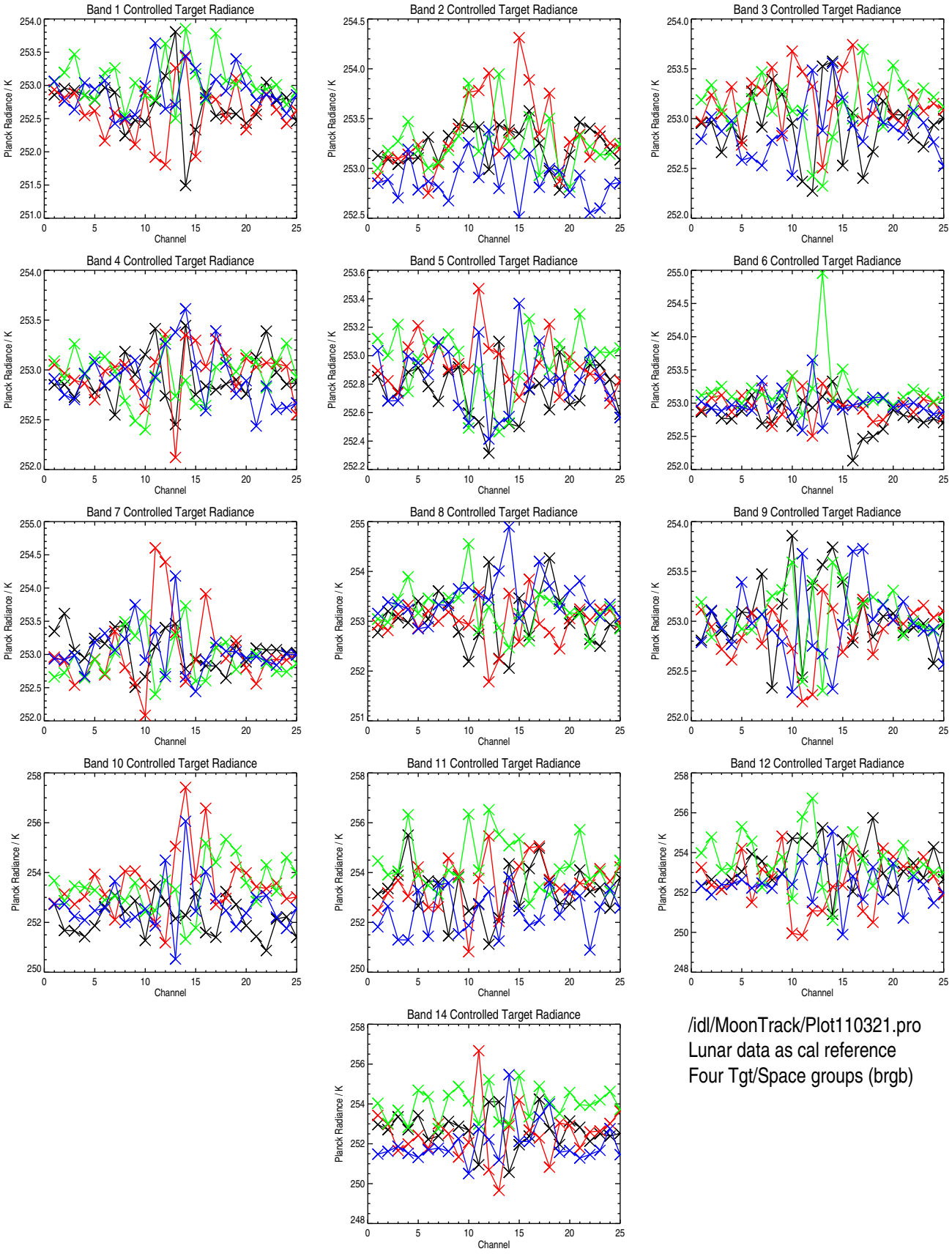

Figure 3.25: Controlled Target Radiance in the four Space-Target groups surrounding the Lunar tracking event on 21 March 2011. See text for additional details. This figure appears to be out of sequence, but is positioned here because the data was taken as an extension to the standard ones made during a Moon tracking event.

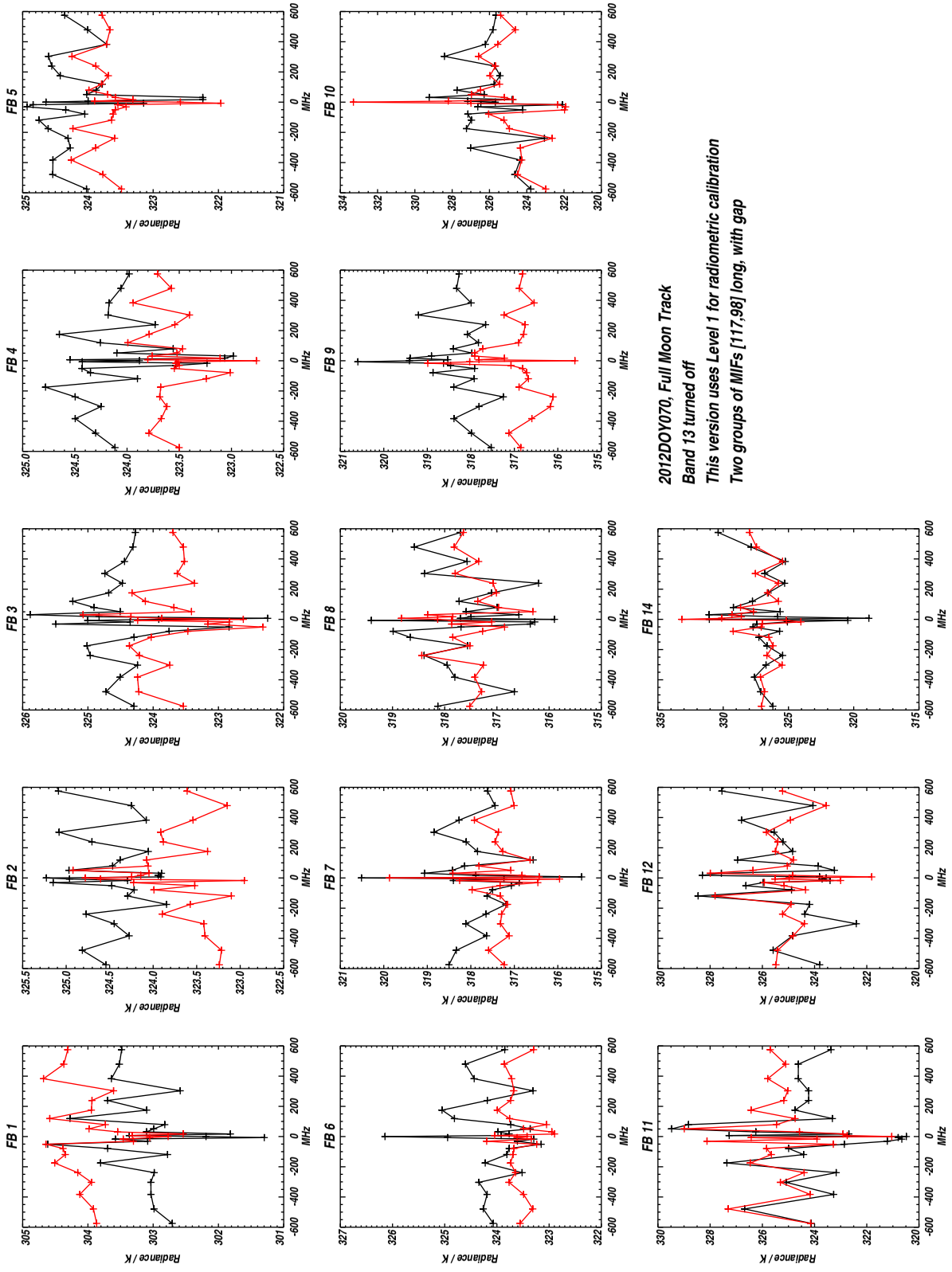

Figure 3.26: Limb radiances while tracking the full Moon on DOY070 of 2012. The L1-calibrated data were split into two segments for comparison. See text for additional details.

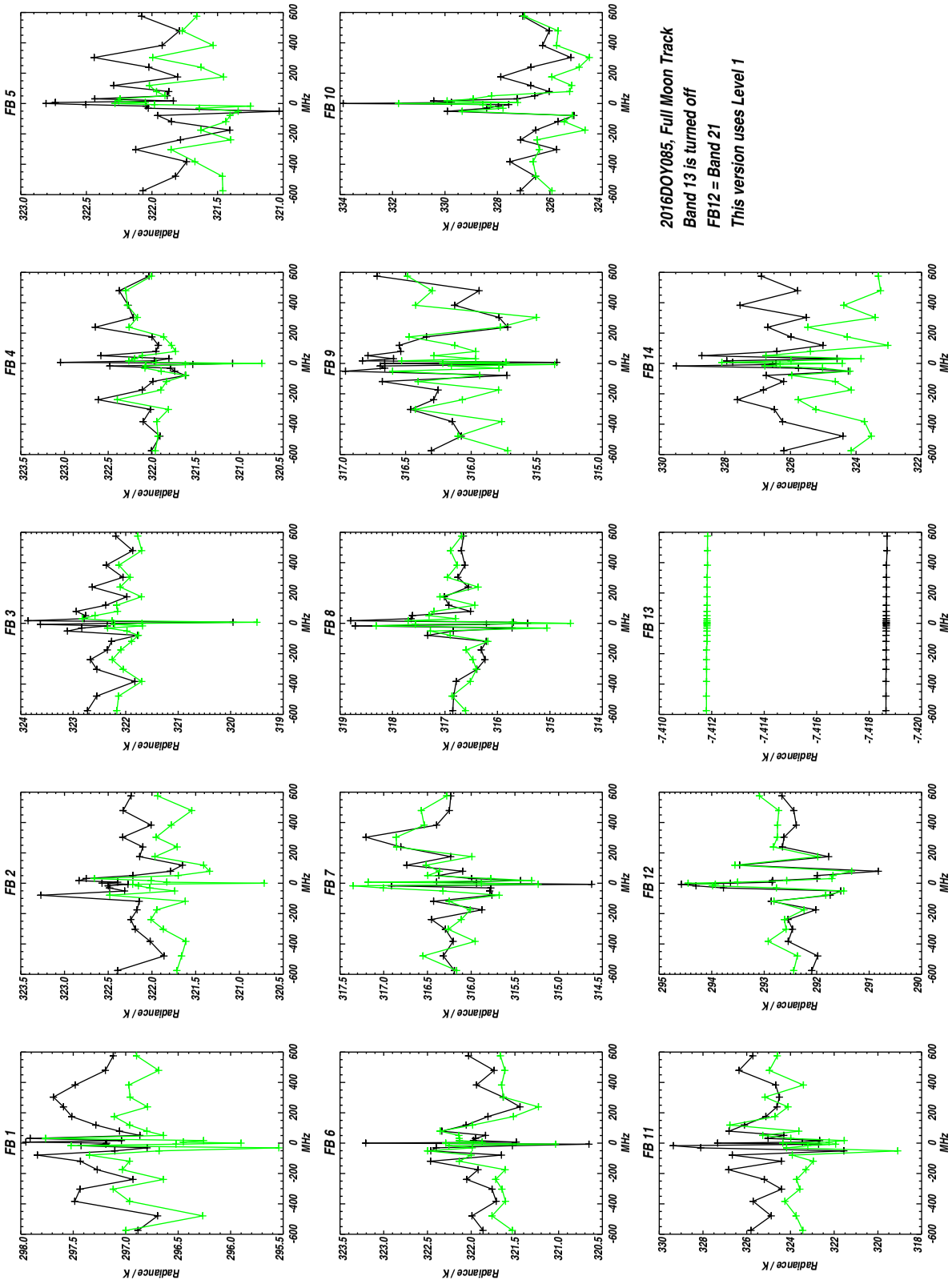

Figure 3.27: Limb radiances while tracking the full Moon on DOY085 of 2016. The time series data has been divided into two segments to give an indication of the noise levels and variations in radiometric calibration between consecutive major frames. These data were created using a modified version of Level 1 software, and hence omit the Moon tracking data taken during the nominal radiometric calibration period.

Chapter 4

Field of View Calibration

Post-launch reanalysis of spillover at the Switching Mirror ports indicated a minor error in the values determined for R2, R3 and R4 (at all of the ports). The revised values are given in Table 4.1 below.

Table 4.1: Spillover Efficiencies Calculated from Radiometer Pattern Integrations

η_r^{MX} (port baffle transmissions)					
$X = L$ Limb	0.99598	0.99344	0.99878	0.99915	0.99894
$X = S$ Space	0.99587	0.99317	0.99874	0.99912	0.99892
$X = T$ Target	0.99575	0.99274	0.99868	0.99910	0.99890

Space Radiance $\dot{P}_\nu^{BB}(2.7°\text{K})$	0.79	0.32	0.16	0.00035
$\dot{P}_{i,s}^{SA}$	$\dot{P}_\nu^{BB}(150°\text{K})$			
$\dot{P}_{i,s}^{S1}$	$\dot{P}_\nu^{BB}(100°\text{K})$			
$\dot{P}_{i,s}^{S2}$	$\dot{P}_\nu^{BB}(140°\text{K})$			
$\dot{P}_{i,s}^{S3}$	$\dot{P}_\nu^{BB}(120°\text{K})$			
$\dot{P}_{i,s}^{O1}$	$\dot{P}_\nu^{BB}([-11,+83]°\text{C})$			
$\dot{P}_{i,s}^{O2}$	$\dot{P}_\nu^{BB}([+18,+62]°\text{C})$			
$\dot{P}_{i,s}^{O3}$	$\dot{P}_\nu^{BB}([+10,+41]°\text{C})$			

Bibliography

[1] Waters, J.W. and Jarnot, R.F., Science Requirements on the EOS MLS Instrument and Data Processing Software, JPL–D14421, Revision 3.0.

[2] Jarnot, R.F., EOS MLS Level 1 Data Processing Algorithm Theoretical Basis, JPL D–15210.

[3] Jarnot, R.F., The Impact of Noise and Gain Variations on Radiometric Precision – a Quantitative Assessment of UARS and EOS MLS, Technical Note RJ.10, available from the author on request.

[4] Jarnot, R.F., Variances and Covariances in Total Power Radiometer Radiances – EOS MLS example, Technical Note RJ.16, available from the author on request.

[5] Jarnot, R.F., Some Observations on the Impacts of Nonlinearity in MLS Signal Chains, MLS Technical Note RJ.20.

[6] Erickson, N., Tolls, V., Near-Field Measurements of the SWAS Antenna, *20th ESTEC Antenna Workshop on Millimetre Wave Antenna Technology and Antenna Measurements*, 18–20 June 1997, Noordwijk, The Netherlands.

[7] Slater, D., Near Field Antenna Measurements, 1991 Artech House, Inc. ISBN 0-89006-361-3.

[8] Slater, D., *et.al.*, A Large Aperture 650 GHz Near-Field Measurement System for the Earth Observing System Microwave Limb Sounder, *Antenna Measurement Techniques Association Conference*, October 2001.

[9] www.nearfield.com